DISSERTATION

FELINE ORAL SQUAMOUS CELL CARCINOMA: A COMPREHENSIVE APPROACH TO IMPROVE TREATMENT OUTCOME

Submitted by

Hiroto Yoshikawa

Graduate Degree Program in Cell and Molecular Biology

In partial fulfillment of the requirements

For the Degree of Doctor of Philosophy

Colorado State University

Fort Collins, Colorado

Summer 2013

Doctoral Committee:

Advisor: Susan M. LaRue

E.J. Ehrhart
Elissa Randall
Douglas Thamm

ABSTRACT

FELINE ORAL SQUAMOUS CELL CARCINOMA: A COMPREHENSIVE APPROACH TO IMPROVE TREATMENT OUTCOME

Feline oral squamous cell carcinoma (SCC) is a devastating disease that responds poorly to traditional treatment modalities. The tumor location directly impacts the patient's ability to eat and drink, and immediate intervention to alleviate clinical signs is important. To design better treatment strategies it is paramount to understand the underlying biological behavior of this poorly defined tumor. This research takes a comprehensive approach in attempt to understand this disease. A number of assays have been developed and applied to elucidate underlying biology. New imaging modalities have been used to better stage the disease and define tumor location. Finally, patients were treated with a new radiation therapy modality, stereotactic radiation therapy (SRT), and outcome was correlated with the biological assays for potential predictive value. This data should inform the development of future clinical trials.

Imaging is an essential step for cancer staging and radiation therapy planning. Cancer cells use glucose at a higher rate than most normal tissues, so 2-^{18}F-fluoro-2-deoxy-D-glucose positron emission tomography (^{18}F-FDG PET) is routinely performed in human oncology because it is a highly sensitive method for identifying areas of higher glucose metabolism. This imaging modality is more frequently used for veterinary oncology staging as well. The goal of the prospective study described in Chapter 2 was to compare gross tumor volume measurements using ^{18}F-FDG PET vs. those using computed tomography (CT) for SRT planning in cats with oral SCC. Twelve cats with confirmed oral SCC underwent pretreatment ^{18}F-FDG PET/CT.

Gross tumor volumes based on contrast-enhanced CT and ^{18}F-FDG PET were measured and compared between cats. Mean PET gross tumor volume was significantly smaller than mean CT gross tumor volume in the mandibular/maxillary SCC group (n=8, *P*=0.002) and for all cats (n=12, *P*=0.006), but not for cats with lingual/laryngeal SCC (n=4, *P*=0.57). Mismatch fraction analysis revealed that most of the lingual/laryngeal patients had a large region of high-^{18}F-FDG activity outside of the CT gross tumor volume. This mismatch fraction was significantly greater in the lingual/laryngeal group than the mandibular/maxillary group (*P*=0.028). The effect of poor spatial resolution of PET imaging was greater when the absolute tumor volume was small. Findings from this study indicated that ^{18}F-FDG PET warrants further investigation as a supplemental imaging modality in cats with oral SCC because it detected presumed regions of primary tumor that were not detected on CT images

For canine and feline patients with tumors in the head region, simultaneous irradiation of the primary tumor and mandibular and retropharyngeal lymph nodes (LNs) is often indicated. The purpose of this study described in Chapter 3 was to assess the reliability of a planning target volume (PTV) expansion protocol for secondary targets (LNs). Two CT image sets from 44 dogs and 37 cats that underwent radiation therapy for tumors in the head region were compared to determine LN repositioning accuracy and precision; planning-CT (for radiation therapy planning) and cone-beam CT (at the time of actual treatment sessions). Eleven percent of dogs and 65 % of cats received treatment to their LNs. In dogs, the mandibular LNs were positioned more caudally (*P*=0.0002) and the right mandibular and right retropharyngeal LNs were positioned more to the left side of the patient (*P*=0.00015 and *P*=0.003, respectively) during treatment compared to the planning CT. In cats, the left mandibular LN was positioned higher (toward roof) than on the planning-CT (*P*=0.028). In conclusion, when the patient

immobilization devices and bony anatomy matching are used to align the primary head target and these LNs are treated simultaneously, an asymmetrical PTV expansion that ranges 4–9 mm (dogs) and 2–4 mm (cats) should be used to ensure that the LNs are within the PTV at least 95% of the time.

Information about the molecular biology of feline oral SCC is still limited. In Chapter 4, 22 archived tumor samples of feline oral SCC were evaluated to develop immunohistochemical assays and to determine if there was correlation to clinical parameters. Immunohistochemistry for Ki67, MVD, and EGFR was performed and scored. Patient survival information was obtained from the medical records. These molecular markers as well as MI were correlated with tumor locations and patient survival time. The 22 tumors showed wide variation in Ki67, MI, MVD, and EGFR. Tongue SCC expressed higher MVD than mandibular/maxillary SCC (P=0.088). Tumor expression of EGFR was inversely proportional to survival time (P=0.097). This study suggests EGFR expression might be a valuable prognostic factor for treatment outcome in feline oral SCC. It also identified higher angiogenesis in tongue SCC as compared to mandibular/maxillary SCC which may account for a different clinical outcome. Further prospective characterization of feline oral SCC may give us a better understanding of the underlying molecular factors that drive its behavior and offer the possibility for future patient-specific treatment plans. In Chapter 5, markers established in Chapter 4 and a number of other potential predictive assays were evaluated in 20 cats prior to treatment with SRT. Survival time (ST) and progression-free interval (PFI) were correlated with mitotic index, several histopathological grading schemes, expression of Ki67 and EGFR, tumor MVD, and tumor oxygen tension (pO2). Median ST and PFI were 106 and 87days, respectively. Overall response rate evaluated 4 weeks post-SRT was 38.5%. Patients with higher MVD had significantly shorter ST than patients with lower MVD (P=0.041). Patients with more keratinized

SCC had significantly shorter PFI than patients with less keratinized SCC (P=0.049). Post-SRT tumor pO2 was significantly lower than pre-SRT tumor pO_2 (P=0.047). In conclusion, although SRT alone did not improve ST and PFI compared to historical controls, MVD and degree of keratinization may be useful prognostic markers and anti-angiogenesis therapy should be considered as an adjuvant treatment.

Cancer stem cell or tumor initiating cell (TIC) theory and telomere biology are actively studied fields in human head and neck (H&N) cancer. In feline oral SCC, which has been advocated as a feline model for human H&N cancer, our knowledge about the TIC and telomere/telomerase biology is limited. Protein expression levels of putative TIC markers of human H&N cancer, CD44 and Bmi-1, were immunohistochemically evaluated for their possible role as prognostic markers in 20 patients with feline oral SCC who underwent SRT. This patient population was part of a clinical trial and information relevant to PFI and ST was available. A combined technique of fluorescent in-situ hybridization and immunofluorescent staining was used to determine telomere length ratio (fractions of very short telomere/average length telomere in the putative cancer stem cells) in the putative TICs that were positive for CD44 and Bmi-1. This was also correlated with treatment outcome. And finally, relative telomerase activity was evaluated by using a novel real-time quantitative polymerase chain reaction assay. Significant inverse correlations were found between PFI or ST and Bmi-1 protein expression in Log-Rank and multivariate Cox proportional hazard analyses (PFI: P<0.047, ST: P<0.013). Those results suggest that Bmi-1 may play important roles in local tumor recurrence and should be used as a novel therapeutic target. Neither the telomere length ratio nor the relative telomerase activity had significant correlations with ST or PFI. A large inter-patient variability in the relative telomerase

activity was noted and this may suggest that telomerase inhibition is not beneficial for the treatment outcome in cats with oral SCC.

In summary, five studies examined different aspects of feline oral squamous cell carcinoma. This information should be useful to develop future treatment strategies. Treatment outcome of this cancer might be improved by adding other modalities that target tumor vasculature and Bmi-1 to SRT.

ACKNOWLEDGEMENT

During my life as a graduate student at the Animal Cancer Center and the Environmental and Radiological Health Sciences, I have had an incredible quantity and quality of support from everybody I have met. First of all, I would like to acknowledge my advisor, Dr. Susan LaRue for her tremendous amount of support and teaching. I would not have been able to even start my career here and may have had to quit pursuing my goal to become a veterinary radiation oncologist/cancer biologist if she had not chosen me as her graduate student in 2008. She was always thoughtful not only for me, but also for my entire family which has always my top priority. She is a great veterinary radiation oncologist and biologist who thinks outside of the box. Therefore, I will be never able to thank her enough for the rest of my career. Second, I would like to acknowledge my committee members, Dr. EJ Ehrhart, Dr. Douglas Thamm, and Dr. Elissa Randall. Dr. Ehrhart is a wonderful veterinary pathologist with whom I spent significant amount of time during my Ph.D. course. He has a very deep and wide knowledge in immunohistochemistry and his histopathological interpretation and explanation were always clear and logical. Dr. Thamm is another very instructive committee member who was always happy to answer any questions I had. He is not only a very intelligent person, but also is always friendly and has a significant passion for teaching. Dr. Randall is also a wonderful committee member and a radiologist who guided my medical imaging-related research in the most appropriate direction. She was always willing to help me and I enjoyed working with her a lot. They, all four committee members, are undoubtedly incredible mentors and I am one of the luckiest students in the world to be able to spend years with them.

Also, I must acknowledge the institutions I have belonged to, the Animal Cancer Center and the Environmental and Radiological Health Sciences. My colleagues in these institutions,

including, but not limited to, Dr. Steve Withrow, Dr. Rod Page, Ms. Barb Rose, Ms. Jenette Shoeneman, Mr. Brad Charles, and Ms. Karen Waldchen, provided me wonderful support throughout the time I spent here.

I am also indebted to people in Dr. Susan Bailey's lab, including Dr. Bailey, Dr. Christine Battaglia, and Dr. David Maranon. They offered me a significant amount of technical help and advice to my telomere study.

I would also like to acknowledge my radiation therapy team, Drs. Custis, Griffin, and Nolan, and Ms. Chana Fullar, Mr. Frank Conway, and Ms. Ann Golden for their help in acquiring and treating patients for my studies. I would also like to acknowledge the radiology team, including Dr. Susan Kraft, Ms. Billie Arceneaux and Mr. Jeff Stewart for technical support in PET/CT imaging. I would also like to acknowledge Dr. Fred Harmon for his help in medical physics in my lymph node project and a class in ERHS, Drs. Jenna Burton, Kelly Carlsten, and Kristen Weishaar for clinical trials coordination, and Drs. Ann Hess and Jens Eickhoff for their support in statistical analysis. I would love to acknowledge the Winn Feline Foundation and the Morris Animal Foundation for their extensive support for my projects and family.

Finally, I would like to acknowledge my family, Noriko, Daichi, and Haruto, family in Japan, Tsuneo, Yoko, Kanae, and Yumiko, grandmother Ayako, and my beautiful cats, Marony, Pemi, and Kuro, for always being with me and their love so that I could keep walking forward.

TABLE OF CONTENTS

CHAPTER 1: INTRODUCTION

Feline oral squamous cell carcinoma is a devastating disease that is poorly responsive to traditional treatment options. Understanding the underlying biological behavior of this cancer is critical for the development of more successful treatment options. This research evaluates the disease from a number of different perspectives. A retrospective evaluation using paraffin embedded tissues was performed to develop and validate immunohistochemical assays that provided baseline information (Chapter 4). A clinical trial that included 20 cats (Chapter 5) was conducted and assays established in Chapter 3 were used to characterize the tumor prior to treatment were performed. Evaluations included histological and immunohistochemistry techniques, tumor oxygen levels, and telomere and stem cell marker expression assays (Chapter 5 and 6). ^{18}F-FDG PET was used to determine if it provided an advantage in tumor staging compared to previous methods (Chapter 2). Because there is no well-defined standard of care for this disease, patients were treated with a new technology, stereotactic radiation therapy (SRT). This technique is administered in less than a week, minimizing time away from their home environment. SRT had never been used in this disease or in any feline head and neck (H&N) cancer, so this research also focused on optimizing the administration of SRT. Chapter 3 addresses how to most accurately deliver dose to regional lymph nodes while also targeting the primary tumor. ^{18}F-FDG PET was evaluated and compared to CT alone to determine any differences in identifying tumor targets and Chapter 2 describes those findings. Finally, in Chapter 5 and 6, all of the pretreatment information was correlated with clinical outcome to identify prognostic parameters. This introduction serves as a comprehensive literature review for the overall body of work (Figure 1.1).

Disease behavior and response to treatment

Squamous cell carcinoma (SCC) is the most common (60-80%) oral malignancy in cats.[1] No breed, gender, or hair coat color predispositions have been identified.[2] Incidence of feline oral cancer has been reported as 45 cases per 100,000 cats, however this seminal report was published more than 35 years ago.[3] Feline oral SCC most commonly affects the mandible, maxilla, and tongue (Figure 1.2). Because of the location, these tumors often impact the cat's ability to eat, drink, and groom, leading to secondary malnutrition and dehydration.

Etiology of this tumor has not been extensively studied. One study reported that the risk of oral SCC is significantly higher in cats who wear a flea control collar or eat canned food. Eating canned tuna cat food is associated with a higher risk than non-tuna canned or dry food.[4] Cats with oral SCC were exposed to environmental tobacco smoke (ETS) were more likely to overexpress p53 protein than those not exposed to ETS although the association was not significant.[5] The relationship between ETS exposure or p53 protein overexpression and patient prognosis has not been evaluated. Bony lysis is a commonly observed characteristic of feline oral SCC,[6,7] leading investigators to evaluate the effect of a bisphosphonates, zoledronic acid, on inhibition of osteolytic activity of the cancer. These studies suggested that the zoledronic acid may inhibit pathological osteolysis caused by feline oral SCC and slow growth rate.

Treatment outcome of this feline cancer is disappointing. Surgery alone rarely provides local tumor control. In two reports from the 1970s and early 1980s, 10 cats with oral SCC were treated surgically.[8,9] All cats were euthanized due to local recurrence within 16 weeks. All recent studies have reported a median survival time (MST) of 44 days for 54 surgically-treated cats.[10] In this study, cats treated with non-steroidal anti-inflammatory drugs (NSAIDs) had significantly

longer MST than those without NSAIDs treatment, although immunohistochemically-evaluated cyclooxygenase-2 expression level was not prognostic. Another study reported outcome of 7 cats with stage III oral SCC of the mandible treated by mandibulectomy, feeding tube placement, and post-surgical radiation therapy.[11] A feeding tube was temporarily (3 to 44 days) used to support food intake post-surgically. Six of the seven cats were euthanized due to local tumor recurrence. MST after surgery was 14 months with one-year survival rate 57%. In another study, 21 cats with oral SCC were treated by mandibulectomy with or without additional radiation and/or chemotherapy.[12] In this study, MST for cats with oral SCC was 7 months and one-year survival was 43%. Minimal improvement has been shown in MST between older studies and more recent studies. Summarizing these previous reports, surgery with additional chemotherapy/radiation therapy seems to provide longer post-treatment survival but local tumor recurrence persists as the primary cause of patient death.

Radiation therapy (XRT) plays a central role in the management of veterinary cancer patients. Historically, orthovoltage, cobalt machines, and linear accelerators using 3 dimensional conformal treatment (3D-CRT) were most commonly used. Radiation therapy has been used as a palliative modality and with curative intent. It has also been combined with surgery and/or chemotherapy. As a palliative treatment for inoperable feline oral SCC, seven cats were treated with weekly 8 Gy treatments on days 0, 7, and 21.[13] MST was 60 days and about 43 % of cases did not complete treatment due to tumor- or XRT-related reasons. The authors of this study concluded that the poor response rate and high complication rate outweighed any benefit. Accelerated XRT consisting of 14 fractions of 3.5 Gy administered twice daily has been evaluated by several groups.[14-16] Although acute and late toxicities were manageable, accelerated XRT alone did not improve treatment outcome. The addition of carboplatin to this XRT regimen

showed modest improvement in MST (163 days) with significantly better MST in cats with complete response (median 379 days).[14,15] In this study, cats with tonsil/buccal mucosa SCC survived significantly longer (mean 724 days) than cats with mandible/maxilla/tongue SCC (median 141 days) but no reason for this difference was addressed in this report.[14] A recent report described accelerated XRT in combination with surgery and neoadjuvant chemotherapy.[16] Three of six cats were still alive (759, 458, and 362 days) and in complete remission at the time of data analysis. The neoadjuvant chemotherapy consisted of bleomycin, piroxicam, and thalidomide, which are immunomodulatory and anti-angiogenic drugs.[17] Although the patient population was small, this aggressive multi-modality treatment protocol should be further investigated.

SRT has recently been introduced in veterinary medicine. Traditional XRT with curative intent is delivered in small doses per fraction, providing greater sparing of normal responding tissues in the field. Higher total doses can be prescribed with small doses per fraction and it generally results in better tumor control. In contrast, SRT delivers higher dose per fraction and is delivered in fewer, usually 1-5, fractions. This is possible because SRT spares normal tissues by minimizing dose to surrounding normal tissues. SRT requires a steep drop-off in dose from the tumor to normal tissues. This requires great accuracy in patient positioning so that a margin added to a primary target (gross tumor volume; GTV)[18] can be decreased. This leads to a smaller final target (planning target volume; PTV) compared to the PTV used in conventional XRT. Prescribed dose is determined by the balance between the normal tissue dose tolerance of the surrounding critical structures (such as brain, eyes, and skin) and tumor control probability. The possibility of radiation-induced late toxicity mainly depends on dose per fraction and total dose.[19] Therefore, a smaller PTV expansion (thus less involvement of surrounding normal tissues

into the PTV) is a benefit resulting in lower dose per fraction and lower total dose to surrounding tissues. SRT for human H&N SCC was first reported in 1991, for the treatment of nasopharyngeal SCC.[20] In this report, a human patient with recurrent oral SCC after surgery and chemotherapy was treated by a single fraction of 20 Gy using a gamma-knife equipped with hundreds of small cobalt-60 sources. This patient was doing well at 7 months post SRT, although the follow-up period was too short to determine treatment durability or toxicity. Several reports utilized SRT as a primary treatment modality for human tumors in the H&N region. [21-23] In these studies, most patients were treated with a fractionated regimen ranging from 3 to 8 fractions with the total dose up to 48 Gy. Overall response rates were about 70%. Treatment-related acute toxicity was absent or manageable and although long-term tumor control did not seem to be improved compared to other definitive treatment regimens, the authors of these studies concluded that SRT for the treatment of H&N SCC was a viable and effective option for selected cases.

In veterinary medicine, our knowledge of SRT is limited. Reports from a group at the University of Florida utilized SRT to treat canine appendicular osteosarcoma and brain tumors;[24,25] however, no study has evaluated the efficacy and toxicity of SRT in feline malignancies. We elected to treat 20 cats with feline oral SCC using SRT and to correlate treatment efficacy with survival time and progression-free interval as endpoints. SRT may have some inherent advantages for a tumor like feline oral SCC, which is assumed to be hypoxic due to its characteristically rapid growth. Previous studies suggested that SRT initiates tumor endothelial cell apoptosis immediately after irradiation and the resulting vascular damage has been hypothesized to indirectly damage tumor cells.[26-28] The paucity of information regarding molecular and cellular characteristics of this disease provides little insight that can predict

response to SRT or other therapy. The main purpose of this body of work is to inform future treatment design.

Evaluations of cellular and molecular biology

Ki67 is a nuclear protein that is expressed in actively proliferating cells and has a biological half-life of approximately 90 min.[29,30] The protein expression of Ki67 is restricted to G1, S, G2, and M phases and is not expressed in G0 (senescence) phase. During G1, S, and G2 phases, Ki67 is detected within the nucleus, and during M phase it is relocated on the surface of the chromosomes.[29] The functional role of Ki67 protein has not been fully discovered yet.[29] However, several studies have shown that silencing Ki67 cDNA inhibits cell proliferation, suggesting Ki67 protein possesses a function that regulates cell cycle progression and cell proliferation.[31,32] Ki67 labeling index (LI) has been suggested to be more sensitive compared to mitotic index (MI) because Ki67 can detect all proliferating cells whereas MI counts only cells in M phase.[29] Clinically, numerous studies in human H&N SCC have evaluated the role of Ki67 as a prognostic marker after different treatment interventions.[33-35] Among them, one study showed that human H&N SCC patients with p53-positive and low Ki67 LI displayed less response to fractionated XRT compared to those with p53-neagtive and higher Ki67 LI.[33] Another study demonstrated that patients with laryngeal/pharyngeal SCC with high Ki67 LI had shorter overall and disease-free survival time after surgical excision.[34] Similarly, a study showed that high Ki67 LI was an independent predictor of local recurrence after total laryngectomy.[35] Several studies evaluated Ki67's role as a prognostic marker in different canine malignancies.[36-38] Among them, in mast cell tumors and mammary carcinoma where surgical resection was the only treatment

modality, patients with higher tumor expression of Ki67 protein had significantly worse outcome compared to those with lower expression.[36,37] Reports in feline oncology have shown that Ki67 LI is a prognostic indicator.[39-41] In one study that included feline patients with surgically resected mammary carcinoma, patients with higher Ki67 LI had decreased survival times compared to those with lower Ki67 LI.[39] Another study showed that high Ki67 LI was an indicator of poor outcome in patients with feline oral SCC. However this study evaluated different treatment modalities including medical palliative treatments.[41] In a report that evaluated treatment outcome in feline patients with nasal/periocular SCC that undergoing fractionated electron beam XRT and Ki67 LI, a positive correlation was observed between the index and disease-free interval was established.[40] In summary, it is likely that SCC responds more favorably to fractionated XRT when the tumor has higher Ki67 LI. This could be because these actively proliferating cells have less time to repair radiation-induced DNA damage. However, actively proliferating cells may result in earlier tumor recurrence if complete surgical excision could be achieved. The role of Ki67 as a prognostic marker in patients with feline oral SCC undergoing SRT has not been evaluated.

Mitotic index (MI) is also used to evaluate proliferating cells. This is a very practical way of estimating the proliferating fraction in a given sample population because of the ease in quantification. The disadvantage is that such as small fraction of cells are in mitosis at any time point. To date, no study evaluating MI in feline oral SCC has been published; however, in human oncology MI has been used for many years as a cell proliferation marker both *in vitro* and *in vivo*.[42] For example, a study in human H&N SCC revealed that proliferative activity expressed with high MI and G2/M cell fraction was a significant prognostic factor in patients who underwent chemotherapy, XRT, or a combination of the two.[43] In human uterine cervical

carcinoma patients, both MI and Ki67 LI were shown to correlate with a reduction of tumor size as measured by MRI after platinum-based chemotherapy.[44] In this study, MI and Ki67 LI showed a significant mutual correlation, although this is still controversial.[45,46] In human cervical SCC patients who underwent fractionated XRT, higher MI was shown to be the strongest indicator of poor survival, followed by tumor volume and Ki67 LI.[47] A report of human cervical carcinoma patients who underwent fractionated XRT showed that low MI and high keratinization were statistically significant indicators of poor survival.[48]

Volume-corrected MI has been evaluated in human patients with oral SCC who underwent either XRT or surgery.[49-51] In these studies, the volume-corrected MI was calculated to account for the neoplastic fraction in a given microscopic field. Patients with lower volume-corrected MI had a significantly better treatment outcome compared to those with higher volume-corrected MI. This suggested that in human H&N SCC patients who underwent fractionated XRT, a reduction of MI after the first 2 Gy irradiation was a favorable indicator of long-term survival. [52] Based on these studies, it is reasonable to suggest that MI may play a prognostic role in feline oral SCC.

Epidermal growth factor receptor (EGFR) is a receptor tyrosine kinase.[53] Multiple ligands can bind to EGFR including epidermal growth factor, transforming growth factor-α, and amphiregulin.[53] Ligand binding leads to conformational changes in the receptor's intracellular domain and this activated EGFR will undergo dimerization and auto-phosphorylation of tyrosine residues of the intraceullular domain.[53] Downstream events are mediated by many proteins (secondary messengers) such as Ras/MAPK, JAK/STATs, and PI-3K/Akt.[53] The final events of EGFR activation depend on the activated downstream messengers and are probably cell type-dependent. Downstream events include cell cycle progression and proliferation, cell survival,

angiogenesis, cell adhesion, differentiation, cell migration and invasion, and radio-and chemo-resistance due to enhanced DNA repair.[54-57] In tumor cells, overexpression of EGFR, due to gene amplification is known to cause self-dimerization/activation in the absence of ligands.[58] Other mutations in the EGFR gene can cause ligand-independent activation of the receptors including a point mutation in the transmembrane domain and loss of the extracellular domain (truncation).[58] In a variety of human malignancies such as non-small cell lung cancer, breast cancer, and H&N SCC, overexpression of EGFR is recognized at mRNA and protein levels.[58-61] Therefore, EGFR has been an attractive therapeutic target in human oncology. Monoclonal antibodies such as cetuximab and tyrosine kinase inhibitors such as gefitinib have been developed and used to treat a variety of human cancers.[62] Clinical studies have revealed that EGFR overexpression is a negative prognostic factor after XRT.[63] A study that treated 155 human H&N patients with conventionally fractionated XRT showed that patients with higher EGFR protein expression had significantly shorter overall survival and disease-free survival and higher rate of loco-regional tumor recurrence.[64] In feline SCC, EGFR expression has been reported but data is still limited.[65] One *in vitro* study evaluated the efficacy of a tyrosine kinase inhibitor (gefitinib) and a small interfering RNA (siRNA) on an oral SCC cell line.[66] The authors observed anti-proliferative activity of gefitinib and found that addition of the siRNA against feline EGFR transcript could overcome the gefitinib resistance that was induced by exposing the cell line to high doses of gefitinib. The authors also reported that the siRNA showed an additive cell-killing effect when it is used with ionizing radiation up to 3 Gy.[66] The efficacy of anti-EGFR monoclonal antibodies against feline oral SCC has not been reported.

Angiogenesis in normal tissues is maintained by a very finely regulated balance between pro- and anti-angiogenic activities.[67] Pro-angiogenic factors include vascular endothelial growth

factor (VEGF), fibroblast growth factor, epidermal growth factor, and platelet-derived growth factor whereas anti-angiogenic factors include thrombospondin-1, angiostatin, and endostatin.[67] Tumor angiogenesis has been described as "wounds that never heal" [68] meaning the effects of pro-angiogenic factors overcome those of anti-angiogenic factors. Upon angiogenesis activation, which may be triggered by many factors, tumor endothelial cells lose attachment to pericytes, which have been shown to suppress proliferative activity of endothelial cells and decrease their dependence on VEGF.[67] p53, a well-known tumor suppressor gene is mutated in up to 50% of many common human malignancies including human H&N SCC.[69] Normal p53 forms a tetramer and has a very short half-life (~20 min) because Mdm2, which is induced by p53 protein, degrades p53 protein immediately.[69] Mutation of the p53 gene results in the loss of its ability to induce Mdm2 protein, leading to accumulation of p53 protein in the cell. This results in a strong immunoreactivity in a large fraction of tumor cells evaluated by immunohistochemistry.[69] p53-positive immunoreactivity has also been reported in feline oral and conjunctival SCC.[5,70,71] Because p53 has been shown to downregulate gene expression of VEGF, cyclooxygenase-2, and hypoxia inducible factor-1 and upregulate that of thrombospondin-1, normal p53 works as an anti-angiogenic factor and its loss-of-function-mutation exacerbates the tumor's chaotic angiogenic activity.[67] Unregulated angiogenic activity results in formation of porous, tortuous, dilated, and sometimes dead-ended vessels.[67] In human cancer patients, anti-angiogenic therapy has been extensively researched and multiple molecular-targeted drugs have been evaluated.[67,72-74] In one study using a human microvascular endothelial cell line, a combination of anti-EGFR, anti-VEGF, and radiation therapy (up to 10 Gy) showed a marked synergistic effect in cell killing.[74] Microvascular density (MVD) has been used to evaluate the degree of angiogenesis in tumor tissues. Typically, MVD is evaluated by quantifying immunohistochemically stained

endothelial cells. Several different antibodies are available to stain the endothelial cells including anti-CD31, anti-CD34, and anti-von Willebrand factor.[75] Methods for counting endothelial cells include computer-aided quantification of positively-stained pixels and manual counting of microvasculature in the tissue.[76,77] A study showed large inter-patient variability in MVD even among the same tumor type.[78] A 1992 study reported that high MVD in human breast cancer patients was a significant indicator of poor overall and relapse-free survival after surgery with or without chemotherapy.[79] A plethora of studies have evaluated a possible role of MVD as a prognostic indicator. Although there are some technical variations, most studies scanned the entire field first at lower power field and then chose areas with the highest angiogenesis (hotspot technique).[78] A human H&N SCC study that treated patients by radical chemoradiotherapy has shown that patients with very low or very high MVD had significantly higher death rates compared to those with intermediate MVD.[78] Another study evaluated changes of MVD before and after 20 Gy of fractionated XRT. Patients who showed >50 % of reduction in MVD compared to the pre-treatment MVD had significantly better overall survival as well as better treatment response after completion of XRT (total 60-70 Gy).[80] In a study that correlated post-surgical tumor recurrence and MVD in human H&N SCC, higher MVD was significantly associated with higher local tumor recurrence.[76] MVD has never been evaluated in feline oral SCC. Considering the importance of local tumor control in feline oral SCC, analyzing MVD using pre-treatment biopsy samples may show a prognostic significance and provide us a direction to improve treatment outcome. In Chapter 4 of this dissertation, immunohistochemistry protocols for those molecular variables (Ki67, EGFR, and MVD) were developed.

Human malignancies contain hypoxic regions due to abnormal tumor vascular function, structure, and organization.[81] Tissue hypoxia affects the biological response of cells to photon

irradiation.[82] Also, hypoxic tumors are known to have less apoptotic potential.[83,84] Tumor hypoxia can result from two different mechanisms; chronic and acute hypoxia.[82] Chronic hypoxia is also called diffusion-limited hypoxia and is a consequence of distance from nearby vasculature. A classic experiment with human bronchial carcinoma revealed that oxygen can diffuse about 100 μm and tumor cells outside this radius are all necrotic.[85] Acute hypoxia is caused by transient closing and re-opening of tumor blood vessels due to their abnormal structure. Increased intra-tumoral pressure due to increased permeability in the tumor vasculature can cause collapse of tumor blood vessels and leads to hypoxia.[82] Multiple methods to measure tissue oxygen tension (pO_2) have been evaluated including oxygen probes, 2-nitroimidazole markers, endogenous hypoxia markers, and hypoxia imaging.[82] Oxygen probes must be inserted into the tissue or tumor. Polarographic needle probes are the most commonly used probe and this system enables multiple points to be measured due to its quick reading time. A major disadvantage of this system is that the probe consumes oxygen due to electrochemical reduction and this leads to underestimation of the tissue pO_2.[86] Another disadvantage is that the measurements from this type of probe become inaccurate when the tissue pO_2 is very low. A luminescence-based fiber-optic system has also been developed. A ruthenium luminophor is incorporated at the probe tip and lifetime of pulsatile fluorescence of the luminophor caused by a diode source is inversely proportional to the tissue pO_2 at the probe tip.[86] The major advantages of this system are that it does not consume local oxygen and the readout is very accurate when the pO_2 is very low, making this system more preferable for tumor oxygen tension measurement over the polarographic system. It has been shown that human H&N cancers are more hypoxic than nearby normal subcutaneous tissues.[87] In human H&N SCC and cervix carcinoma, tumor hypoxia has been shown to be a prognostic factor for outcomes after fractionated XRT.[88-97] In these studies,

the definition of tumor hypoxia somewhat varies although it is typically defined as median or mean pO_2< 5-10 mm Hg. To date, no study has evaluated tumor pO_2 in feline oral SCC. Although the polarographic probes were used in these studies, several studies have shown that the luminescence system can produce comparable results to the polarographic system.[98,99] Tumor oxygen levels following fractionated XRT have shown an improvement in oxygen status.[100] Radiation biological consequences associated with SRT may be different from that following conventional fractionated XRT. Post-SRT *in vivo* oxygen measurement in spontaneous cancer patients has not been reported in human or veterinary medicine. In Chapter 5 of this dissertation, pre-SRT tumor pO_2 as well as histopathological grading and immunohistochemiral variables were correlated with treatment outcome in cats with oral SCC after SRT.

For many years tumors have been thought to arise from a single cell as a result of a series of random mutations. In this "clonal expansion model", mutational events occur in many different types of cells, including stem cells, differentiating cells, and somatic cells.[101] Because of the natural selection pressure, cells with more aggressive phenotypes such as those having more effective proliferation or less oxygen or nutrient dependence survive and create larger clonal populations than other mutated cells with less advantageous phenotypes. Because cells with several different phenotypes can survive and expand their population, a heterogeneous tumor cell population will be created after repeating this mutation-expansion cycle. It has been suggested that these multiple mutations occur infrequently in a specific single cell due to their random nature and that there must be a significant time gap between mutations.[101] In contrast, in the last decade, a novel model called the cancer stem cell or tumor initiating cell (TIC) theory has been proposed based on experimental findings in human leukemia.[102] In these experiments, leukemia cells were sorted based on cell-surface marker expression, and a small fraction of cells

with a specific marker had highly effective capability to form a phenotypically heterogeneous tumor population in immunocompromised animals. In this model, multiple mutations occur in a normal stem cell which is thought to have a longer lifespan permiting the accumulation of multiple random mutations over a long time period of time, whereas more differentiated cells are thought not to live long enough.[101] The mutated normal stem cell, which is now called cancer stem cell or TIC, gives rise to its descendant cells (these cells will differentiate) and self-renews to maintain its own population. This results in a heterogeneous cancer cell population which has a similar phenotypic diversity to the original tumor sample harvested from a patient. Since the discovery of TIC in human leukemia, the research related to TIC in many different types of human malignancies expanded. Of clinical importance is the relative resistance of TICs to chemotherapy and XRT compared to non-TICs. Research indicates that TICs may create fewer reactive oxygen species after irradiation and have more efficient DNA damage-repair mechanisms.[103-108] Recently published studies investigated characteristics of TICs isolated from feline oral SCC and feline mammary carcinoma and revealed that these cells are also more resistant to exposure to radiation and chemotherapy.[109,110] The accumulating evidence supporting the TIC in human H&N SCC makes this potentially important in the biology of feline oral SCC. In human H&N SCC, CD44 has been shown to be a TIC marker and CD44-positive TICs expressed mRNA and protein of Bmi-1 significantly more than CD44-negative cancer cells (non-TICs).[111]

CD44 is a transmembrane receptor that is involved in cell-cell and cell-matrix interactions.[112] In human CD44, at least 11 isoforms (standard form and v1-v10) have been discovered but all isoforms are created from a single gene by alternative splicing and post-translational modifications.[112-114] Ligands for CD44 include hyaluronic acid (HA), osteopontin,

serglycin, collagens, fibronectin, and laminin. Many are involved in maintenance of tissue structure. CD44 has three different structural sections; intracellular, transmembrane, and extracellular domains. The intracellular and transmembrane domains are highly conserved between mammalian species.[112] Although the extracellular domain contains variable sections (due to alternative splicing), the receptor region for HA is thought to be highly conserved.[112] It has been observed that many CD44 isoforms are expressed in a variety of normal human organs such as skin, gastrointestinal mucosa, thyroid, lymphocytes, prostate, and cervix.[115] CD44 has been proposed as a CSC marker in human H&N SCC and cancers of the pancreas, colorectum, prostate, cervix, and breast.[116] Activation of CD44 by HA binding causes signaling cascades mediated by Nanog and Stat-3, which result in multi-drug resistance (MDR) gene expression and protein expression of P-glycoprotein, with an ultimate consequence of multi-drug resistance in multiple human cancers.[117,118] Furthermore, activation of CD44 also causes anti-apoptotic signals and tumor proliferation in human breast and ovarian cancers.[118] Interestingly, CD44 has been shown to "team-up" with EGFR to enhance downstream events leading to cellular invasion, proliferation, and escape from apoptosis in human H&N SCC.[119] The clinical role of CD44 as a prognostic indicator has been studied extensively with variable results. In a microarray and immunohistochemical study of 52 human patients with H&N SCC who underwent fractionated XRT, higher CD44 expression at the mRNA and protein levels was a significant indicator for local recurrence.[120] Recently, a small study evaluated the frequency of successful xenograft implantation, which is one of the default characteristics of TICs, using CD44-positive human H&N SCC.[121] A higher frequency of CD44-positive SCC, as quantified by flow cytometry, was a significant indicator of shorter post-surgical disease control. Patients with successful xenograft implantation had significantly shorter post-surgical loco-regional disease control time compared

to patients without successful implantation. Another study with 135 patients with H&N SCC (located on the tongue, oro/hypopharynx, larynx, and other oral cavity) revealed that patients with higher CD44 protein expression had significantly shorter 5-year survival times than those with lower CD44 expression.[122] When outcome was analyzed after sorting patients into different groups based on tumor location, oro/hypopharyngeal and laryngeal SCC still had shorter survival times. The negative impact of high CD44 expression has also been reported by a Japanese group. This study also indicated that human patients with hypopharyngeal SCC with higher CD44 protein expression developed distant metastasis more frequently than those with lower CD44 expression.[123] These two studies had poorly documented or controlled treatment regimens. In contrast, a study from Spain evaluated CD44 expression immunohistochemically in 54 human patients with surgically excised H&N SCC and reported that loss of CD44 expression had a significantly negative impact on patient survival.[124] Interestingly, CD44 isoforms seem to play different roles in human ovarian cancers.[125] One hundred and forty two patients with surgically resected primary ovarian cancers and 265 patients with metastatic lesions were immunohistochemically evaluated for protein expression of CD44s (standard isoform), CD44-variant (v) 4, -v5, -v6, -v9, and -v10. CD44-v10 protein expression in the primary ovarian cancer was a significant indicator of improved survival whereas its expression in the metastatic lesion was a statistically significant indicator of poor survival.[125] However, additional treatment modalities such as postoperative chemotherapy were not clearly specified. In cats, two studies used CD44 and CD133 as a CSC marker in mammary carcinoma and oral SCC, respectively. Those studies showed that cancer cells positive for the marker had a higher capability of tumor sphere formation compared to cancer cells negative for the marker.[110,126] Compared to human H&N SCC, research of CSC in feline oral SCC is significantly limited and there is no standard

CSC marker for feline oral SCC. Based on the accumulating reports of CD44 as a CSC marker in human H&N SCC and the similarity between that human cancer and feline oral SCC, CD44 protein expression was evaluated for prognostic significance in patients with feline oral SCC.

Bmi-1, another CSC marker, was also evaluated. Bmi-1 is a member of the polycomb group of proteins that have essential roles in gene silencing during embryonic development and in DNA damage response.[127] While H2AX is a well-known DNA damage-sensing protein, another pathway that requires Bmi-1 but not H2AX to recognize DNA double-strand damage (DSD) exists.[127,128] It seems likely that Bmi-1 recognizes the DNA DSD earlier than H2AX and starts ubiquitinizing histones close to the DSD site. This eventually leads to cell cycle arrest at check points and allows cells to repair DNA damage.[127,129] If the damage is too serious to repair, the cell undergoes apoptosis or senescence to prevent possible mutagenesis. This mechanism has been thought to be, at least partially, a cause of resistance to XRT in cancer cells with Bmi-1 expression.[128] One of the key features of stem cells is the ability to undergo self-renewal.[128] Tumor suppressor proteins $P16^{INK4}$ and $p14^{ARF}$, as well as the hedgehog pathway have been shown to be involved in the self-renewal activation.[130,131] Bmi-1 has also been reported to play multiple roles in tumorigenesis and progression. These include, but are not limited to, causing epithelial-mesenchymal transition, silencing tumor suppressors such as PTEN, blocking p53-mediated apoptosis, activating telomerase, and reducing intracellular reactive oxygen species.[128,132] Bmi-1 is found in many normal tissues such as lymphocytes, hair follicles, intestinal crypt, and skin basal cells.[133-136] As research focused on the role of CSCs, Bmi-1 also gained attention due to its participation in DNA repair and self-renewal. Bmi-1 has been tested as a therapeutic target for small interfering RNA, broad spectrum histone deacetylase inhibitors, and artemisinin.[106,128,137-139] Successful delivery of these drugs might be the next challenge to

overcome.[128] The clinical role of Bmi-1 as a prognostic indicator has also been studied. In human non-small cell lung carcinoma, immunohistochemically evaluated Bmi-1 expression was significantly higher in patients with advanced stages compared to those with lower stages.[140] In a study of 62 human patients with oligodendroglial tumors, high Bmi-1 protein expression was an indicator of poor prognosis.[141] Another study with 46 human patients with nasopharyngeal carcinoma, tumors negative for Bmi-1 had significantly higher 5-year survival rate than those with positive Bmi-1 protein expression.[142] Conversely, the same authors reported that high Bmi-1 protein expression in human tongue SCC was an indicator of better local tumor control after surgery (n=73).[143] The authors attributed the inconsistent results between studies to the different types of tumors.[143] In cats, a study showed that the Bmi-1 gene coding region and its protein sequence are 97% and 99% homologous to human gene and protein of Bmi-1, respectively.[144] Although Bmi-1 has been studied in relation to feline leukemia virus-induced malignancies, its role as a stem cell marker and a prognostic indicator in feline SCC has not been evaluated.[145-147]

Eukaryotic chromosomes are coiled to be stored efficiently in a nucleus by interacting with many proteins such as histone. DNA damage such as DSB is usually repaired quickly by appropriate repairing mechanisms; however, defective repair pathways can lead to many different types of chromosome and chromatid aberrations. The aberration is lethal when certain structures such as dicentrics and rings are formed. If the cell can survive or the aberration is not a lethal type, genetic information is often misplaced. The broken chromosome is often referred as ‘sticky end’ as this is easily inappropriately re-joined. In normal cells, however, the end of the chromosome is protected by a ‘cap’ that consists of many different types of proteins as well as special hexonuclear DNA sequences (5’-TTAGGG-3’ in humans) called telomeres. The telomeric DNA sequence is about 10-15 kb in length in humans and has a 3’ overhang.

Structurally, this 3' overhang loops back to the double-strand telomeric DNA with the help of telomere binding proteins such as TRF1 and TRF2 complexes.[148,149] In each cell division, cells lose up to 100 base pairs of telomeric DNA because the 5' end cannot be replicated efficiently by DNA polymerases during S phase of the cell cycle due to the end-replication problem.[149,150] When the telomere length becomes too short, normal cells lose proliferative ability and the cell goes into replicative senescence (Hayflick limit).[151] If the cell escapes senescence and continues proliferating, the telomere length becomes critically short and its protective cap is lost. This leads to inappropriate joining of chromosome ends and genetic instability.[149] In a normal cell, a DNA damage-sensing pathway is activated at this point to prevent further cell division and the cell undergoes apoptosis. However, there are at least two methods to maintain the telomere length so that the cell can continue proliferating. The first method is to activate a reverse transcriptase to elongate the telomeric sequence. This enzyme is called telomerase and consists of mainly two components; telomerase reverse transcriptase (TERT) and telomerase RNA component that acts as a template for telomere elongation.[149] Many normal tissues possess very weak or undetectable telomerase activity that may reside in normal stem cells.[152] The other method, called alternative lengthening of telomeres (ALT), utilizes recombination-based inter-chromosomal exchanges of telomere sequences.[153,154] It is not clear if these two methods are mutually exclusive, but approximately 90% of human cancers have been shown to express telomerase.[150] Specifically in human H&N SCC, telomerase activity was detected in 90-100% of clinical tumor samples whereas it was not detected in adjacent normal tissues.[152] Therefore, anti-telomerase therapy such as telomerase enzyme inhibitors and telomerase-targeted immunotherapy is a potential new therapeutic modality and many agents are currently under experimental and clinical investigation.[155] Knowledge about telomerase and telomere biology in feline malignancies is

scarce.[156,157] A previous study showed that cats also have telomere sequences at the end of their chromosomes.[158] Although a study evaluated telomere length in feline peripheral blood mononuclear cells, telomere length in feline cancer has not been investigated.[159] In feline oral SCC, one study reported that the only sample of feline oral SCC they evaluated was telomerase-positive.[156] We investigated the telomerase-activation status in our feline samples of oral SCC to obtain better knowledge in a larger cohort. In this evaluation, we utilized a new, improved method compared to more classical type of telomerase activity analysis which is called telomeric repeat-amplification protocol (TRAP) and involves polymerase chain reaction (PCR) and gel electrophoresis. On the other hand, our method utilized real-time quantitative PCR that allows us more accurate quantification.[160] Because the telomere is often referred to a biological clock, telomere length has been evaluated for its clinical role as a prognostic indicator, with ambiguous conclusions.[161] This has been evaluated using both tumor tissues and peripheral blood.[161-165] The most commonly used technique is a southern-blot based technique called terminal restriction fragments (TRF). Other methods include a flow cytometry-based technique (Flow-FISH) and slot-blot.[161] Evaluation of telomere length specifically in CSCs is of great importance if the CSC is the key cancer cell phenotype that has the greatest impact on treatment outcome. When a clinically obtained sample is used for TRF assay, different types of cells in the tumor sample such as tumor cells, inflammatory cells, and stromal cells are all homogenized together and then the DNA fragment samples are sorted by size via electrophoresis. The data obtained from this technique represents average telomere length among various cell types, since the ability to discriminate cell types via cell morphology is lost during homogenization. In 2002, Meeker et al. reported a novel method to evaluate telomere length only in the target cells (TELI-FISH).[166] With this method, target cells were labeled using immunofluorescence techniques and telomere

DNA was viewed by hybridizing telomere sequence-specific peptide nucleic acid. The study reported that telomere length obtained by TELI-FISH and TRF using cell lines (which did not include non-tumor cells) showed significant mutual correlation.[166] Since CD44 and Bmi-1 have been suggested as a CSC marker for human H&N SCC as described above, these two proteins are candidates for evaluation of prognostic significance as a putative CSC marker for feline oral SCC. In Chapter 6, the roles of CD44 and Bmi-1 protein expression levels and telomere length in the putative CSCs as a prognostic marker are evaluated.

^{18}F-FDG PET for delineation of possible tumoral regions.

CT is an essential imaging modality for the computerized XRT planning. CT images include not only information about disease extent, but also information about heterogeneous tissue proton density.[18] For example, bones have higher proton density, which attenuates more radiation whereas fat has lower proton density. This information is used to calculate attenuation of radiation dose. This might be particularly important for patients with feline oral SCC because this disease often involves bones such as the mandible and maxilla.[167] Sophisticated planning software and stereotactic verification provides the tools for selective radiation delivery. However this makes accurate identification of the target much more important. Identification of the tumor and surrounding normal tissue structures is dependent on the image interpretation by the attending radiation oncologists and radiologists. The gross tumor volume (GTV) is defined as volume where gross tumor can be identified.[18] This structure is then used as a template for additional tumor related structures. Of particular importance for SRT is the planning target volume (PTV). This takes into account any potential variation in position accuracy.[18] CT is the

most commonly used imaging modality to identify the GTV and this process relies on interpretation of changes such as mass-effect, contrast enhancement, and bone lysis. Magnetic resonance (MR) imaging is often used to help define intracranial tumors. MR does not provide tissue density information or distinct visualization of bony landmarks required for patient setup so the MR images are generally fused with a CT scan of the patient in the same position.[168]

Recently, a novel imaging modality, PET, has been introduced to veterinary medicine. Various compounds, depending on the intent of the study, are conjugated with a radioactive isotope and evaluated using emission tomography. During the same study the patients also are imaged with computed tomography and the images are fused. PET and CT image fusion allows for far better identification of the specific anatomic regions that are enhancing from positron emission. ^{18}F-FDG is the most commonly used compound in human and veterinary oncology.[169] ^{18}F-FDG is a glucose analog that enters into cells by cell-surface glucose transporters (GLUTs) and then undergoes phosphorylation by hexokinase.[170,171] The resultant compound, ^{18}F-FDG-6-phosphate, is a substrate of neither further glycolytic reactions nor glucose-6-phosphatase that removes the phosphate group. Therefore, ^{18}F-FDG-6-phosphate is metabolically trapped in the cell. While this compound stays in the cell, ^{18}F undergoes positron decay.[171] Emitted positrons undergo annihilation reactions, producing two 511 keV photons which travel in opposite directions. These annihilation photons collide with PET detectors and the data is processed to create a PET image. Therefore, ^{18}F-FDG PET provides a "map" of levels of glucose metabolism. This functional imaging is often interpreted alongside a CT image because the anatomical imaging from CT aids in localization of the ^{18}F-FDG-avid region. These two imaging modalities can be even fused and overlaid. However, there are some limitations of ^{18}F-FDG PET imaging. First, ^{18}F-FDG is not a cancer-specific tracer. This radioisotope compound is known to be taken

up not only by malignant cells, but also by inflammatory cells and various normal tissues with high glucose consumption such as brain, salivary gland, and cardiac muscle.[172] Second, in addition to the non-specificity of ^{18}F-FDG, there are multiple factors that affect FDG uptake in malignant cells. These include hypoxia, tumor perfusion, density of cancer cells, blood glucose and insulin concentrations, and hexokinase activity.[172] Third, the resolution of PET imaging is not as fine as CT or magnetic resonance imaging (MRI) images. While the resolution of CT and MRI images are known to be at millimeter (mm) or even sub-mm level, the current resolution of PET images is reported to be about 5 mm.[169]

Nevertheless, ^{18}F-FDG PET imaging has become an important tool for patient management in human oncology. The value of ^{18}F-FDG PET for tumor delineation for XRT planning has been evaluated,[173-179] and although conclusions from these studies are not consistent, ^{18}F-FDG PET imaging has impacted tumor delineation in patients with human H&N cancer.[175-179] Second, ^{18}F-FDG PET has improved staging of patients with human H&N cancer because of higher sensitivity for detection of cervical nodal status compared to CT/MRI.[180] Finally, ^{18}F-FDG PET imaging is now being used to evaluate treatment response.[181-187] A number of studies have concluded that ^{18}F-FDG PET combined with conventional imaging modalities such as CT or MRI can detect residual primary or nodal disease more accurately with higher sensitivity and specificity compared to CT or MRI alone.[181-185,187] In veterinary medicine, there are few reports utilizing ^{18}F-FDG PET, probably due to its lack of availability. No studies have evaluated its role in feline oral SCC. One goal of the work described here (Chapter 2) was to evaluate the impact of ^{18}F-FDG PET for delineation of GTV.

Accurate delivery of SRT to regional lymph nodes

Stereotactic radiation therapy is a novel technique that can spare normal surrounding tissues by avoidance. To do so, this technique requires higher accuracy in patient positioning and radiation delivery compared to fractionated XRT, where normal tissues are spared by delivering small doses per fraction. Intensity-modulation is also a major advancement in medical physics that allows us to create heterogeneous dose distribution and steep dose drop-off. Utilizing these technologies, SRT with intensity modulation is capable of treating tumors with higher dose while exposing surrounding normal tissues to lower dose. This allows the dose to be delivered in far fewer fractions (1-5) than conventional treatment, and acute radiation effects are minimized.

Prior to SRT, patients must first undergo imaging examination so a treatment plan can be created. CT imaging is often used because of the density information, although images can be fused with MR or PET studies to provide different information. When the patients then undergo SRT, they must be positioned as closely to the planning imaging as possible. For cyberknife treatment, fiducial markers are placed into the tumor before imaging, and these markers are used for stereotactic verification during treatment. For linear accelerator based systems, on-board imaging systems (OBI) are used so the tumor position can be verified using orthogonal kV x-rays or cone beam computed tomography (CBCT). Two different types of margins must be added to the GTV to account for inaccuracy in treatment administration.[18] The first margin, internal margin (IM), is to take into account errors caused by internal physiological movements and variation in shape, size, and position. Chest wall motion due to respiration is a good example of this type of error. Clinically, this type of error may be difficult to eliminate completely but can be minimized by using appropriate techniques such as suspending respiration. The other margin,

set-up margin (SM), is to take into account errors related to patient repositioning. For SRT, this particular type of margin has to be minimized by using any techniques to decrease the amount of surrounding non-tumoral regions that are included in PTV, which is the final target structure. These techniques include patient immobilization devices such as thermoplastic face mask and bite block and Vac-Lok type cushions. IM and SM will be added to the GTV to create the PTV. These two margins can be reduced further by utilizing imaging verification systems such as kV-imaging and cone-beam CT (CBCT). The kV-imaging is mainly used to align bony landmarks. In our institution, two orthogonal kV-images are obtained to align PTVs that are relatively immobile in respect to the bony anatomy, such as PTVs within the brain, nasal cavity, extremities, and vertebrae. CBCT is particularly useful for patients with more mobile tumors such as those in the thoracic or abdominal cavities. SRT requires one of these imaging modalities to verify patient positioning.

Tumors in the head region are good candidates for SRT because this region is accurately repositionable with appropriate devices and there are fewer organs undergoing physiological movement. Gamma knife, the very first SRT equipment, was specially designed for intracranial diseases.[188] Previous studies in human XRT have revealed that a PTV expansion of less than 2 mm is required by using a thermoplastic face mask and bite block and Vac-Lok vacuum bag for patients with tumors in the head region.[189,190] In veterinary XRT, previous studies utilizing bite-block type immobilization and have shown that accuracy of 2-3 mm can be achieved for repositioning patients with tumors in the head region.[191,192] Another study has shown that their immobilization device can reduce the PTV margin to 6-7 mm that has to be otherwise up to 10 mm with their system.[193] A different device was evaluated and 2 mm of PTV expansion for the treatment of the head region would be sufficient.[194]

As with the human tumors, malignancies in dogs and cats are known to spread loco-regionally and/or systemically. In the head region, canine oral melanoma, canine mast cell tumor, and canine tonsilar/sublingual squamous cell carcinoma are the most common diseases that spread through regional lymph nodes (LN).[167] In the head region, there are three main lymph centers; mandibular LNs, retropharyngeal LNs, and parotid LNs.[195] Among them, mandibular and retropharyngeal LNs are frequently considered as a "checkpoint" and evaluated due to their accessibility and drainage pattern. Radiation therapy is often used to treat these LNs prophylactically or when there is evidence of tumor metastasis. With fractionated XRT, an extensive PTV expansion is used to make sure these secondary targets are included in the field. In this treatment regimen, more normal tissue structures are included and this can result in increase of acute effects. However late effects, which are dose limiting, are minimized because of the sparing effects of fractionation. When using SRT, expansion of radiation field into normal tissues must be minimized. If these regional LNs are treated at the same time as the primary disease, accuracy of target positioning becomes an issue because the primary disease is geographically separated from these LNs. OBI allows for primary tumor verification using small PTV expansions. Re-positioning multiple targets at the same time is more difficult than re-positioning only a single target, and this is confounded by the fact that unlike the primary tumor, the regional nodes are not secured to bony anatomy and may require greater SM. The proximity of critical normal structures around these LNs such as esophagus, trachea, and skin prevent unlimited expansion of the SM. These normal structures can be a dose-limiting and overdosing leads to severe radiation-induced late toxicity. Therefore, knowing the variation in positioning of these LNs for a specific set of immobilization devices is critical so that these LNs can be included with minimal PTV expansions. The purpose of Chapter 3 was to evaluate accuracy and

precision of immobilization devices and to elucidate appropriate set-up PTV margins for secondary targets such as regional lymph nodes.

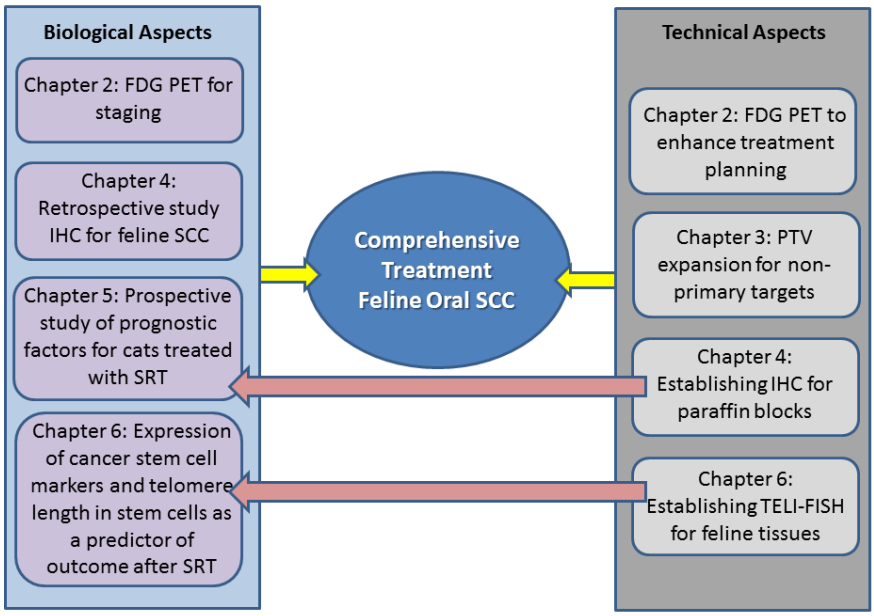

Figure 1.1: Overview and relationship of each study conducted in this comprehensive approach to feline oral SCC.

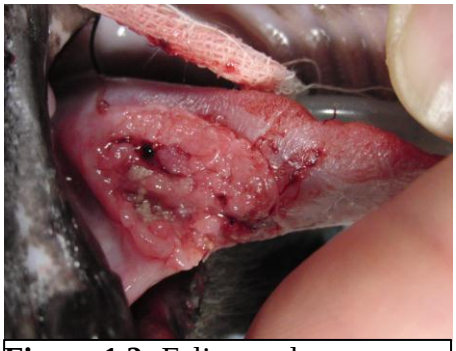

Figure 1.2: Feline oral squamous cell carcinoma in the ventral aspect of the tongue.

BIBLIOGRAPHY

1. Moore AS, Ogilvie GK. Tumors of the alimentary tract In: Stecher Y, ed. *Feline Oncology*: Veterinary Learning Systems, 2001;271-294.

2. Dorn CR, Taylor DO, Schneider R. Sunlight exposure and risk of developing cutaneous and oral squamous cell carcinomas in white cats. *J Natl Cancer Inst* 1971;46:1073-1078.

3. Dorn CR, Priester WA. Epidemiologic analysis of oral and pharyngeal cancer in dogs, cats, horses, and cattle. *J Am Vet Med Assoc* 1976;169:1202-1206.

4. Bertone ER, Snyder LA, Moore AS. Environmental and lifestyle risk factors for oral squamous cell carcinoma in domestic cats. *J Vet Intern Med* 2003;17:557-562.

5. Snyder LA, Bertone ER, Jakowski RM, et al. p53 expression and environmental tobacco smoke exposure in feline oral squamous cell carcinoma. *Vet Pathol* 2004;41:209-214.

6. Wypij JM, Fan TM, Fredrickson RL, et al. In vivo and in vitro efficacy of zoledronate for treating oral squamous cell carcinoma in cats. *J Vet Intern Med* 2008;22:158-163.

7. Martin CK, Werbeck JL, Thudi NK, et al. Zoledronic acid reduces bone loss and tumor growth in an orthotopic xenograft model of osteolytic oral squamous cell carcinoma. *Cancer Res* 2010;70:8607-8616.

8. Emms SG, Harvey CE. Preliminary results of maxillectomy in the dog and cat. *J Small Anim Pract* 1986;27:291-306.

9. Bostock DE. The prognosis in cats bearing squamous cell carcinoma. *J Small Anim Pract* 1972;13:119-125.

10. Hayes AM, Adams VJ, Scase TJ, et al. Survival of 54 cats with oral squamous cell carcinoma in United Kingdom general practice. *J Small Anim Pract* 2007;48:394-399.

11. Hutson CA, Willauer CC, Walder EJ, et al. Treatment of mandibular squamous cell carcinoma in cats by use of mandibulectomy and radiotherapy: seven cases (1987-1989). *J Am Vet Med Assoc* 1992;201:777-781.

12. Northrup NC, Selting KA, Rassnick KM, et al. Outcomes of cats with oral tumors treated with mandibulectomy: 42 cases. *J Am Anim Hosp Assoc* 2006;42:350-360.

13. Bregazzi VS, LaRue SM, Powers BE, et al. Response of feline oral squamous cell carcinoma to palliative radiation therapy. *Vet Radiol Ultrasound* 2001;42:77-79.

14. Fidel J, Lyons J, Tripp C, et al. Treatment of oral squamous cell carcinoma with accelerated radiation therapy and concomitant carboplatin in cats. *J Vet Intern Med* 2011;25:504-510.

15. Fidel JL, Sellon RK, Houston RK, et al. A nine-day accelerated radiation protocol for feline squamous cell carcinoma. *Vet Radiol Ultrasound* 2007;48:482-485.

16. Marconato L, Buchholz J, Keller M, et al. Multimodal therapeutic approach and interdisciplinary challenge for the treatment of unresectable head and neck squamous cell carcinoma in six cats: a pilot study. *Vet Comp Oncol* 2012.

17. Teo SK. Properties of thalidomide and its analogues: implications for anticancer therapy. *AAPS J* 2005;7:E14-19.

18. Khan F. Treatment planning I: Isodose distributions. *The physics of radiation therapy*. 3rd ed. Philadelphia: Lippincott Williams & Wilkins, 2003;199-227.

19. Hall E, Giaccia A. Clinical response of normal tissues. *Radiobiology for the radiologist*. 6th ed, 2006;327-348.

20. Kondziolka D, Lunsford LD. Stereotactic radiosurgery for squamous cell carcinoma of the nasopharynx. *Laryngoscope* 1991;101:519-522.

21. Kawaguchi K, Yamada H, Horie A, et al. Radiosurgical treatment of maxillary squamous cell carcinoma. *Int J Oral Maxillofac Surg* 2009;38:1205-1207.

22. Siddiqui F, Patel M, Khan M, et al. Stereotactic body radiation therapy for primary, recurrent, and metastatic tumors in the head-and-neck region. *Int J Radiat Oncol Biol Phys* 2009;74:1047-1053.

23. Kodani N, Yamazaki H, Tsubokura T, et al. Stereotactic body radiation therapy for head and neck tumor: disease control and morbidity outcomes. *J Radiat Res* 2011;52:24-31.

24. Coomer A, Farese J, Milner R, et al. Radiation therapy for canine appendicular osteosarcoma. *Vet Comp Oncol* 2009;7:15-27.

25. Farese JP, Milner R, Thompson MS, et al. Stereotactic radiosurgery for treatment of osteosarcomas involving the distal portions of the limbs in dogs. *J Am Vet Med Assoc* 2004;225:1567-1572, 1548.

26. Fuks Z, Kolesnick R. Engaging the vascular component of the tumor response. *Cancer Cell* 2005;8:89-91.

27. Garcia-Barros M, Paris F, Cordon-Cardo C, et al. Tumor response to radiotherapy regulated by endothelial cell apoptosis. *Science* 2003;300:1155-1159.

28. Park HJ, Griffin RJ, Hui S, et al. Radiation-Induced Vascular Damage in Tumors: Implications of Vascular Damage in Ablative Hypofractionated Radiotherapy (SBRT and SRS). *Radiat Res* 2012;177:311-327.

29. Scholzen T, Gerdes J. The Ki-67 protein: from the known and the unknown. *J Cell Physiol* 2000;182:311-322.

30. Heidebrecht HJ, Buck F, Haas K, et al. Monoclonal antibodies Ki-S3 and Ki-S5 yield new data on the 'Ki-67' proteins. *Cell Prolif* 1996;29:413-425.

31. Schluter C, Duchrow M, Wohlenberg C, et al. The cell proliferation-associated antigen of antibody Ki-67: a very large, ubiquitous nuclear protein with numerous repeated elements, representing a new kind of cell cycle-maintaining proteins. *J Cell Biol* 1993;123:513-522.

32. Starborg M, Gell K, Brundell E, et al. The murine Ki-67 cell proliferation antigen accumulates in the nucleolar and heterochromatic regions of interphase cells and at the periphery of the mitotic chromosomes in a process essential for cell cycle progression. *J Cell Sci* 1996;109 (Pt 1):143-153.

33. Raybaud-Diogene H, Fortin A, Morency R, et al. Markers of radioresistance in squamous cell carcinomas of the head and neck: a clinicopathologic and immunohistochemical study. *J Clin Oncol* 1997;15:1030-1038.

34. Liu M, Lawson G, Delos M, et al. Prognostic value of cell proliferation markers, tumour suppressor proteins and cell adhesion molecules in primary squamous cell carcinoma of the larynx and hypopharynx. *Eur Arch Otorhinolaryngol* 2003;260:28-34.

35. Acikalin MF, Oner U, Tel N, et al. Prognostic significance of Ki-67 expression for patients with laryngeal squamous cell carcinoma primarily treated by total laryngectomy. *Eur Arch Otorhinolaryngol* 2004;261:376-380.

36. Abadie JJ, Amardeilh MA, Delverdier ME. Immunohistochemical detection of proliferating cell nuclear antigen and Ki-67 in mast cell tumors from dogs. *J Am Vet Med Assoc* 1999;215:1629-1634.

37. Pena LL, Nieto AI, Perez-Alenza D, et al. Immunohistochemical detection of Ki-67 and PCNA in canine mammary tumors: relationship to clinical and pathologic variables. *J Vet Diagn Invest* 1998;10:237-246.

38. Phillips BS, Kass PH, Naydan DK, et al. Apoptotic and proliferation indexes in canine lymphoma. *J Vet Diagn Invest* 2000;12:111-117.

39. Yerushalmi R, Woods R, Ravdin PM, et al. Ki67 in breast cancer: prognostic and predictive potential. *Lancet Oncol* 2010;11:174-183.

40. Melzer K, Guscetti F, Rohrer Bley C, et al. Ki67 reactivity in nasal and periocular squamous cell carcinomas in cats treated with electron beam radiation therapy. *J Vet Intern Med* 2006;20:676-681.

41. Bergkvist GT, Argyle DJ, Morrison L, et al. Expression of epidermal growth factor receptor (EGFR) and Ki67 in feline oral squamous cell carcinomas (FOSCC). *Vet Comp Oncol* 2011;9:106-117.

42. Sealy R, Immerman A, Shepstone B. Mitotic index in human squamous cell carcinoma. *Acta Radiol Ther Phys Biol* 1972;11:59-64.

43. Smilek P, Dusek L, Vesely K, et al. Prognostic significance of mitotic and apoptotic index and the DNA cytometry in head and neck cancer. *Neoplasma* 2005;52:199-207.

44. Kamoi S, Ohaki Y, Amano Y, et al. Pre-treatment mitotic index versus computer-quantitated Ki-67 nuclear antigen labeling index as predictors of response to neoadjuvant chemotherapy in uterine cervical carcinoma. *J Nippon Med Sch* 2003;70:219-226.

45. Rudolph P, Peters J, Lorenz D, et al. Correlation between mitotic and Ki-67 labeling indices in paraffin-embedded carcinoma specimens. *Hum Pathol* 1998;29:1216-1222.

46. Sarbia M, Bittinger F, Porschen R, et al. The prognostic significance of tumour cell proliferation in squamous cell carcinomas of the oesophagus. *Br J Cancer* 1996;74:1012-1016.

47. Nakano T, Oka K, Ishikawa A, et al. Immunohistochemical prediction of radiation response and local control in radiation therapy for cervical cancer. *Cancer Detect Prev* 1998;22:120-128.

48. Gasinska A, Urbanski K, Gruchala A, et al. A ratio of apoptosis to mitosis, proliferation pattern and prediction of radiotherapy response in cervical carcinoma. *Neoplasma* 2002;49:379-386.

49. Hirvikoski P, Kumpulainen E, Virtaniemi J, et al. p53 expression and cell proliferation as prognostic factors in laryngeal squamous cell carcinoma. *J Clin Oncol* 1997;15:3111-3120.

50. Imai Y, Sasaki T, Fujibayashi T. Volume-corrected mitotic index as a prognostic factor in oral squamous cell carcinomas. *Oral Oncol* 2001;37:72-76.

51. Tomasino RM, Daniele E, Bazan V, et al. Prognostic significance of cell kinetics in laryngeal squamous cell carcinoma: clinicopathological associations. *Cancer Res* 1995;55:6103-6108.

52. Kraxner H, Tamas L, Jaray B, et al. Search for prognostic factors in head and neck cancer. *Acta Otolaryngol Suppl* 1997;527:145-149.

53. McGill MA, McGlade CJ. Cellular signaling In: Strauss M,Watt M, eds. *The basic science of oncology*. 4th ed. New York: McGraw-Hill, Medical Pub. Division, 2005;142-166.

54. Baumann M, Krause M. Targeting the epidermal growth factor receptor in radiotherapy: radiobiological mechanisms, preclinical and clinical results. *Radiother Oncol* 2004;72:257-266.

55. Herbst RS. Review of epidermal growth factor receptor biology. *Int J Radiat Oncol Biol Phys* 2004;59:21-26.

56. Zips D, Krause M, Yaromina A, et al. Epidermal growth factor receptor inhibitors for radiotherapy: biological rationale and preclinical results. *J Pharm Pharmacol* 2008;60:1019-1028.

57. Arteaga CL. Epidermal growth factor receptor dependence in human tumors: more than just expression? *Oncologist* 2002;7 Suppl 4:31-39.

58. Weinberg R. Growth factors and their receptors. *The biology of cancer*: Garland Science, Taylor & Francis Group, 2007;119-158.

59. Rubin Grandis J, Melhem MF, Barnes EL, et al. Quantitative immunohistochemical analysis of transforming growth factor-alpha and epidermal growth factor receptor in patients with squamous cell carcinoma of the head and neck. *Cancer* 1996;78:1284-1292.

60. Grandis JR, Tweardy DJ. TGF-alpha and EGFR in head and neck cancer. *J Cell Biochem Suppl* 1993;17F:188-191.

61. Grandis JR, Tweardy DJ. Elevated levels of transforming growth factor alpha and epidermal growth factor receptor messenger RNA are early markers of carcinogenesis in head and neck cancer. *Cancer Res* 1993;53:3579-3584.

62. Russell JS, Colevas AD. The use of epidermal growth factor receptor monoclonal antibodies in squamous cell carcinoma of the head and neck. *Chemother Res Pract* 2012;2012:761518.

63. Langer CJ. Exploring biomarkers in head and neck cancer. *Cancer* 2012;118:3882-3892.

64. Ang KK, Berkey BA, Tu X, et al. Impact of epidermal growth factor receptor expression on survival and pattern of relapse in patients with advanced head and neck carcinoma. *Cancer Res* 2002;62:7350-7356.

65. Looper JS, Malarkey DE, Ruslander D, et al. Epidermal growth factor receptor expression in feline oral squamous cell carcinomas. *Vet Comp Oncol* 2006;4:33-40.

66. Bergkvist GT, Argyle DJ, Pang LY, et al. Studies on the inhibition of feline EGFR in squamous cell carcinoma: enhancement of radiosensitivity and rescue of resistance to small molecule inhibitors. *Cancer Biol Ther* 2011;11:927-937.

67. Bergers G, Benjamin LE. Tumorigenesis and the angiogenic switch. *Nat Rev Cancer* 2003;3:401-410.

68. Dvorak HF. Tumors: wounds that do not heal. Similarities between tumor stroma generation and wound healing. *N Engl J Med* 1986;315:1650-1659.

69. Weinberg R. p53 and apoptosis: master gurdian and executioner. *The biology of cancer*: Garland Science, Taylor & Francis Group 2007;307-356.

70. Tannehill-Gregg SH, Levine AL, Rosol TJ. Feline head and neck squamous cell carcinoma: a natural model for the human disease and development of a mouse model. *Vet Comp Oncol* 2006;4:84-97.

71. Sironi G, Riccaboni P, Mertel L, et al. p53 protein expression in conjunctival squamous cell carcinomas of domestic animals. *Vet Ophthalmol* 1999;2:227-231.

72. Ellis LM, Hicklin DJ. VEGF-targeted therapy: mechanisms of anti-tumour activity. *Nat Rev Cancer* 2008;8:579-591.

73. Kerbel RS, Kamen BA. The anti-angiogenic basis of metronomic chemotherapy. *Nat Rev Cancer* 2004;4:423-436.

74. Bozec A, Formento P, Ciccolini J, et al. Response of endothelial cells to a dual tyrosine kinase receptor inhibition combined with irradiation. *Mol Cancer Ther* 2005;4:1962-1971.

75. Schor AM, Pendleton N, Pazouki S, et al. Assessment of vascularity in histological sections: effects of methodology and value as an index of angiogenesis in breast tumours. *Histochem J* 1998;30:849-856.

76. Erovic BM, Neuchrist C, Berger U, et al. Quantitation of microvessel density in squamous cell carcinoma of the head and neck by computer-aided image analysis. *Wien Klin Wochenschr* 2005;117:53-57.

77. Weidner N. Current pathologic methods for measuring intratumoral microvessel density within breast carcinoma and other solid tumors. *Breast Cancer Res Treat* 1995;36:169-180.

78. Koukourakis MI, Giatromanolaki A, Sivridis E, et al. Cancer vascularization: implications in radiotherapy? *Int J Radiat Oncol Biol Phys* 2000;48:545-553.

79. Weidner N, Folkman J, Pozza F, et al. Tumor angiogenesis: a new significant and independent prognostic indicator in early-stage breast carcinoma. *J Natl Cancer Inst* 1992;84:1875-1887.

80. Lovey J, Lukits J, Remenar E, et al. Antiangiogenic effects of radiotherapy but not initial microvessel density predict survival in inoperable oropharyngeal squamous cell carcinoma. *Strahlenther Onkol* 2006;182:149-156.

81. Weinberg R. Dialogue replaces monologue: heterotypic interactions and the biology of angiogenesis. *The biology of cancer*: Garland Science, Taylor & Francis Group, 2007;527-586.

82. Hall E, Giaccia A. Oxygen effect and reoxygenation. *Radiobiology for the radiologist*. 6th ed, 2006;85-105.

83. Hockel M, Schlenger K, Hockel S, et al. Hypoxic cervical cancers with low apoptotic index are highly aggressive. *Cancer Res* 1999;59:4525-4528.

84. Graeber TG, Osmanian C, Jacks T, et al. Hypoxia-mediated selection of cells with diminished apoptotic potential in solid tumours. *Nature* 1996;379:88-91.

85. Thomlinson RH, Gray LH. The histological structure of some human lung cancers and the possible implications for radiotherapy. *Br J Cancer* 1955;9:539-549.

86. Griffiths JR, Robinson SP. The OxyLite: a fibre-optic oxygen sensor. *Br J Radiol* 1999;72:627-630.

87. Terris DJ, Dunphy EP. Oxygen tension measurements of head and neck cancers. *Arch Otolaryngol Head Neck Surg* 1994;120:283-287.

88. Nordsmark M, Bentzen SM, Rudat V, et al. Prognostic value of tumor oxygenation in 397 head and neck tumors after primary radiation therapy. An international multi-center study. *Radiother Oncol* 2005;77:18-24.

89. Nordsmark M, Overgaard M, Overgaard J. Pretreatment oxygenation predicts radiation response in advanced squamous cell carcinoma of the head and neck. *Radiother Oncol* 1996;41:31-39.

90. Brizel DM, Sibley GS, Prosnitz LR, et al. Tumor hypoxia adversely affects the prognosis of carcinoma of the head and neck. *Int J Radiat Oncol Biol Phys* 1997;38:285-289.

91. Fyles A, Milosevic M, Hedley D, et al. Tumor hypoxia has independent predictor impact only in patients with node-negative cervix cancer. *J Clin Oncol* 2002;20:680-687.

92. Knocke TH, Weitmann HD, Feldmann HJ, et al. Intratumoral pO2-measurements as predictive assay in the treatment of carcinoma of the uterine cervix. *Radiother Oncol* 1999;53:99-104.

93. Milosevic M, Fyles A, Hedley D, et al. The human tumor microenvironment: invasive (needle) measurement of oxygen and interstitial fluid pressure. *Semin Radiat Oncol* 2004;14:249-258.

94. Lyng H, Sundfor K, Trope C, et al. Disease control of uterine cervical cancer: relationships to tumor oxygen tension, vascular density, cell density, and frequency of mitosis and apoptosis measured before treatment and during radiotherapy. *Clin Cancer Res* 2000;6:1104-1112.

95. Nordsmark M, Overgaard J. A confirmatory prognostic study on oxygenation status and loco-regional control in advanced head and neck squamous cell carcinoma treated by radiation therapy. *Radiother Oncol* 2000;57:39-43.

96. Stadler P, Becker A, Feldmann HJ, et al. Influence of the hypoxic subvolume on the survival of patients with head and neck cancer. *Int J Radiat Oncol Biol Phys* 1999;44:749-754.

97. Brizel DM, Dodge RK, Clough RW, et al. Oxygenation of head and neck cancer: changes during radiotherapy and impact on treatment outcome. *Radiother Oncol* 1999;53:113-117.

98. Seddon BM, Honess DJ, Vojnovic B, et al. Measurement of tumor oxygenation: in vivo comparison of a luminescence fiber-optic sensor and a polarographic electrode in the p22 tumor. *Radiat Res* 2001;155:837-846.

99. Wen B, Urano M, Humm JL, et al. Comparison of Helzel and OxyLite systems in the measurements of tumor partial oxygen pressure (pO2). *Radiat Res* 2008;169:67-75.

100. Dunst J, Hansgen G, Lautenschlager C, et al. Oxygenation of cervical cancers during radiotherapy and radiotherapy + cis-retinoic acid/interferon. *Int J Radiat Oncol Biol Phys* 1999;43:367-373.

101. Weinberg R. Multi-step tumorigenesis. *The biology of cancer*: Garland Science, Taylor & Francis Group, 2007;399-462.

102. Lapidot T, Sirard C, Vormoor J, et al. A cell initiating human acute myeloid leukaemia after transplantation into SCID mice. *Nature* 1994;367:645-648.

103. Shay JW, Wright WE. Telomeres and telomerase in normal and cancer stem cells. *FEBS Lett* 2010;584:3819-3825.

104. Wang J, Sakariassen PO, Tsinkalovsky O, et al. CD133 negative glioma cells form tumors in nude rats and give rise to CD133 positive cells. *Int J Cancer* 2008;122:761-768.

105. Singh SK, Clarke ID, Terasaki M, et al. Identification of a cancer stem cell in human brain tumors. *Cancer Res* 2003;63:5821-5828.

106. Chen YC, Chang CJ, Hsu HS, et al. Inhibition of tumorigenicity and enhancement of radiochemosensitivity in head and neck squamous cell cancer-derived ALDH1-positive cells by knockdown of Bmi-1. *Oral Oncol* 2010;46:158-165.

107. Diehn M, Cho RW, Lobo NA, et al. Association of reactive oxygen species levels and radioresistance in cancer stem cells. *Nature* 2009;458:780-783.

108. Tabor MH, Clay MR, Owen JH, et al. Head and neck cancer stem cells: the side population. *Laryngoscope* 2011;121:527-533.

109. Pang LY, Blacking TM, Else RW, et al. Feline mammary carcinoma stem cells are tumorigenic, radioresistant, chemoresistant and defective in activation of the ATM/p53 DNA damage pathway. *Vet J* 2012.

110. Pang LY, Bergkvist GT, Cervantes-Arias A, et al. Identification of tumour initiating cells in feline head and neck squamous cell carcinoma and evidence for gefitinib induced epithelial to mesenchymal transition. *Vet J* 2012;193:46-52.

111. Prince ME, Sivanandan R, Kaczorowski A, et al. Identification of a subpopulation of cells with cancer stem cell properties in head and neck squamous cell carcinoma. *Proc Natl Acad Sci U S A* 2007;104:973-978.

112. Goodison S, Urquidi V, Tarin D. CD44 cell adhesion molecules. *Mol Pathol* 1999;52:189-196.

113. Oliveira DT, Odell EW. Expression of CD44 variant exons by normal oral epithelia. *Oral Oncol* 1997;33:260-262.

114. Assimakopoulos D, Kolettas E, Patrikakos G, et al. The role of CD44 in the development and prognosis of head and neck squamous cell carcinomas. *Histol Histopathol* 2002;17:1269-1281.

115. Fox SB, Fawcett J, Jackson DG, et al. Normal human tissues, in addition to some tumors, express multiple different CD44 isoforms. *Cancer Res* 1994;54:4539-4546.

116. Brunner TB, Kunz-Schughart LA, Grosse-Gehling P, et al. Cancer stem cells as a predictive factor in radiotherapy. *Semin Radiat Oncol* 2012;22:151-174.

117. Bourguignon LY, Earle C, Wong G, et al. Stem cell marker (Nanog) and Stat-3 signaling promote MicroRNA-21 expression and chemoresistance in hyaluronan/CD44-activated head and neck squamous cell carcinoma cells. *Oncogene* 2012;31:149-160.

118. Bourguignon LY, Peyrollier K, Xia W, et al. Hyaluronan-CD44 interaction activates stem cell marker Nanog, Stat-3-mediated MDR1 gene expression, and ankyrin-regulated multidrug efflux in breast and ovarian tumor cells. *J Biol Chem* 2008;283:17635-17651.

119. Wang SJ, Bourguignon LY. Role of hyaluronan-mediated CD44 signaling in head and neck squamous cell carcinoma progression and chemoresistance. *Am J Pathol* 2011;178:956-963.

120. de Jong MC, Pramana J, van der Wal JE, et al. CD44 expression predicts local recurrence after radiotherapy in larynx cancer. *Clin Cancer Res* 2010;16:5329-5338.

121. Joshua B, Kaplan MJ, Doweck I, et al. Frequency of cells expressing CD44, a head and neck cancer stem cell marker: correlation with tumor aggressiveness. *Head Neck* 2012;34:42-49.

122. Kokko LL, Hurme S, Maula SM, et al. Significance of site-specific prognosis of cancer stem cell marker CD44 in head and neck squamous-cell carcinoma. *Oral Oncol* 2011;47:510-516.

123. Uwa N, Kataoka TR, Torii I, et al. CD44 expression is related to poor prognosis of hypopharyngeal squamous cell carcinoma. *Acta Otolaryngol* 2011;131:323-329.

124. Gonzalez-Moles MA, Bravo M, Ruiz-Avila I, et al. Adhesion molecule CD44 as a prognostic factor in tongue cancer. *Anticancer Res* 2003;23:5197-5202.

125. Rodriguez-Rodriguez L, Sancho-Torres I, Mesonero C, et al. The CD44 receptor is a molecular predictor of survival in ovarian cancer. *Med Oncol* 2003;20:255-263.

126. Barbieri F, Wurth R, Ratto A, et al. Isolation of stem-like cells from spontaneous feline mammary carcinomas: phenotypic characterization and tumorigenic potential. *Exp Cell Res* 2012;318:847-860.

127. Gieni RS, Ismail IH, Campbell S, et al. Polycomb group proteins in the DNA damage response: a link between radiation resistance and "stemness". *Cell Cycle* 2011;10:883-894.

128. Cao L, Bombard J, Cintron K, et al. BMI1 as a novel target for drug discovery in cancer. *J Cell Biochem* 2011;112:2729-2741.

129. Lee K, Adhikary G, Balasubramanian S, et al. Expression of Bmi-1 in epidermis enhances cell survival by altering cell cycle regulatory protein expression and inhibiting apoptosis. *J Invest Dermatol* 2008;128:9-17.

130. Siddique HR, Saleem M. Role of BMI1, a stem cell factor, in cancer recurrence and chemoresistance: preclinical and clinical evidences. *Stem Cells* 2012;30:372-378.

131. Liu S, Dontu G, Mantle ID, et al. Hedgehog signaling and Bmi-1 regulate self-renewal of normal and malignant human mammary stem cells. *Cancer Res* 2006;66:6063-6071.

132. Dimri GP, Martinez JL, Jacobs JJ, et al. The Bmi-1 oncogene induces telomerase activity and immortalizes human mammary epithelial cells. *Cancer Res* 2002;62:4736-4745.

133. Reinisch CM, Uthman A, Erovic BM, et al. Expression of BMI-1 in normal skin and inflammatory and neoplastic skin lesions. *J Cutan Pathol* 2007;34:174-180.

134. Umar S. Intestinal stem cells. *Curr Gastroenterol Rep* 2010;12:340-348.

135. Claudinot S, Nicolas M, Oshima H, et al. Long-term renewal of hair follicles from clonogenic multipotent stem cells. *Proc Natl Acad Sci U S A* 2005;102:14677-14682.

136. Raaphorst FM, van Kemenade FJ, Fieret E, et al. Cutting edge: polycomb gene expression patterns reflect distinct B cell differentiation stages in human germinal centers. *J Immunol* 2000;164:1-4.

137. Liu L, Andrews LG, Tollefsbol TO. Loss of the human polycomb group protein BMI1 promotes cancer-specific cell death. *Oncogene* 2006;25:4370-4375.

138. Wang E, Bhattacharyya S, Szabolcs A, et al. Enhancing chemotherapy response with Bmi-1 silencing in ovarian cancer. *PLoS One* 2011;6:e17918.

139. Bommi PV, Dimri M, Sahasrabuddhe AA, et al. The polycomb group protein BMI1 is a transcriptional target of HDAC inhibitors. *Cell Cycle* 2010;9:2663-2673.

140. Vrzalikova K, Skarda J, Ehrmann J, et al. Prognostic value of Bmi-1 oncoprotein expression in NSCLC patients: a tissue microarray study. *J Cancer Res Clin Oncol* 2008;134:1037-1042.

141. Hayry V, Tynninen O, Haapasalo HK, et al. Stem cell protein BMI-1 is an independent marker for poor prognosis in oligodendroglial tumours. *Neuropathol Appl Neurobiol* 2008;34:555-563.

142. Song LB, Zeng MS, Liao WT, et al. Bmi-1 is a novel molecular marker of nasopharyngeal carcinoma progression and immortalizes primary human nasopharyngeal epithelial cells. *Cancer Res* 2006;66:6225-6232.

143. Hayry V, Makinen LK, Atula T, et al. Bmi-1 expression predicts prognosis in squamous cell carcinoma of the tongue. *Br J Cancer* 2010;102:892-897.

144. Kinnon S, Fulton R. Nucleotide sequence of the feline Bmi-1 coding region. *DNA Seq* 1999;10:335-338.

145. Fujino Y, Ohno K, Tsujimoto H. Molecular pathogenesis of feline leukemia virus-induced malignancies: insertional mutagenesis. *Vet Immunol Immunopathol* 2008;123:138-143.

146. Tsatsanis C, Fulton R, Nishigaki K, et al. Genetic determinants of feline leukemia virus-induced lymphoid tumors: patterns of proviral insertion and gene rearrangement. *J Virol* 1994;68:8296-8303.

147. Levy LS, Lobelle-Rich PA, Overbaugh J, et al. Coincident involvement of flvi-2, c-myc, and novel env genes in natural and experimental lymphosarcomas induced by feline leukemia virus. *Virology* 1993;196:892-895.

148. Griffith JD, Comeau L, Rosenfield S, et al. Mammalian telomeres end in a large duplex loop. *Cell* 1999;97:503-514.

149. Blasco MA. Telomeres and human disease: ageing, cancer and beyond. *Nat Rev Genet* 2005;6:611-622.

150. Weinberg R. Eternal life: Cell immortalization and tumorigenesis. *The biology of cancer*: Garland Science, Taylor & Francis Group 2007;357-398.

151. Weaver RF. DNA replication II: detailed mechanism In: Reidy PE, ed. *Molecular biology*. 4th ed ed. New York: Roerig-Blong, J., 2008;684-717.

152. Mao L, El-Naggar AK, Fan YH, et al. Telomerase activity in head and neck squamous cell carcinoma and adjacent tissues. *Cancer Res* 1996;56:5600-5604.

153. Hanahan D, Weinberg RA. The hallmarks of cancer. *Cell* 2000;100:57-70.

154. Bryan TM, Englezou A, Gupta J, et al. Telomere elongation in immortal human cells without detectable telomerase activity. *EMBO J* 1995;14:4240-4248.

155. Harley CB. Telomerase and cancer therapeutics. *Nat Rev Cancer* 2008;8:167-179.

156. Cadile CD, Kitchell BE, Biller BJ, et al. Telomerase activity as a marker for malignancy in feline tissues. *Am J Vet Res* 2001;62:1578-1581.

157. McKevitt TP, Nasir L, Wallis CV, et al. A cohort study of telomere and telomerase biology in cats. *Am J Vet Res* 2003;64:1496-1499.

158. Hirota J, Usui R, Satoh T, et al. Telomere position on the cat chromosome. *J Vet Med Sci* 1996;58:1025-1026.

159. Brummendorf TH, Mak J, Sabo KM, et al. Longitudinal studies of telomere length in feline blood cells: implications for hematopoietic stem cell turnover in vivo. *Exp Hematol* 2002;30:1147-1152.

160. Herbert BS, Hochreiter AE, Wright WE, et al. Nonradioactive detection of telomerase activity using the telomeric repeat amplification protocol. *Nat Protoc* 2006;1:1583-1590.

161. Svenson U, Roos G. Telomere length as a biological marker in malignancy. *Biochim Biophys Acta* 2009;1792:317-323.

162. Sakoff JA, De Waal E, Garg MB, et al. Telomere length in haemopoietic stem cells can be determined from that of mononuclear blood cells or whole blood. *Leuk Lymphoma* 2002;43:2017-2020.

163. Barwell J, Pangon L, Georgiou A, et al. Is telomere length in peripheral blood lymphocytes correlated with cancer susceptibility or radiosensitivity? *Br J Cancer* 2007;97:1696-1700.

164. Svenson U, Ljungberg B, Roos G. Telomere length in peripheral blood predicts survival in clear cell renal cell carcinoma. *Cancer Res* 2009;69:2896-2901.

165. Svenson U, Nordfjall K, Stegmayr B, et al. Breast cancer survival is associated with telomere length in peripheral blood cells. *Cancer Res* 2008;68:3618-3623.

166. Meeker AK, Gage WR, Hicks JL, et al. Telomere length assessment in human archival tissues: combined telomere fluorescence in situ hybridization and immunostaining. *Am J Pathol* 2002;160:1259-1268.

167. Liptak JM, SJ W. Cancer of the gastrointestinal tract In: Withrow SJ,DM V, eds. *Small Animal Clinical Oncology*, 2007;455-435.

168. LJ F, SL K. Imaging in oncology In: Withrow SJ, DM V,RL P, eds. *Small Animal Clinical Oncology*. 5th ed, 2013;98-110.

169. Lawrence J, Rohren E, Provenzale J. PET/CT today and tomorrow in veterinary cancer diagnosis and monitoring: fundamentals, early results and future perspectives. *Vet Comp Oncol* 2010;8:163-187.

170. Workman RBJ, Coleman RE. Fundamentals of PET and PET/CT imaging In: Workman RBJ,Coleman RE, eds. *PET/CT essentials for clinical practice*. New York: Springer, 2006;1-22.

171. Basu S, Kwee TC, Surti S, et al. Fundamentals of PET and PET/CT imaging. *Ann N Y Acad Sci* 2011;1228:1-18.

172. Vallabhajosula S. (18)F-labeled positron emission tomographic radiopharmaceuticals in oncology: an overview of radiochemistry and mechanisms of tumor localization. *Semin Nucl Med* 2007;37:400-419.

173. Scarfone C, Lavely WC, Cmelak AJ, et al. Prospective feasibility trial of radiotherapy target definition for head and neck cancer using 3-dimensional PET and CT imaging. *J Nucl Med* 2004;45:543-552.

174. Nishioka T, Shiga T, Shirato H, et al. Image fusion between 18FDG-PET and MRI/CT for radiotherapy planning of oropharyngeal and nasopharyngeal carcinomas. *Int J Radiat Oncol Biol Phys* 2002;53:1051-1057.

175. Ciernik IF, Dizendorf E, Baumert BG, et al. Radiation treatment planning with an integrated positron emission and computer tomography (PET/CT): a feasibility study. *Int J Radiat Oncol Biol Phys* 2003;57:853-863.

176. Leong T, Everitt C, Yuen K, et al. A prospective study to evaluate the impact of FDG-PET on CT-based radiotherapy treatment planning for oesophageal cancer. *Radiother Oncol* 2006;78:254-261.

177. Schinagl DA, Vogel WV, Hoffmann AL, et al. Comparison of five segmentation tools for 18F-fluoro-deoxy-glucose-positron emission tomography-based target volume definition in head and neck cancer. *Int J Radiat Oncol Biol Phys* 2007;69:1282-1289.

178. Daisne JF, Duprez T, Weynand B, et al. Tumor volume in pharyngolaryngeal squamous cell carcinoma: comparison at CT, MR imaging, and FDG PET and validation with surgical specimen. *Radiology* 2004;233:93-100.

179. Paulino AC, Koshy M, Howell R, et al. Comparison of CT- and FDG-PET-defined gross tumor volume in intensity-modulated radiotherapy for head-and-neck cancer. *Int J Radiat Oncol Biol Phys* 2005;61:1385-1392.

180. Ng SH, Yen TC, Liao CT, et al. 18F-FDG PET and CT/MRI in oral cavity squamous cell carcinoma: a prospective study of 124 patients with histologic correlation. *J Nucl Med* 2005;46:1136-1143.

181. Kitagawa Y, Nishizawa S, Sano K, et al. Prospective comparison of 18F-FDG PET with conventional imaging modalities (MRI, CT, and 67Ga scintigraphy) in assessment of combined intraarterial chemotherapy and radiotherapy for head and neck carcinoma. *J Nucl Med* 2003;44:198-206.

182. Menda Y, Graham MM. Update on 18F-fluorodeoxyglucose/positron emission tomography and positron emission tomography/computed tomography imaging of squamous head and neck cancers. *Semin Nucl Med* 2005;35:214-219.

183. Andrade RS, Heron DE, Degirmenci B, et al. Posttreatment assessment of response using FDG-PET/CT for patients treated with definitive radiation therapy for head and neck cancers. *Int J Radiat Oncol Biol Phys* 2006;65:1315-1322.

184. Goerres GW, Schmid DT, Bandhauer F, et al. Positron emission tomography in the early follow-up of advanced head and neck cancer. *Arch Otolaryngol Head Neck Surg* 2004;130:105-109; discussion 120-101.

185. Ong SC, Schoder H, Lee NY, et al. Clinical utility of 18F-FDG PET/CT in assessing the neck after concurrent chemoradiotherapy for Locoregional advanced head and neck cancer. *J Nucl Med* 2008;49:532-540.

186. Schoder H, Fury M, Lee N, et al. PET monitoring of therapy response in head and neck squamous cell carcinoma. *J Nucl Med* 2009;50 Suppl 1:74S-88S.

187. Kostakoglu L, Goldsmith SJ. PET in the assessment of therapy response in patients with carcinoma of the head and neck and of the esophagus. *J Nucl Med* 2004;45:56-68.

188. Leksell L. The stereotaxic method and radiosurgery of the brain. *Acta Chir Scand* 1951;102:316-319.

189. Tryggestad E, Christian M, Ford E, et al. Inter- and intrafraction patient positioning uncertainties for intracranial radiotherapy: a study of four frameless, thermoplastic mask-based immobilization strategies using daily cone-beam CT. *Int J Radiat Oncol Biol Phys* 2011;80:281-290.

190. Verhey LJ, Goitein M, McNulty P, et al. Precise positioning of patients for radiation therapy. *Int J Radiat Oncol Biol Phys* 1982;8:289-294.

191. Charney SC, Lutz WR, Klein MK, et al. Evaluation of a head-repositioner and Z-plate system for improved accuracy of dose delivery. *Vet Radiol Ultrasound* 2009;50:323-329.

192. Mayer MN, Waldner CL, Elliot KM, et al. Comparison of interfractional variation in canine head position using palpation and a head-repositioning device. *Vet Radiol Ultrasound* 2010;51:472-476.

193. Kent MS, Gordon IK, Benavides I, et al. Assessment of the accuracy and precision of a patient immobilization device for radiation therapy in canine head and neck tumors. *Vet Radiol Ultrasound* 2009;50:550-554.

194. Harmon J, Van Ufflen D, Larue S. Assessment of a radiotherapy patient cranial immobilization device using daily on-board kilovoltage imaging. *Vet Radiol Ultrasound* 2009;50:230-234.

195. Bezuidenhout AJ. The lymphatic system. *Miller's anatomy of the dog* 3rd ed. Philadelphia, Pa. ; London: Saunders, 1993;717-757.

CHAPTER 2: COMPARISON BETWEEN ^{18}F-FLUORO-2-DEOXY-D-GLUCOSE POSITRON EMISSION TOMOGRAPHY AND CONTRAST-ENHANCED COMPUTED TOMOGRAPHY FOR MEASURING GROSS TUMOR VOLUME IN CATS WITH ORAL SQUAMOUS CELL CARCINOMA

Brief summary

Feline oral squamous cell carcinoma (SCC) is a very invasive cancer and local recurrence of the tumor is the most common reason of treatment failure. ^{18}F-fluoro-2-deoxy-D-glucose positron emission tomography (^{18}F-FDG PET) is increasingly being used for veterinary oncology staging as it highlights areas with higher glucose metabolism. The goal of the current prospective study was to compare gross tumor volume (GTV) measurements using ^{18}F-FDG PET (GTV_{PET}) versus those using computed tomography (CT) (GTV_{CT}) for stereotactic radiation therapy planning in cats with oral SCC. Twelve cats with confirmed oral SCC underwent pre-treatment ^{18}F-FDG PET/CT. GTV based on contrast-enhanced CT and ^{18}F-FDG PET were measured and compared among cats. Mean GTV_{PET} was significantly smaller than mean GTV_{CT} in the mandibular/maxillary SCC group (n=8, P=0.002) and for the total number of patients (n=12, *P*=0.006), but not in the lingual/laryngeal group (n=4, *P*=0.57). Mismatch fraction analysis revealed that most of the lingual/laryngeal patients had a large region of high-^{18}F-FDG activity outside of the GTV_{CT}. This mismatch fraction was significantly greater in the lingual/laryngeal group than the mandibular/maxillary group (*P*=0.028). The effect of poor spatial resolution of PET imaging was greater when the absolute tumor volume was small. Findings from this study indicated that ^{18}F-FDG PET warrants further investigation as a supplemental imaging modality in cats with oral SCC because it detected regions of possible primary tumor that were not detected on CT images.

Introduction

Accurate measurement of GTV is important for successful radiation therapy (XRT) in cats with oral squamous cell carcinoma (SCC) because geographically missed tumor cells could lead to a failure in local tumor control. Computer-based three-dimensional planning tools typically use electron density maps to calculate radiation attenuation associated with tissue heterogeneity and to date, computed tomography (CT) has been the only imaging modality that could provide this information. However, CT has some limitations when it is used for delineation of gross tumor volume in that it does not always allow discrimination of infiltrative tumors from surrounding non-tumor reactive regions or normal adjacent tissues. To address the limitations of CT for oncologic staging and XRT planning, imaging modalities that are metabolically or functionally based are the current standard in human medicine and are increasingly being used for veterinary patients. [1-4] Positron emission tomography (PET) is one of the most commonly used functional imaging studies and 2-[^{18}F]-fluoro-2-deoxy-D-glucose (^{18}F-FDG) is one of the most commonly used radioisotopes. This glucose-analog radiotracer accumulates in areas with high glucose uptake and high cellular metabolism.[3,5] Increased glucose metabolism can be seen in tumor tissues as well as areas of inflammation or infection. Some normal organs such as the brain and the cardiac muscle also have high glucose metabolism.

Recent technological advances allow co-registration of PET images with CT images (PET/CT) so that functional and anatomical images can be viewed simultaneously (Figure 2.1). Several human studies have concluded that metabolic gross tumor volume based solely on ^{18}F-FDG PET is generally smaller than gross tumor volume derived from CT or magnetic resonance imaging (MRI). [6-11] However, ^{18}F-FDG PET often detects disease outside the gross tumor volume that is based on CT/MRI and thereby reduces the likelihood of geographic miss of the

primary tumor in XRT planning. In one study, ^{18}F-FDG PET was found to be superior to CT/MRI in detecting cervical nodal status.[12] In other human studies, ^{18}F-FDG PET was found to yield a high negative predictive value for detecting nodal metastases and primary disease, and ^{18}F-FDG PET combined with CT/MRI was described as the most reliable imaging modality for evaluating treatment response.[13-15]

Feline oral SCC has been proposed to be the feline counterpart of human head and neck SCC.[16,17] This tumor is the most common malignancy seen in the feline oral cavity, accounting for approximately 65% of all oral tumors.[18] Risk factors such as environmental tobacco smoke, high intake of canned food, and the use of flea collars have been previously identified.[18,19] Treatment outcome for cats with oral SCC is often disappointing and most patients die or are euthanized due to failure in local tumor control even after multimodal treatment.[18,19] Some veterinary reports have described the use of ^{18}F-FDG PET for dogs and cats in the fields of oncology, physiology, and behavioral medicine. [20-26] No veterinary studies were found that described the use of this new imaging modality for XRT planning. The objective of this prospective study was to compare PET and CT gross tumor volume measurements for stereotactic radiation therapy (SRT) planning in a cohort of feline patients with oral SCC. Based on previous studies in humans, we hypothesized that ^{18}F-FDG PET would allow detection of additional possible tumor regions and that gross tumor volumes based solely on PET imaging would not completely overlap with gross tumor volumes based on CT imaging.

Materials and Methods

Cats: Client-owned feline patients with histopathologically-confirmed oral SCC were prospectively recruited during the period of January 2010 to July 2011. All cats were presented for treatment at the Flint Animal Cancer Center, Colorado State University. The study protocol was approved by and conducted in accordance with requirements of the CSU Institutional Animal Care and Use Committee. Each cat was assigned to a mandibular/maxillary or a lingual/laryngeal group based on the location of the grossly visible tumor.

PET-CT Scanning Procedures: All patients were fasted at least 12 hours. The anesthetic protocol was tailored to individual patients' medical and physical conditions so as to maintain the best standard of care. An identical standardized drug scheme was not used for all patients in the study. Pre-anesthetic drugs included atropine and either methadone or hydromorphone, and anesthetic induction agents included ketamine or propofol, with or without midazolam or diazepam. Upon anesthetic induction, patients were instrumented with two intravenous catheters, an intra-arterial catheter for blood pressure monitoring and a urinary catheter with a urine collection bag. One intravenous catheter was dedicated exclusively for injection of the radioactive isotope. Anesthesia was maintained with isoflurane or sevoflurane inhalation, typically with 1-2 % of admixture rate. Normal body temperature was maintained by appropriate warming devices (Baer hugger, Arizant Healthcare, Eden Prairie, MN) as needed. Patient positioning for PET/CT scanning was done to provide concurrent immobilization and CT simulation for XRT using a thermoplastic bite block (Patterson Medical, Cedarburg, WI) and mask system (Civco Systems, Orange City, IA) as previously reported.[27,28] Dorsal or ventral positioning was chosen for the best exposure and access to the tumor and regional lymph nodes for modulated teletherapy beams and modifiers. Extended urinary catheter tubing was placed

through the two bores of the PET/CT gantries and the urinary bag was placed in a lead container behind the PET camera. Whole body PET/CT imaging was performed using the same scanner for all cats (Philips Gemini TF Big Bore 16-slice scanner, Philips Medical Systems, Andover, MA). Orthogonal pilot views were obtained to prescribe the CT and PET series. Immediately after positioning and planning, the cats were injected intravenously with 0.17 mCi per kg +/- 10% ^{18}F-FDG.

After injection of the radioisotope, a volumetric (helical) low-dose CT scan was obtained pre-contrast through the body and reconstructed at 5.0 mm contiguous intervals at 600 mm field of view for the PET acquisition and 2.0 mm contiguous intervals at 350 mm field of view for improved resolution and radiation therapy planning. The following CT acquisition parameters were used: 120 KV, 100 mAs/slice, 0.75 second rotation time, 0.813 pitch and 0.75 mm X 16 detector width. A second whole-body helical low dose CT pass after injection with 0.7 g/kg of iohexol (Omnipaque ™ 350, GE Healthcare, Princeton, NJ, USA) contrast media was acquired using the scan parameters and reconstruction protocol above.

The animal was maintained under anesthesia and in position until one hour post- ^{18}F-FDG injection, at which time the PET data collection was initiated. The PET acquisition consisted of 8 to 9 frames (beds), each 18.0 cm in cranial-caudal length. Acquisition time was 1.5 minutes per bed. The range of times for the collection of the PET series was 12 to 13.5 minutes. Non-attenuation corrected PET images were reconstructed using the 3D-row action maximum likelihood algorithm (RAMLA) method. CT attenuation-corrected images of the PET data were reconstructed using the line-of-response TruFlight (LOR-TF) RAMLA method (identified as BLOB-OS-TF for this scanner) and the pre-contrast CT dataset. After image

acquisition, all patients were recovered from anesthesia and isolated until their radiation level reached the institutional safety requirement.

Measurement of gross tumor volumes: For each cat, post-contrast CT and PET image datasets were exported to the PET/CT scanner's image viewing workstation (Extended brilliance workspace, EBW, version 4.5.3, Philips Healthcare Nederland B.V., Veenpluis, the Netherlands) and loaded into the XRT planning software (Eclipse treatment planning system, TPS, version 8.6.0, Varian Medical Systems, Palo Alto, CA). Using a freehand contouring tool, gross tumor volume based exclusively on post-contrast CT images (GTV_{CT}) was contoured by one of the authors who had expertise in XRT planning. A board-certified veterinary radiologist interpreted the CT images independently and modified the contours as needed for final determination of GTV_{CT} for each cat. The GTV_{PET} was then calculated based solely on the ^{18}F-FDG PET images, using a modified thresholding technique and the workstation's image analysis software.[7] Thresholding was done by two board certified veterinary radiologists and was based on selection of the standardized uptake value (SUV) [29] that completely surrounded the entire tumor and best delineated the FDG avidity. This was done while reviewing the ^{18}F-FDG PET uptake pattern on images using a standard window level setting. Once the SUV threshold was determined, the workstation's software was used to automatically draw a volume of interest (VOI) around the tumor and calculate GTV_{PET}. Modifications in the VOI were made as needed to eliminate regions outside of the patient body (such as the oral cavity and endotracheal tube) that exhibited artifactual hypermetabolic activity. After the GTV_{PET} was finalized for each cat, the first author copied the VOI onto the post-contrast CT image in the treatment planning system and used this for subsequent comparisons.

Comparisons between CT and PET gross tumor volumes: All statistical tests were selected and performed by a statistical consultant, using commercially available software (SigmaPlot ver 12, Systat Software, San Jose, CA and GraphPad Prism ver 5.03, GraphPad Software, La Jolla, CA). A *P*-value < 0.05 was considered statistically significant for all tests. Once the CT and PET VOI's for each cat were imported into the treatment planning system, GTV based on each VOI were calculated using the "measure volume" tool in the treatment planning system. A two-tailed paired t-test was used to compare mean values for GTV_{CT} versus GTV_{PET}. Comparisons were performed for all cats and for cats assigned to mandibular/maxillary (M/M) and lingual/laryngeal (L/L) groups.

The degree of GTV_{CT} and GTV_{PET} overlapping was calculated using a mismatch fraction as described in a previous study.[7] By using the "Boolean operators" tool in the treatment planning system, a structure defined as "only in GTV_{PET} but not in GTV_{CT}" was created. Then a mismatch fraction defined as "mismatch GTV_{PET} to GTV_{CT}" was calculated using the following formula:

(volume of GTV_{PET} that is not overlapped by GTV_{CT}) / (entire GTV_{CT})*100

The Mann-Whitney rank sum test was then used to compare mismatch fractions for cats assigned to mandibular/maxillary and lingual/laryngeal groups.

Results

Cats: Twelve feline patients with oral SCC were included in this study. All patients had no history of previous treatment except for one (patient #11 had tumor recurrence after surgical

debulking). Breeds represented were domestic short hair (8), domestic longhair (3), and Siamese (1). Eight cats were neutered males and four were neutered females. Average patient age and body weight at the time of diagnosis were 12 years old and 4.8 kg, respectively. Clinical stages for tumors were stage II (n=6), stage III (n=3), and stage IV (n=3), based on a previously published feline oral SCC staging scheme.[19] Eight cats were assigned to the M/M group and four were assigned to the L/L group.

Comparisons of gross tumor volumes: GTVs measured for each patient using PET are summarized in Figure 2.2A.

The average of the mean SUV for GTV_{PET} was 5.5 (standard deviation (SD)=1.7) and the median of the mean SUVs was 5.2. The average of the maximum SUVs was 10.1 (SD=5.03) and the median of the maximum SUVs was 8.95. The selected SUV threshold that best encompassed the GTV_{PET} ranged from 2.4 to 3.8 (median value 3.2). Mean GTV_{CT} (14.7, SD=9.6) was significantly larger than mean GTV_{PET} (11.0, SD=7.5) (P=0.006) when all 12 cats were analyzed. For the 8 cats in the M/M group, mean GTV_{CT} (18.0, SD=7.9) was significantly larger than GTV_{PET} (13.2, SD=7.7) (P=0.002). For the 4 cats in the L/L group, no statistically significant difference was found between mean GTV_{CT} (8.1, SD=10.3) and mean GTV_{PET} (6.5, SD=5.5) (P=0.57). Mismatch fractions defined as "mismatch GTV_{PET} to GTV_{CT}" for each patient are summarized in Figure 2.2A. Cats in the L/L group (median=41.6, mean=53.9, SD=52.0) had a significantly higher mismatch fraction than cats in the M/M group (median=4.2, mean=8.3, SD=11.5) (P=0.028, Figure 2.2B).

Discussion

In this study, we incorporated ^{18}F-FDG PET into the XRT plans for 12 feline patients with oral SCC with the ultimate goal of improving targeted delivery. Our protocols were based on those previously described for humans with head and neck SCC.[6,7,11,30] The use of FDG-PET/CT yielded GTVs that, in some feline patients, were asymmetrically or only partially overlapping with the GTV_{CT}. This finding supported our hypothesis that the information provided by ^{18}F-FDG PET would lead to the detection of additional possible tumor areas outside of the volumes indicated by CT alone. The use of metabolic ^{18}F-FDG PET imaging to better detect all potential tumor regions may be particularly critical for SRT planning in order to avoid geographical miss because failure in local tumor control is the most common reason for death/euthanasia in feline patients with oral SCC. Affected cats in this study were to be treated with SRT, which employs a high dose per fraction to tumor and has a very sharp drop-off at tumor margins to spare surrounding tissues. Target tumor volumes in SRT do not employ an additional microscopic tumor margin, which is called clinical target volume and is used in conventional XRT.[31]

Our finding that GTV_{CT} was significantly larger than GTV_{PET} was consistent with some reports describing XRT planning for humans with head and neck SCC.[7-9] In one of those studies, it was concluded that ^{18}F-FDG-PET/CT was the more accurate imaging tool compared to CT/MRI, even though GTVs derived from PET were significantly larger than surgically excised tumor volumes.[7] In our feline study, a reference standard such as a surgically or microscopically-determined tumor volume was not available as all cats were treated with radiation alone. We also did not measure GTVs more than one time using more than one observer. Therefore possible effects of outside factors such as thresholding methods, resolution of the imaging device, size of

the patient, and degree of contrast enhancement on calculated gross tumor volumes remain unknown. Both GTV_{CT} and GTV_{PET} in the L/L group of cats tended to be smaller than GTVs in the M/M group. While not statistically significant, this difference between two tumor groups may warrant further investigation in terms of the usefulness of this imaging modality for XRT planning of small anatomic regions. It is possible that ^{18}F-FDG PET could overestimate the metabolic volume more when a tumor is small due to PET imaging's relatively poor spatial resolution compared to CT and MRI.[4,22,32,33] The in-plane and longitudinal resolution at best was 5 mm with our system. The effect of resolution could be especially exaggerated when determining tumor volumes for anatomic structures of the feline head that differ greatly in size (ie. maxilla/mandible compared to the smaller tongue). Also, a hypermetabolic region reconstructed by the PET system could extend into the air cavity adjacent to an oral mass due to the increased range of positrons in air and could require modification of contours drawn for oral tumors (Figure 2.3).[8] The current resolution limits of PET as well as the presence of hypermetabolic peritumor reactions could therefore preclude its use for determining accurate margins for small tumors and small patients. In spite of this limitation, we propose that PET's greatest advantage may be in providing increased conspicuity of hypermetabolic regions outside of the primary tumor. In our study, the mismatch fraction between PET and CT gross tumor volumes was significantly larger for the lingual/laryngeal group of cats. Patients with L/L SCC had ^{18}F-FDG avid regions that were not overtly abnormal on post-contrast CT images (Figure 2.4).

In cats, as in people, there is high vascularity in the lingual/sublingual area. This high vascularity can make accurate differentiation of contrast enhanced abnormal regions challenging. A recent study describing the usefulness of CT for characterizing feline oral SCC reported that

this tumor showed varying types of contrast enhancement patterns, mass effect and a high frequency of adjacent osteolysis and that CT examination more accurately identify mass extension than radiographs.[34] Our findings were discordant with this previous study in that we encountered feline oral SCC patients without direct bone involvement, with minimal contrast enhancement and with minimal mass effect. It is therefore possible that, depending on the location, CT examination alone may have accurately detected tumoral changes in one area but missed changes in other parts of the same tumor. It is also possible that, because ^{18}F-FDG tracers are not cancer-specific, some of the hypermetabolic regions detected in PET scans of our cats could have contained a mixture of tumor cells and reactive tissues. Full volume histopathology was not performed in any of our cats. However, even in a terminal study, it would be difficult to perfectly correlate imaging and histopathological findings on a millimeter or sub-millimeter level and to exactly confirm the cell composition of a given area seen on images.

The lower specificity of ^{18}F-FDG can also make interpretation of SUV challenging. In human oncology studies, SUV has been reported to be a valuable tool for certain tumor types to distinguish tumor grades, benign from metabolic tumors, and to quantitatively assess treatment response.[1,3,13,35] Many reports have attempted to find an optimum protocol for SUV thresholding and delineating XRT target volumes for human cancer patients, but currently there are no widely-accepted, standardized methods.[4,36] For that reason, we chose to define the volumes subjectively using a consensus of two observers and to determine SUV threshold levels individually for each patient instead of using an arbitrary, fixed, universal SUV threshold. This was more time consuming, but the goal was to use a technique that could still be simply implemented in a clinical setting.

Clinically, PET imaging has other drawbacks that may limit its widespread use in feline oral SCC patients. First, the protocol for PET/CT imaging requires a prolonged period of anesthesia. This is an important consideration given that many feline SCC patients are debilitated, geriatric and may have concurrent medical issues such as renal failure. Second, radioisotopes and imaging equipment are not widely available. Third, the cost of examination is high and may be prohibitive for some owners.

In conclusion, although there are some important limitations of ^{18}F-FDG PET for SRT planning in cats with oral SCC, this imaging modality allowed us to detect potential tumoral regions that were not detected using contrast-enhanced CT, especially in the patients with L/L SCC. Until a cancer-specific tracer is developed and spatial resolution is improved, we recommend combining results of post-contrast CT and ^{18}F-FDG PET imaging with results of clinical examination for SRT planning in order to include all potential tumor regions within the treatment volume. Future, controlled prospective studies are needed to determine whether XRT based on ^{18}F-FDG PET imaging yield increased survival times and success rates of local tumor control in feline oral SCC patients.

Acknowledgement

The authors would like to thank Morris Animal Foundation, the Winn Feline Foundation, the Department of Environmental and Radiological Sciences and CSU Animal Cancer Center for financial support. The authors would also like to thank Dr. Ann Hess for statistical analysis; Ms. Billie Arceneaux and Mr. Jeff Stewart for technical support in PET/CT imaging; and Drs. Jenna Burton, Kelly Carlsten, and Kristen Weishaar for clinical trials coordination.

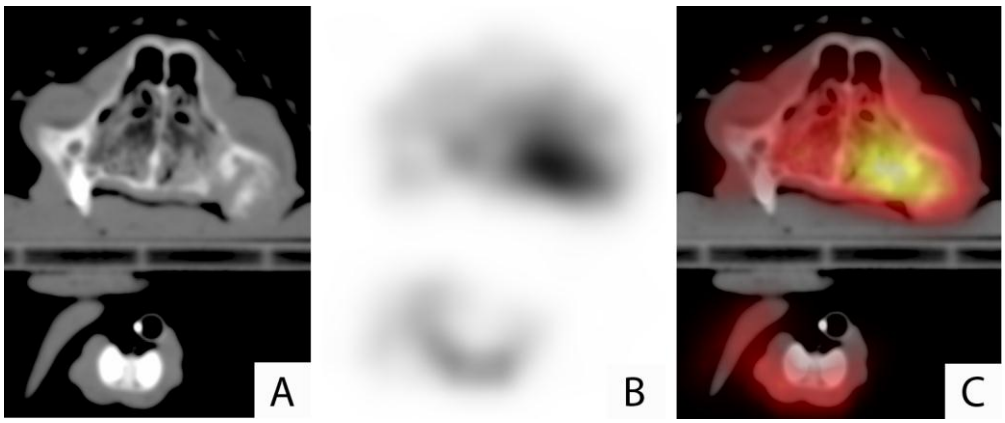

Figure 2.1: Transverse images acquired of a patient with feline oral squamous cell carcinoma. (A) post-contrast CT, (B) ^{18}F-FDG PET, and (C) ^{18}F-FDG PET/CT. Note the ^{18}F-FDG avid and osteolytic lesion involving the left maxilla.

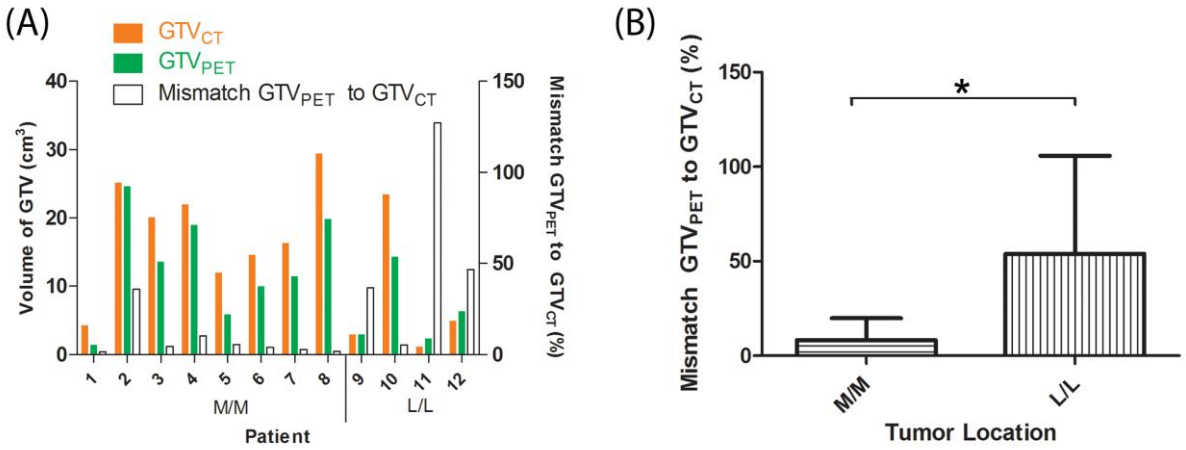

Figure 2.2: (A) Graph summarizing GTV$_{CT}$ and GTV$_{PET}$ for each feline patient (orange and green bars, respectively, left Y axis, cm3) as well as the mismatch fractions for GTV$_{PET}$ to GTV$_{CT}$ (white bar, right Y axis, %). (B) Means of mismatch fractions for mandibular/maxillary and lingual/laryngeal tumors. Bar: Standard deviation of the mean. M/M=mandibular/maxillary tumor, L/L=lingual/laryngeal tumor. Asterisk: *P*=0.028.

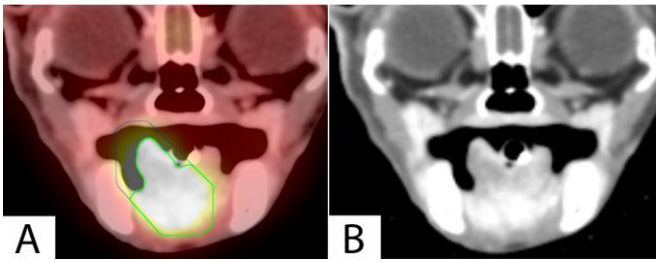

Figure 2.3: (A) 18F-FDG PET/CT and (B) post-contrast CT images of a cat with lingual squamous cell carcinoma (patient #12). Note the ^{18}F-FDG avid region (blue) is extending outside of the tongue into the oral cavity. The GTV_{PET} (green) was created by modifying the ^{18}F-FDG avid region (blue) to exclude the non-tissue area in the air of the oral cavity.

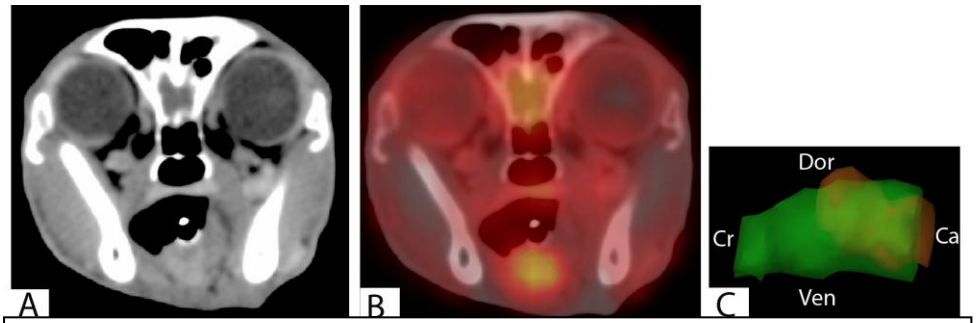

Figure 2.4: Images of a minimally contrast-enhancing CT tissue region (A) that is ^{18}F-FDG avid on the PET/CT image (B) in a cat with lingual SCC (patient #11). The green line in (B) represents GTV_{PET}. (C) Lateral view of GTV_{CT} and GTV_{PET}. Note the larger GTV_{PET} (green) compared to the GTV_{CT} (orange) especially at the cranial portion of the lesion. Cr; cranial, Ca; caudal, Dor; dorsal, Ven; ventral.

BIBLIOGRAPHY

1. Bar-Shalom R, Valdivia AY, Blaufox MD. PET imaging in oncology. *Semin Nucl Med* 2000;30:150-185.

2. Grosu AL, Piert M, Weber WA, et al. Positron emission tomography for radiation treatment planning. *Strahlenther Onkol* 2005;181:483-499.

3. Heron DE, Andrade RS, Beriwal S, et al. PET-CT in radiation oncology: the impact on diagnosis, treatment planning, and assessment of treatment response. *Am J Clin Oncol* 2008;31:352-362.

4. MacManus M, Nestle U, Rosenzweig KE, et al. Use of PET and PET/CT for radiation therapy planning: IAEA expert report 2006-2007. *Radiother Oncol* 2009;91:85-94.

5. Vallabhajosula S. (18)F-labeled positron emission tomographic radiopharmaceuticals in oncology: an overview of radiochemistry and mechanisms of tumor localization. *Semin Nucl Med* 2007;37:400-419.

6. Ciernik IF, Dizendorf E, Baumert BG, et al. Radiation treatment planning with an integrated positron emission and computer tomography (PET/CT): a feasibility study. *Int J Radiat Oncol Biol Phys* 2003;57:853-863.

7. Daisne JF, Duprez T, Weynand B, et al. Tumor volume in pharyngolaryngeal squamous cell carcinoma: comparison at CT, MR imaging, and FDG PET and validation with surgical specimen. *Radiology* 2004;233:93-100.

8. Geets X, Daisne JF, Tomsej M, et al. Impact of the type of imaging modality on target volumes delineation and dose distribution in pharyngo-laryngeal squamous cell carcinoma: comparison between pre- and per-treatment studies. *Radiother Oncol* 2006;78:291-297.

9. Geets X, Tomsej M, Lee JA, et al. Adaptive biological image-guided IMRT with anatomic and functional imaging in pharyngo-laryngeal tumors: impact on target volume delineation and dose distribution using helical tomotherapy. *Radiother Oncol* 2007;85:105-115.

10. Nishioka T, Shiga T, Shirato H, et al. Image fusion between 18FDG-PET and MRI/CT for radiotherapy planning of oropharyngeal and nasopharyngeal carcinomas. *Int J Radiat Oncol Biol Phys* 2002;53:1051-1057.

11. Schinagl DA, Vogel WV, Hoffmann AL, et al. Comparison of five segmentation tools for 18F-fluoro-deoxy-glucose-positron emission tomography-based target volume definition in head and neck cancer. *Int J Radiat Oncol Biol Phys* 2007;69:1282-1289.

12. Ng SH, Yen TC, Liao CT, et al. 18F-FDG PET and CT/MRI in oral cavity squamous cell carcinoma: a prospective study of 124 patients with histologic correlation. *J Nucl Med* 2005;46:1136-1143.

13. Andrade RS, Heron DE, Degirmenci B, et al. Posttreatment assessment of response using FDG-PET/CT for patients treated with definitive radiation therapy for head and neck cancers. *Int J Radiat Oncol Biol Phys* 2006;65:1315-1322.

14. Goerres GW, Schmid DT, Bandhauer F, et al. Positron emission tomography in the early follow-up of advanced head and neck cancer. *Arch Otolaryngol Head Neck Surg* 2004;130:105-109; discussion 120-101.

15. Ong SC, Schoder H, Lee NY, et al. Clinical utility of 18F-FDG PET/CT in assessing the neck after concurrent chemoradiotherapy for Locoregional advanced head and neck cancer. *J Nucl Med* 2008;49:532-540.

16. MacEwen EG. Spontaneous tumors in dogs and cats: models for the study of cancer biology and treatment. *Cancer Metastasis Rev* 1990;9:125-136.

17. Tannehill-Gregg SH, Levine AL, Rosol TJ. Feline head and neck squamous cell carcinoma: a natural model for the human disease and development of a mouse model. *Vet Comp Oncol* 2006;4:84-97.

18. Moore AS, Ogilvie GK. Tumors of the alimentary tract In: Stecher Y, ed. *Feline Oncology*: Veterinary Learning Systems, 2001;271-294.

19. Liptak JM, SJ W. Cancer of the gastrointestinal tract In: Withrow SJ,DM V, eds. *Small Animal Clinical Oncology*, 2007;455-435.

20. Hansen AE, McEvoy F, Engelholm SA, et al. FDG PET/CT imaging in canine cancer patients. *Vet Radiol Ultrasound* 2011;52:201-206.

21. Irimajiri M, Miller MA, Green MA, et al. Cerebral metabolism in dogs assessed by (18)F-FDG PET: a pilot study to understand physiological changes in behavioral disorders in dogs. *J Vet Med Sci* 2010;72:1-6.

22. Lawrence J, Rohren E, Provenzale J. PET/CT today and tomorrow in veterinary cancer diagnosis and monitoring: fundamentals, early results and future perspectives. *Vet Comp Oncol* 2010;8:163-187.

23. LeBlanc AK, Jakoby BW, Townsend DW, et al. 18FDG-PET imaging in canine lymphoma and cutaneous mast cell tumor. *Vet Radiol Ultrasound* 2009;50:215-223.

24. Leblanc AK, Miller AN, Galyon GD, et al. Preliminary evaluation of serial (18) FDG-PET/CT to assess response to toceranib phosphate therapy in canine cancer. *Vet Radiol Ultrasound* 2012;53:348-357.

25. LeBlanc AK, Wall JS, Morandi F, et al. Normal thoracic and abdominal distribution of 2-deoxy-2-[18F]fluoro-D-glucose (18FDG) in adult cats. *Vet Radiol Ultrasound* 2009;50:436-441.

26. Lee MS, Lee AR, Jung MA, et al. Characterization of physiologic 18F-FDG uptake with PET-CT in dogs. *Vet Radiol Ultrasound* 2010;51:670-673.

27. Harmon J, Van Ufflen D, Larue S. Assessment of a radiotherapy patient cranial immobilization device using daily on-board kilovoltage imaging. *Vet Radiol Ultrasound* 2009;50:230-234.

28. Yoshikawa H, Harmon JF, Custis JT, et al. Repeatability of a Planning Target Volume Expansion Protocol for Radiation Therapy of Regional Lymph Nodes in Canine and Feline Patients with Head Tumors. *Vet Radiol Ultrasound* 2012;53:667-672.

29. Workman RBJ, Coleman RE. Fundamentals of PET and PET/CT imaging In: Workman RBJ,Coleman RE, eds. *PET/CT essentials for clinical practice*. New York: Springer, 2006;1-22.

30. Leong T, Everitt C, Yuen K, et al. A prospective study to evaluate the impact of FDG-PET on CT-based radiotherapy treatment planning for oesophageal cancer. *Radiother Oncol* 2006;78:254-261.

31. Khan F. Treatment planning I: Isodose distributions. *The physics of radiation therapy*. 3rd ed. Philadelphia: Lippincott Williams & Wilkins, 2003;199-227.

32. Basu S, Kwee TC, Surti S, et al. Fundamentals of PET and PET/CT imaging. *Ann N Y Acad Sci* 2011;1228:1-18.

33. Lee JA. Segmentation of positron emission tomography images: some recommendations for target delineation in radiation oncology. *Radiother Oncol* 2010;96:302-307.

34. Gendler A, Lewis JR, Reetz JA, et al. Computed tomographic features of oral squamous cell carcinoma in cats: 18 cases (2002-2008). *J Am Vet Med Assoc* 2010;236:319-325.

35. Smyth EC, Shah MA. Role of (1)(8)F 2-fluoro-2-deoxyglucose positron emission tomography in upper gastrointestinal malignancies. *World J Gastroenterol* 2011;17:5059-5074.

36. Zaidi H, El Naqa I. PET-guided delineation of radiation therapy treatment volumes: a survey of image segmentation techniques. *Eur J Nucl Med Mol Imaging* 2010;37:2165-2187.

CHAPTER 3: REPEATABILITY OF A PLANNING TARGET VOLUME EXPANTION PROTOCOL FOR RADIATION THERAPY OF REGIONAL LYMPH NODES IN CANINE AND FELINE PATIENTS WITH HEAD TUMORS

Brief Summary

For canine and feline patients with head tumors, simultaneous irradiation of the primary tumor and mandibular and retropharyngeal lymph nodes (LNs) is often indicated. The purpose of this study was to assess the repeatability of a planned target volume (PTV) expansion protocol for these LNs. Two CT image sets from 44 dogs and 37 cats that underwent radiation therapy (XRT) for head tumors were compared to determine LN repositioning accuracy and precision; planning CT (for XRT planning) and cone-beam CT (at the time of actual treatment sessions). Eleven percent of dogs and 65% of cats received treatment to their LNs. In dogs, the mandibular LNs were positioned more caudally (P=0.0002) and the right mandibular and right retropharyngeal LNs were positioned more to the left side of the patient (P=0.00015 and P=0.003, respectively). In cats, the left mandibular LN was positioned higher (towards roof) than on the planning CT (P=0.028). In conclusion, when patient immobilization devices and bony anatomy matching are used to align the primary head target and these LNs are treated simultaneously, an asymmetrical PTV expansion that ranges 4 to 9 mm (dogs) and 2 to 4 mm (cats), depending on the directions of couch movement, should be used to include the LNs within the PTV at least 95% of the time.

Introduction

The radiation dose that can be prescribed to malignant structures is determined by the balance between therapeutic benefit and possible damage to surrounding normal tissues. Intensity modulated radiation therapy (IMRT) can administer precise dose to targets and decrease dose to regional normal tissue structures. Since the dose distribution to the tissues in the radiation field is not uniform, the ability to accurately position the patient for treatment is an important factor in the successful administration of IMRT. Many positioning apparatuses are commercially available and are used at the initial imaging acquisition, typically computed tomography (CT) that is utilized for computer-based radiation planning. This initial patient setup must be replicated as accurately as possible for each of the actual treatments, but there are inevitable errors in patient repositioning which need to be addressed. The International Commission on Radiation Units and Measurement suggests to use two margins to take this uncertainty into account: internal margin and setup margin.[1] Whereas the former is to compensate for physiological variations of the organ such as internal movement, size, and shape, the latter is to take into account setup inaccuracy and patient movement during the treatment session. The two margins are added to clinical target volume (CTV) to create planning target volume (PTV). Because smaller CTV-to-PTV expansion decreases the volume of normal tissues that receive a clinically relevant dose, extensive efforts have been made in human and veterinary medicine to immobilize radiation therapy (XRT) patients with higher repositioning accuracy, thereby decreasing setup margins.[2-11] In our institution, patients treated with IMRT are set up with a custom-made bite block (made from thermoplastic pellets, Civco model MT-APS 3A, Civco Medical Solutions, Kalona, IA), a modified thermoplastic face mask (Civco model MT-APU), an indexed carbon fiber treatment table, a custom-made carbon fiber bridge to hold the

bite block, a carbon fiber base plate (Civco model MT-20100CF), and a Styrofoam bead style cushion (Civco model MT-VL-37) (Figure 3.1-A).

A previous study from our institution, using two orthogonal kilovoltage (kV) images (kV-kV matching) taken by on-board imaging device, confirmed that a 2 mm PTV margin for the primary cranial target was appropriate to take into account inter-fractional patient setup inaccuracy.[3]

When treating tumors in the head region, it is sometimes necessary to also treat regional lymph nodes (LN), most commonly the mandibular and retropharyngeal LNs. These LNs are readily identifiable on the planning CT scan.[12] However, unlike the primary tumor, which is generally in a fixed position relative to bony landmarks, these LNs may not be repositioned as consistently as the primary tumor. Thus, a 2 mm PTV margin may not be adequate to consistently include the LN targets. An inadequate PTV margin may result in a geographic miss of these LNs (decreasing the probability of tumor control) and in an unacceptably increased dose to the surrounding normal tissues leading to unexpected treatment complications. To avoid these possible problems, better understanding regarding patient positioning reproducibility is essential for each setup device combination and the structures of interest. We hypothesized that with the setup devices mentioned above, a PTV margin greater than 2 mm is needed for these LNs. The current study was conducted to test this hypothesis by retrospectively evaluating LN position variability using kV cone-beam CT images captured immediately after each daily patient setup with kV-kV imaging.

Materials and Methods

Forty-four dogs and 37 cats with primary tumors of the head that underwent XRT at the Colorado State University Flint Animal Cancer Center between March 2010 and December 2011 and had cone-beam CT images acquired at the time of XRT were included. After inducing general anesthesia, all patients were positioned on an indexed CT and XRT couch-top with a custom-made thermoplastic face mask and bite block, a carbon fiber baseplate, a carbon fiber support bridge, and a Styrofoam bead style cushion (Figure 3.1-B and C). The rest of the patient body was positioned either on a U-shaped foam cushion, a large Styrofoam bead style cushion, or a folded towel. All patient setups were performed by experienced radiation therapists.

XRT planning was performed as described before.[3] Briefly, post contrast planning CT images with 2 mm thickness were imported into the XRT planning software (Eclipse treatment planning system, version 8.6.0, Varian Medical Systems, Palo Alto, CA). Digitally reconstructed radiographs and the treatment isocenter were created during the planning process. Simulation isocenter was identified using 1.5 mm metal bead markers (Spee-D-Mark model SDM-BB15, Civco), typically placed on the thermoplastic facemask.

To compare and match the patient positioning with digitally reconstructed radiographs, two orthogonal kV images were taken using on-board imaging devices (kV-kV matching) equipped on a linear accelerator (Varian Trilogy). In this study, dorsal and lateral kV images were taken for all patients. We used a "spyglass" image comparison tool which allows us to evaluate and align anatomical structures from two different CT image sets by overlaying them on a computer screen. With this tool, appropriate couch shifts (X, Y, and Z directions, as well as couch rotation) were applied. This correction was performed as part of regular patient

positioning procedure. After any required patient position correction was made, a cone-beam CT was taken for later evaluation of variability in LN positions using the "high quality head" setting with 2 mm slice thickness, 512 x 512 pixel field of view, and a full-fan bowtie filter. Typically, the cone-beam CT was taken immediately after the treatment session or before the treatment session but after the kV-kV matching. No positioning correction was performed after cone-beam CT acquisition. Each cone-beam CT image set was saved and imported into the Eclipse TPS where it was fused with the planning CT based on CT pixel data. Subjective evaluation regarding fusion quality, especially focusing on bony anatomy was performed. Both sides of mandibular and medial retropharyngeal LNs were contoured on the original planning CT and on each treatment session cone-beam CT. Structures for these LNs from cone-beam CTs were then copied and pasted on to the planning CT so that all contoured LNs from the same patient but from the different timeframes could be visualized on the planning CT (Figure 3.2).

In order to obtain the coordinates of the center of the LNs, a mock-treatment beam was placed and the beam was aligned to the center of mass of each LN using the "align field to structure tool". The coordinates of the center of each LN, as X (horizontal), Y (vertical), and Z (longitudinal), as well as the volume of each LN at the time of planning CT (LN Vol), were recorded. A set up error for each cone-beam CT series was calculated by subtracting coordinates of center of mass of each LN in each cone-beam CT from coordinates of center of mass of the corresponding LN in the planning CT. To evaluate the possible correlation between the magnitude of setup errors and patient body weight (BW), medical records were reviewed to collect patient body weight at the time of the planning CT. Also, to evaluate the possible correlation between the magnitude of set up errors and the distance (Dist) from the caudal edge of the carbon fiber bridge to the each LN, Z coordinate of the most caudal CT image of the

carbon fiber bridge in the planning CT was subtracted from the Z coordinates of the center of the each LN from the planning CT.

All statistical analyses were conducted using commercially available software (SigmaPlot version 12, Systat Sowtware, San Jose, CA). For all analyses, a p value < 0.05 was considered to be significant. Accuracy was defined as an average of set up errors of each axis and is used to estimate systematic LN positioning errors relative to the planning CT baseline. The standard deviation of set up errors x 2 (2SD) was used to estimate precision (variability). A two-tailed, one-sample t-test was used to evaluate whether there was any tendency of the LN to shift in a particular direction (ie. + or -) in each axis. Patient BW, LN Vol, and Dist were correlated with precision errors of each dog. Dogs and cats with multiple cone-beam CTs were used in this correlation analysis. A Pearson product moment correlation analysis or Spearman rank order correlation analysis was performed depending on normality of data distribution.

Suggested PTV expansions were determined for each axis (+ and -) as a sum of the average error and the 2SD if the average error was proved to be significant by the t-test. If the average error was not significant, 2SD was used as a suggested PTV expansion to ensure the LN would be included within the PTV margin 95% of the time.

Results

Among the 44 dogs and 37 cats with head and neck tumors, tumor locations included 20 nasal/maxillary, 21 skull/intracranial, two neck, and one mandible region in dogs; and nine mandible, seven each nasal, pituitary, and lingual/sublingual, five maxilla, one laryngeal, and one dorsal neck in cats. All dogs and 28 of 37 cats (76 %) were positioned in ventral recumbency

and the remaining nine cats (24 %) were positioned in dorsal recumbency with their mandible secured in the bite block.

XRT protocols ranged from one to 20 fractions in dogs and from one to three fractions in cats. Among the 44 dogs and 37 cats, five dogs (11 %) and 24 cats (65 %) had their mandibular and retropharyngeal LNs treated at the same time as the primary head and neck tumors.

An example of the overlaid CT image is shown in Figure 3.2 demonstrating the locations of the LNs from daily cone-beam CTs relative to the original LN locations on the planning CT. Setup accuracy and precision of each LN of the dogs and cats is summarized in Table 3.1 and Table 3.2, respectively. Facing the CT/radiation machine from the foot of the couch, directions of X, Y, and Z are positive to the right (lateral), down (vertical), and towards the CT/radiation machine (longitudinal), respectively. A two-sided, one-sample t-test revealed minor but statistically significant systematic errors in dogs in the Z axis of the left mandibular LN (P=0.0002), the X and Z axes of the right mandibular LN (P=0.0002 and 0.00002, respectively), and all 3 axes of the right retropharyngeal LN (P=0.0033, 0.0001, and 0.0004, respectively). In cats, statistically significant systematic error was found only in the Y axis of left mandibular LN (P=0.0278).

In dogs and cats, the total numbers of patients, the median of analyzed cone-beam CT per animal, and the median and range of LN Vol, Dist for each LN, and patient BW used in the correlation analysis are summarized in Table 3.3 and Table 3.4, respectively. Correlation analysis between 2SD of mean of setup errors and BW, LN Vol, and Dist revealed no statistically significant correlations in dogs. In cats, a significant inverse correlation was found

between the 2SD of mean of right RP LN Z axis and LN Vol (P=0.0162, correlation coefficient; -0.731).

Discussion

XRT plays an important role in controlling canine and feline head and neck malignancies and at our institution, we have been treating them using a highly accurate and precise linear accelerator that is capable of delivering radiation doses stereotactically. A previous study from our institution concluded that a 2-4 mm PTV expansion is appropriate to take into account inter-fractional setup variability for the primary tumor in the head region when the custom-made immobilization devices described previously are used.[3] We currently use a 2 mm expansion for the primary tumor because we can confirm bony anatomic accuracy using kV-kV matching. However, sometimes regional LNs must also be treated. Generally, LNs are soft tissue structures that are not firmly adhered to bony structures and may move relative to surrounding bone, somewhat like prostate and bladder tumors.[13-20] Because we were concerned that a 2 mm of CTV-to-PTV expansion for the draining LNs of the head area was inadequate, this study was conducted to elucidate optimal PTV expansion for them, specifically for the simultaneous treatment of the primary tumor and these LNs.

By retrospectively evaluating the location of each LN using CT and daily treatment session cone-beam CTs, we found that more than 2 mm of PTV expansion is needed for these LNs. In dogs and cats, for the mandibular LNs, our study showed that larger PTV expansion is needed for the X (lateral) and Z (longitudinal) directions, compared to the Y (vertical) direction. Considering all dogs and about 75% of the cats in the current study were positioned in ventral

recumbency, the mandibular LNs resting against the neck-supporting cushion, creating less variation in the Y direction in comparison to the X and Z direction. Our study also showed that both mandibular LNs in dogs were located more caudally during positioning for treatment than in the planning CT. This could be due to differences in the positioning technique used by CT compared to the XRT technicians. However, because of the retrospective nature of this study, we were unable to sort patients by person who performed CT and radiation setup. Although a controlled prospective study with a single person performing these setups may help to clarify the influence of inter-technician variability, we would speculate that the situation in this current study can be found in many of the veterinary radiation oncology facilities. More caudal positioning of mandibular LNs at the time of treatment was not observed in cats. A plausible reason for this difference between dogs and cats may be the difference of head and body size between dogs and cats. Smaller feline heads may have smaller positioning variability. This speculation is supported by the smaller PTV expansion in cats in comparison to dogs summarized in Table 3.2 and 3.1, respectively.

In dogs, the exact reason why only the right mandibular LN showed a statistically significant tendency to be positioned more to the left side of the patient is unclear, but the same tendency was found in the right retropharyngeal LN. Also, not only the right mandibular LN, but also the right retropharyngeal LN showed a statistically significant tendency to be positioned more caudally. In cats, our study revealed that the left mandibular LN was repositioned higher in the treatment session than the planning CT. The exact reason of these statistically significant tendencies is unclear but the clinical routine specific to our institution might be a reason. In this current study, no correlation was found between the setup precision errors in dogs and patient BW, volume of the LNs, or the distance between the edge of the teeth-supporting bridge and

each LN. Even though there was a wide variation in the patient BW and in the distance (Table 3.3), finding no correlation was not surprising because there were also many different breeds in this study. This suggests that the wide variety of shape of their head and neck might have complicated the correlation analysis. In cats, we found an inverse relationship between the setup precision error of the right retropharyngeal LN Z axis and the volume of LN. Considering the fact that feline heads have less variability in size and shape between individual cats than canines, this relationship in the current study was an interesting finding. We need to verify this finding in a future study with a larger patient population of cats because of the limited number of cases in this correlation analysis (10 cats).

Overall, when the patient immobilization devices and bony anatomy matching are used to align the primary target in the head region and treat the mandibular and retropharyngeal LNs simultaneously, we demonstrated that larger PTV expansions are needed for these LNs. We suggest applying an asymmetrical PTV expansion that ranges 6 to 9 mm, 5 to 8 mm, and 5 to 8 mm for dogs and 2 to 4 mm, 2 to 3 mm, and 2 to 4 mm for cats (both X, Y, and Z, direction, respectively) (Table 3.1 and Table 3.2). Developing devices that can help repositioning caudal head and cranial neck area more accurately might reduce this larger (compared to the 2 mm for the primary tumor) PTV expansion.

Acknowledgement

The authors would like to thank Dr. Ann Hess for her support in statistical analyses, and Dr. Lynn Griffin, Dr. Michael Nolan, Mr. Frank Conway, and Ms. Chana Fuller for their support in patient acquisition and treatment setup.

Table 3.1: Repositioning accuracy and precision for inclusion of regional lymph nodes in dogs receiving radiation therapy for head tumors. Numbers in parenthesis indicate the total numbers of cone-beam CTs evaluated. In the suggested expansion, facing the CT/radiation machine from the foot of the couch, + for X, Y, and Z axes indicate right, down, and towards the CT/radiation machine, respectively.

Lymph node (n)	Axis	Average error (accuracy) (cm)	t-test (*P*-value)	2SD (precision) (cm)	Suggested PTV expansion (cm)	
					+	-
L Man LN	X	0.06	0.076	0.69	0.7	0.7
(107)	Y	-0.01	0.539	0.5	0.5	0.5
	Z	-0.13	0.00024	0.68	0.6	0.8
R Man LN	X	-0.14	0.00015	0.72	0.6	0.9
(106)	Y	0.02	0.416	0.5	0.5	0.5
	Z	-0.14	0.00002	0.63	0.5	0.8
L RP LN	X	-0.04	0.217	0.55	0.6	0.6
(89)	Y	0.02	0.244	0.4	0.4	0.4
	Z	-0.03	0.202	0.45	0.5	0.5
R RP LN	X	-0.08	0.0033	0.5	0.6	0.6
(83)	Y	0.15	0.00011	0.66	0.8	0.5
	Z	-0.12	0.00045	0.62	0.5	0.7

LN, lymph node; Man, mandibular; PTV, planning target volume; RP, retropharyngeal; SD, standard deviation

Table 3.2: Repositioning accuracy and precision for inclusion of regional lymph nodes in cats receiving radiation therapy for head tumors. Numbers in parenthesis indicate the total numbers of cone-beam CTs evaluated. In the suggested expansion, facing the CT/radiation machine from the foot of the couch, + for X, Y, and Z axes indicate right, down, and towards the CT/radiation machine, respectively.

Lymph node (n)	Axis	Average error (accuracy) (cm)	t-test (*P*-value)	2SD (precision) (cm)	Suggested PTV expansion (cm)	
					+	-
L Man LN	X	-0.01	0.63	0.29	0.3	0.3
(62)	Y	-0.03	0.028	0.22	0.2	0.2
	Z	-0.03	0.2	0.33	0.3	0.3
R Man LN	X	0.04	0.15	0.38	0.4	0.4
(57)	Y	0.03	0.06	0.23	0.2	0.2
	Z	-0.02	0.49	0.37	0.4	0.4
L RP LN	X	0.01	0.45	0.28	0.3	0.3
(52)	Y	-0.01	0.79	0.32	0.3	0.3
	Z	-0.01	0.6	0.18	0.2	0.2
R RP LN	X	0	0.96	0.23	0.2	0.2
(46)	Y	0.01	0.71	0.23	0.2	0.2
	Z	0	0.89	0.21	0.2	0.2

LN, lymph node; Man, mandibular; PTV, planning target volume; RP, retropharyngeal; SD, standard deviation

Table 3.3: Volume of lymph nodes, distance from the edge of the teeth-supporting bridge to the center of each lymph node, and body weight for dogs receiving radiation therapy for head tumors.

Lymph node (number)	median # of CBCTs/dog	LN Vol (cm^3) Median (Range)	Dist (cm) Median (Range)	BW (kg) Median (Range)
L Man LN (33)	2	1.21 (0.19-3.34)	9.19 (0.19-3.34)	24.7 (5.3-45.1)
R Man LN (32)	3	1.23 (0.23-4.43)	9.3 (4.23-14.0)	24.3 (5.3-45.1)
L RP LN (29)	2	1.02 (0.16-3.35)	12.2 (5.89-18.5)	23.8 (5.3-43.7)
R RP LN (26)	2.5	1.09 (0.11-3.45)	12.3 (6.48-19.1)	22.7 (5.3-43.7)

BW, Body weight; CBCT, Cone-beam CT; Dist, Distance; LN, Lymph node; Man, Mandibular; RP, Retropharyngeal; Vol, Volume

Table 3.4: Volume of lymph nodes, distance from the edge of the teeth-supporting bridge to the center of each lymph node, and body weight for cats receiving radiation therapy for head tumors.

Lymph node (number)	median # of CBCTs/cat	LN Vol (cm^3) Median (Range)	Dist (cm) Median (Range)	BW (kg) Median (Range)
L Man LN (15)	3	0.17 (0.05-0.47)	5.02 (3.35-6.71)	5.1 (2.4-8.6)
R Man LN (14)	3	0.21 (0.05-0.66)	4.85 (3.25-5.99)	4.8 (2.4-8.6)
L RP LN (12)	3	0.19 (0.1-0.46)	6.76 (5.52-8.92)	4.8 (2.4-8.6)
R RP LN (10)	3	0.21 (0.09-0.44)	6.66 (5.45-7.84)	5.35 (2.4-8.6)

BW, Body weight; CBCT, Cone-beam CT; Dist, Distance; LN, Lymph node; Man, Mandibular; RP, Retropharyngeal; Vol, Volume

Figure 3.1: (A) Components of the cranial immobilization device. (B and C) An example of the setup of a canine patient on the radiation therapy couch top.

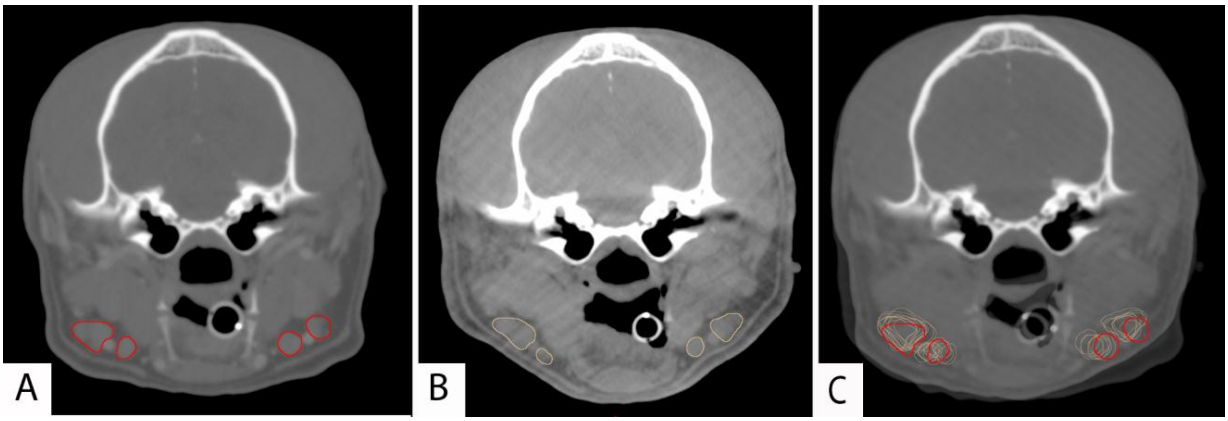

Figure 3.2: An example of the planning CT and cone-beam CT images used for the setup error evaluation. (A) A planning CT image with the mandibular LNs contoured in the red. (B) A cone-beam CT image with the mandibular LNs contoured in brown. (C) A fused image of the A and B. Note the well-aligned bony structures and some positioning differences of the LNs and the skin.

BIBLIOGRAPHY

1. ICRU. Prescribing, recording, and reporting photon beam therapy (supplement to ICRU Report 50). ICRU report 62. Bethesda, Maryland. International Commission on Radiation Units and Measurements, 1999.

2. Charney SC, Lutz WR, Klein MK, Jones PD. Evaluation of a head-repositioner and Z-plate system for improved accuracy of dose delivery. Vet Radiol Ultrasound 2009;50:323-329.

3. Harmon JF, Ufflen DV, LaRue SM. Assesment of a radiotherapy patient cranial immobilization device using daily on-board kilovoltage imaging. Vet Radiol Ultrasound 2009;50:230-234.

4. Kent MS, Gordon IK, Benavides I, Primas P, Young J. Assessment of the accuracy and precision of a patient immobilization device for radiation therapy in canine head and neck tumors. Vet Radiol Ultrasound 2009;50:550-554.

5. Mayer MN, Waldner CL, Elliot KM, Sidhu N. Comparison of interfractional variation in canine head position using palpation and a head-repositioning device. Vet Radiol Ultrasound 2010;51:472-476.

6. Devereux C, Grundy G, Littman P. Plastic molds for patient immobilization. Int J Radiat Oncol Biol Phys 1976;1:553-557.

7. Gilbeau L, Octave-Prignot M, Loncol T, Renard L, Scalliet P, Grégoire V. Comparison of setup accuracy of three different thermoplastic masks for the treatment of brain and head and neck tumors. Radiother Oncol 2001;58:155-162.

8. Houweling AC, van der Meer S, van der Wal E, Terhaard CH, Raaijmakers CP. Improved immobilization using an individual head support in head and neck cancer patients. Radiother Oncol 2010;96:100-103.

9. Jones D, Hafermann MD. A radiolucent bite-block apparatus. Int J Radiat Oncol Biol Phys 1987;13:129-132.

10. Tryggestad E, Christian M, Ford E, Kut C, Le Y, Sanguineti G, Song DY, Kleinberg L. Inter- and intrafraction patient positioning uncertainties for intracranial radiotherapy: a study of four frameless, thermoplastic mask-based immobilization strategies using daily cone-beam CT. Int J Radiat Oncol Biol Phys 2011;80:281-290.

11. Verhey LJ, Goitein M, McNulty P, Munzenrider JE, Suit HD. Precise positioning of patients for radiation therapy. Int J Radiat Oncol Biol Phys 1982;8:289-294.

12. Kneissl S, Probst A. Comparison of computed tomographic images of normal cranial and upper cervical lymph nodes with corresponding E12 plastinated-embedded sections in the dog. Vet J 2007;174:435-438.

13. Bezuidenhout AJ. The lymphatic system. In: Evans HE editor. Miller's anatomy of the dog. 3rd ed. Philadelphia, W.B.Saunders. p. 717-757.

14. Byrne TE. A review of prostate motion with considerations for the treatment of prostate cancer. Med Dosim 2005;30:155-161.

15. Greer PB, Dahl K, Ebert MA, Wratten C, White M, Denham JW. Comparison of prostate set-up accuracy and margins with off-line bony anatomy corrections and online implanted fiducial-based corrections. J Med Imaging Radiat Oncol 2008;52:511-516.

16. Lattanzi J, McNeely S, Hanlon A, Das I, Schultheiss TE, Hanks GE. Daily CT localization for correcting portal errors in the treatment of prostate cancer 1998;41:1079-1086.

17. Lerma FA, Liu B, Wang Z, Yi B, Amin P, Liu S, Feng Y, Yu CX. Role of image-guided patient repositioning and online planning in localized prostate cancer IMRT. Radiother Oncol 2009;93:18-24.

18. Nieset JR, Harmon JF, Larue SM. Use of cone-beam computed tomography to characterize daily urinary bladder variations during fractionated radiotherapy for canine bladder cancer. Vet Radiol Ultrasound. 2011;52:580-588.

19. Rosenthal SA, Roach M 3rd, Goldsmith BJ, Doggett EC, Pickett B, Yuo HS, Soffen EM, Stern RL, Ryu JK. Immobilization improves the reproducibility of patient positioning during six-field conformal radiation therapy for prostate carcinoma. Int J Radiat Oncol Biol Phys 1993;27:921-926.

20. Sripadam R, Stratford J, Henry AM, Jackson A, Moore CJ, Price P. Rectal motion can reduce CTV coverage and increase rectal dose during prostate radiotherapy: A daily cone-beam CT study. Radiother Oncol 2009;90:312-317.

CHAPTER 4: Immunohistochemical characterization of feline oral squamous cell carcinoma

Brief Summary

This study was performed to evaluate the expression of Ki67 and epidermal growth factor receptor (EGFR), mitotic index (MI), and microvascular density (MVD) in feline oral squamous cell carcinoma (SCC) using immunohistochemistry on archival tumor tissues and to seek a correlation between these markers and clinical parameters. Twenty-two archived tumor samples of feline oral SCC were evaluated. Immunohistochemistry for Ki67, MVD, and EGFR was performed and scored. Patient survival information was obtained from the medical records. These molecular markers as well as MI were correlated with tumor locations and patient survival time. The 22 tumors showed wide variation in Ki67, MI, MVD, and EGFR. Tongue SCC expressed higher MVD than mandibular/maxillary SCC (P=0.088). Tumor expression of EGFR was inversely proportional to survival time (P=0.097). This study suggests EGFR expression might be a valuable prognostic factor for treatment outcome in feline oral SCC. It also identified higher angiogenesis in tongue SCC as compared to mandibular/maxillary SCC which may account for a different clinical outcome. Further prospective characterization of feline oral SCC may give us a better understanding of the underlying molecular factors that drive its behavior and offer the possibility for future patient-specific treatment plans.

Introduction

Squamous cell carcinoma (SCC) is the most common feline oral malignancy.[1] It arises from the mucosal epithelial cells in the oral cavity and can invade nearby bone.[2] Although regional lymph node involvement and distant metastasis are relatively rare, local disease progression interferes with food and water consumption and reduces patient quality of life.

Historically, treatment outcomes from surgery, chemotherapy, radiation therapy (XRT) or combinations of these treatments have been discouraging enough to deter owners from pursuing treatment.[3-8] Two studies which employed surgical resection of the feline oral SCC reported poor local control and survival time.[6,8] Another two studies which treated feline oral SCC with XRT showed no obvious improvement in either survival time or quality of life.[3,9] To improve treatment outcome of this devastating disease, further understanding of the biology of this tumor is essential. To date, most of the underlying biology of this tumor still remains a mystery. It is our opinion that cellular and molecular characterization involving measurable tumor parameters like mitotic index (MI), Ki67, microvascular density (MVD), and epidermal growth factor receptor (EGFR) may help elucidate aspects of feline oral SCC biological and clinical behavior.

Determination of tumor MI is a simple and quick way to estimate the proportion of proliferating cells. Mitotic index has been studied extensively in human oncology.[10,11] For example, studies have shown that a higher MI value is predictive for local tumor recurrence, patient survival, and treatment response in humans with cervical SCC.[12-14] In another study it was reported that human patients with head and neck (H&N) SCC who had reduction of MI after the first fraction of XRT tended to a have longer survival time than patients who had increased MI.[15] Due to the similarities between human and feline oral SCC,[16] MI could be of prognostic significance in feline cases of oral SCC.

Ki67 is a nuclear antigen with expression restricted to actively proliferating cells.[17] While the role of Ki67 in cell cycle control is unclear, its expression is widely used as a measure of the growth fraction within a cell population.[17] Cats with nasal and periocular SCC treated with electron beam XRT and that presented with fewer Ki67-positive-cells had a shorter median disease free survival time compared to cats with the same tumors and with higher Ki67

reactivity.[18] Conversely, it was shown that human patients with H&N SCC who had high protein expression of Ki67 and an absence of p53 protein expression showed excellent outcome after XRT even if disease was advanced.[19] These studies suggest that SCC with more proliferating cells, identified by high Ki67 expression, responds better to XRT. Human laryngeal and hypopharyngeal SCC, treated with surgery alone, had an inverse relationship between disease free survival time and Ki67 expression,[20,21] implying that SCCs with high Ki67 expression are more likely to recur without ancillary perisurgical treatment.

The importance of tumor angiogenesis has been extensively studied in human oncology. Microvascular density is an indicator of angiogenesis in the tissue microenvironment, and can be assessed by using the endothelial marker von Willebrand factor (vWf).[22-24] In human SCC, MVD correlates with histopathological grade, nodal metastasis, and patient outcome.[22,25-27] MVD has not been studied in feline oral SCC.

Epidermal growth factor receptor is a transmembrane receptor tyrosine kinase that controls downstream pathways such as cell cycle regulation, apoptosis, and differentiation.[28] In human H&N carcinoma, EGFR expression is a strong independent prognostic indicator for overall and disease free survival time and is a good predictor for locoregional relapse.[29] As a result, EGFR is a good therapeutic target in human oncology and some anti-EGFR drugs have been approved as anti-cancer drugs.[28] In cats, EGFR was shown to be a prognostic indicator in feline cutaneous SCC and EGFR was expressed in feline oral SCC,[30,31] however, its clinical significance is not well studied and only a few reports suggested that clinically-obtained feline oral SCC and cultured feline oral SCC cell lines express EGFR.[30,32]

The goal of this study was to deepen our understanding about feline oral SCC by retrospectively evaluating some cellular and molecular characteristics in archival paraffin

embedded feline oral SCC tissues, and by correlating the obtained data with the clinical outcome as well as the tumor location.

Materials and methods

Patient selection: Archived paraffin embedded feline oral SCC tissues from 42 cats collected over an eleven year period (1997-2008) were obtained from the Diagnostic Laboratory at Colorado State University. All tumors were confirmed as feline oral SCC by a boarded pathologist. Twenty-two of 42 blocks were not decalcified and 20 of 42 blocks were considered decalcified based on the presence or absence of bony tissue in the H&E stained slides. These 20 blocks were excluded due to the impact of the decalcification process on immunohistochemistry (IHC) staining.[30,33] The remaining 22 blocks consisted of tissues from 13 neutered males, one intact male, and eight spayed female cats. Breeds included ten domestic short hair, nine domestic long hair, one Siamese, one Ragdoll, and one Persian. The median age of the cats was 10.5 years (range, 5 to 19 years). Tumor locations included six maxillary, three mandibular, two buccal mucosa, two laryngeal, and nine tongue/sublingual. Corresponding patient records were reviewed. If needed, additional information was obtained through a questionnaire distributed to the referring veterinarians to verify information regarding date of diagnosis and death/euthanasia, as well as reason of death/euthanasia.

MI: Mitotic index was determined by counting mitotic cells in ten random high power fields (HPFs) (400x magnification) of hematoxylin and eosin (H&E) stained slides. The slides were read twice by a single author without knowledge of patient survival time. Then the total numbers of cells in mitosis were divided by the numbers of HPFs counted to obtain an average MI

(MIave). The maximum number of mitotic cells in these HPFs for each patient was also recorded as MImax and used for analysis. These results were confirmed by a boarded pathologist.

Western analysis: Briefly, the SCCF1 cell line (Cell line supplied by Dr. Thomas Rosol, the Ohio State University, Columbus, OH) was maintained as published previously.[16] The cells were lysed using a commercial lysis buffer (Lysis buffer contains M-PER mammalian protein extraction reagent; Thermo Fisher Scientific, Fremont CA, SDS, protease inhibitor; Roche, Indianapolis, IN, sodium orthovanadate, and phenylmethanesulfonyl fluoride). Lysate supernatant was stored at -80 ℃ until analyzed. Protein concentration in the lysate was measured using a commercially available kit (BCA protein assay reagent, Thermo Fisher Scientific, Fremont CA). The cell lysate was electrophoresed with a protein molecular weight ladder (Precision plus protein kaleidoscope standards, Bio-Rad Laboratories, Hercules, CA) and horizontally blotted onto a polyvinylidene difluoride membrane (PVDF membrane, Bio-Rad Laboratories, Hercules, CA). The membrane was incubated with blocking buffer (Superblock, Thermo Fisher Scientific, Fremont CA) for 1 hour, then the membrane was incubated with mouse anti-human monoclonal EGFR antibody (ab-10, Thermo Fisher Scientific, Fremont CA) (diluted in the blocking buffer 1:50) overnight at 4 ℃ followed by incubation with a goat anti-mouse secondary antibody conjugated with horseradish peroxidase (1:10,000 diluted in TBST, Millipore, Billerica, MA) for two hours at room temperature. The band was visualized with a chemiluminescent enzyme substrate (SuperSignal West Pico, Thermo Fisher Scientific, Fremont CA). A CCD camera equipped chemiluminescent imager (ChemiDoc XRS system, Bio-Rad Laboratories, Hercules, CA) was used to capture images.

Sample preparation for IHC: Tumor samples were sectioned to 5 µm thickness and mounted on positively-charged glass slides.

IHC: The IHC protocols used are described in detail elsewhere.[30] Briefly, the slides were deparaffinized and rehydrated through graded xylene and alcohol. Antigen retrieval was conducted with citrate buffer (Dako target retrieval solution, Dako, Carpinteria, CA) for Ki67 and vWf (the latter used as an endothelial marker for MVD analysis) and with protease (Dako cytomation proteolytic enzyme, Dako, Carpinteria, CA) for EGFR. This was followed by incubation with a blocking reagent (Background sniper, Biocare medical, Concord, CA) for ten minutes. The primary antibody {mouse anti-human Ki67 monoclonal 1:50 dilution (MIB-1, Dako, Carpinteria, CA); rabbit anti-human polyclonal vWf 1:300 dilution (A0082, Dako, Carpinteria, CA); EGFR 1:50 dilution}was applied and incubated overnight at 4 ℃. Slides were then incubated with 3% hydrogen peroxide for 10 minutes, followed by incubation with a universal secondary antibody {(Dako Envision+ Dual link, Dako, Carpinteria, CA) for Ki67 and vWf, (Dako Envision+, Dako, Carpinteria, CA) for EGFR} for 20 min at room temperature. A diaminobenzidine substrate kit (DAB substrate kit for peroxidase, Vector Laboratories, Burlingame, CA) was utilized to detect immunoreactive complexes. The slides were counterstained with Mayer's hematoxylin and permanently mounted. Appropriate positive control slides were used for each batch and for all antibodies (feline lymph nodes for Ki67 and feline urinary bladder for vWf and EGFR). Negative controls were stained exactly the same as tumor slides except for omission of the primary antibody.

Grading of IHC stains: The evaluation of Ki67 and EGFR was completed by two readers who graded all slides independently based on criteria described below. Discrepancies were reviewed together at a multihead microscope and consensus was reached. Grading was confirmed by a boarded pathologist. If no consensus was obtained, the reading was repeated.

Scoring of the protein expression of Ki67: Ki67 staining was evaluated using our own scoring system. The system is based on the percent of positively-stained tumor cells (0; 0%, 1; 1-5%, 2; 6-20%, 3; 21-50%, 4; ≥51%)(Ki67%) and the average intensity of positively stained tumor cells (0; negative, 1; weak, 2; moderate, 3; strong, 4; very strong)(Ki67int). The percentage of positive cells and intensity were multiplied to obtain a total score of 0 - 16 (Ki67total).

Scoring of the protein expression of EGFR: EGFR was evaluated based on a previously published method.[30] The percent of positively stained tumor cells was graded as 0; 0%, 1; <10%, 2; 11-30%, 3; 31-60%, and 4; ≥61% (EGFR%). The intensity of positively stained tumor cells was graded as 0; negative, 1; weak, 2; moderate, 3; strong (EGFRint). The percent of positive cells and intensity were multiplied to obtain a total score (EGFRtotal).

MVD analysis: Microvascular density analysis was done by evaluating blood vessels positive for vWf. Image analysis was performed using a microscope (Carl Zeiss Axioplan 2 imaging scope, Carl Zeiss, Thornwood, New York) equipped with a CCD camera (AxioCam HRc Carl Zeiss camera, Carl Zeiss, Thornwood, New York) and image analysis software (Axio Vision 4.3 system software, Carl Zeiss, Thornwood, New York). Briefly, the entire tumor section was scanned under low power (40x magnification) to determine the highest microvascular density area (hot spot) close to tumor cells.[23] Then, at 200x magnification, two distinct hot spots were picked from each slide and captured. MVD was expressed as the ratio of positively-stained pixels of representative endothelium over the total amount of image pixels (MVD%). The actual numbers of pixels of positively stained endothelial cells (MVD#) was also determined.

Tumor locations and molecular markers: Analysis was performed to evaluate if there was any relationship between tumor location and expression of these molecular markers. Locations included mandible, maxilla, and tongue/sublingual. Mandible and maxilla were combined into a

single group to increase statistical power. Because of the smaller sample population, laryngeal and buccal mucosa were excluded from this analysis. A two-sample t-test was used to evaluate differences in molecular marker expression between tumor locations. The normality assumption was verified using normal-probability plots.

Overall survival time (OST) and correlation analysis between OST and tumor locations/markers: OST was defined as the time from diagnosis to either death or last follow-up evaluation. Data from patients with an unknown date of death were censored at the time of the last known follow-up.

Statistical Analysis: All statistical tests were two-sided, and *P*-values <0.05 were considered significant. For each case, MIave and MImax were correlated with Ki67 scores. The association between Ki67 scores and MI scores was evaluated by performing a non-parametric Spearman's rank correlation analysis. The Kaplan–Meier methodology was used to estimate the median OST. The comparison of OST between tumor location groups was performed using the log-rank test. Multivariate Cox proportional hazard analysis was performed to determine the prognostic significance of the molecular markers for predicting OST. The proportional hazard assumption was verified using plots of the log (-log) survival curves and Schoenfeld residuals. Statistical data analyses were performed using commercially available software (SAS, version 9.2, SAS Institute Inc, Cary, NC).

Results

Western analysis: We confirmed cross-reactivity of the EGFR antibody by performing western analysis even though this antibody was previously reported to cross react with feline tissue.[30] Human EGFR was reported to be 170 kDa in size[34] and feline EGFR protein has a similar

molecular weight.[35] Only a single intense band was observed at approximately 170 kDa (Figure 4.1), suggesting that this antibody cross-reacts and is specific for feline EGFR protein.

IHC: Ki67 exhibited nuclear, vWf cytoplasmic, and EGFR membranous and cytoplasmic localization respectively (Figure 4.2). The median and range of scores for each marker in all patients (22 cats) is summarized in Table 4.1.

MI and Ki67 grades: There were significant correlations between MImax and Ki67int (*P*=0.05, 95%CI; 0.01, 0.73), MImax and Ki67 total (*P*=0.004, 95%CI; 0.23, 0.82), and MIave and Ki67total (*P*=0.04, 95%CI; 0.05, 0.75).

Tumor location and molecular markers: *P*-values of the t-test were summarized in Table 4.1. Although not significant, the tongue tumor group tended to have higher MVD% compared to mandible/maxilla group (*P*=0.088). Other markers showed no difference based on tumor location.

OST and correlation analysis between OST and tumor location/marker: Among 22 cats, there were 14 death events in this cohort. The median survival time of the 14 cats was 10.5 days. Although not statistically significant, Cox proportional hazard analysis revealed an inverse relationship between EGFRtotal and OST (*P*=0.097, hazard ratio= 1.91, 95% confidence interval: 0.97 -1.47) (Figure 4.3). A cutoff value of 2 for EGFRtotal was determined based on the median of the patient population. All other markers showed no significant correlations. There was no statistically significant difference in OST between the maxilla/mandible group and the tongue/sublingual group.

Discussions

Feline oral SCC is resistant to conventional treatments,[3,4,7,8] but the mechanism of resistance is still unknown. The main purposes of this retrospective study was to analyze MI,

Ki67, MVD, and EGFR within a larger patient population than previous studies[18,30] in order to understand and characterize the biology of feline oral SCC better, as well as to seek a correlation between these markers and clinical outcome.

We found significant positive correlations between some Ki67 scores and MI scores. To our knowledge, this is the first report that showed a significant correlation between MI and Ki67 scores in feline oral SCC. Ki67 is expressed in all cell cycle phases of actively proliferating cells but not in quiescent cells (G0).[17] In contrast, mitotic index takes into account cells in mitosis but not cells in other cell cycle phases or G0. Melzer *et al*. reported that there was a correlation between Ki67 reactivity and disease free intervals in feline nasal and periocular SCC.[18] In dogs with cutaneous mast cell tumors, Ki67 was shown to be a prognostic factor.[36] Both Ki67 and MI are known to be related to patient outcomes in human breast cancer and lung SCC.[37-39] Thus, observing correlations between the two indices in this study was not surprising. However, the correlations we found may imply that many feline oral SCC cells positive for Ki67 are able to pass cell cycle checkpoints and continue proliferating rather than undergoing senescence or apoptosis which are both Ki67 negative processes.[17] Given the role of Ki67 and MI in human and veterinary oncology as a prognostic factor in multiple tumor types, we expected to see significant correlations between these two markers and patient OST. Our study did not find a statistically significant correlation with patient OST, possibly due to the smaller sample size in the current study.

EGFR is a transmembrane growth hormone receptor and activation of its receptor-coupled tyrosine kinase leads to activation of signaling cascades such as cell cycle regulation and cytoskeleton reorganization.[28] In humans, EGFR is known to be a prognostic indicator in many malignancies including H&N SCC.[40] Although not statistically significant, we found a negative

correlation between EGFRtotal and OST. Considering that EGFR activation leads to cell cycle progression, invasion, and inhibition of apoptosis and accumulating data that suggest similarities between human H&N SCC and feline oral SCC, this trend suggests that EGFR may be useful as a prognostic indicator for OST in cats with oral SCC.[16,40] Because of the retrospective nature of our current study, treatments that patients received varied widely from no treatment to more aggressive treatments such as multiple radical surgical excisions or XRT (data not shown). As demonstrated in Figure 4.3, there was an initial drop of patient survival in both EGFR low and EGFR high groups. This drop was attributed to euthanasia elected by owners immediately following diagnosis. We performed a secondary survival analysis including only patients who lived more than 7 days. In this secondary analysis, EGFRtotal was not prognostic for patient survival but showed a similar trend (P=0.14) as in the original analysis (P=0.097), supporting the negative trend that we found in the primary analysis. Despite some limitations (small patient population, wide treatment variety), the negative trend we showed in this study was an interesting finding. If a well-controlled prospective study can verify this correlation, drugs targeting the EGFR pathway may be beneficial to cats with oral SCC.

Tumor vascularization is an important factor for tumor oxygen and nutrient supply as well as for tumor metastasis.[41] Tumors tend to create less organized and less dense vascular networks compared to normal vasculature.[42] This structural difference might result in ineffective oxygen delivery to tumor cells creating hypoxic areas. vWf has been used to identify endothelial cells to evaluate MVD.[23] A so called “hot spot” technique has been widely used to quantify MVD and correlations between MVD and outcome in several human tumors have been reported.[23] In the current study, neither MVD% nor MVD# correlated with patient survival time. However, MVD% in tongue SCC tended to be higher than MVD% in mandibular and maxillary

SCC. This result may indicate higher vascularity in feline oral SCC of the tongue although the tongue may normally have higher MVD thus this comparison is of uncertain significance. We quantified MVD within the tumor tissue ("hot spot" technique), not within the normal tongue, but it is unclear whether the vascularity of the normal tissue had an influence on the MVD in the tumor. Based on our clinical experience, we feel that feline oral SCC in the tongue is more difficult to treat but this may be due to its location and higher impact on a patient's ability to eat. At this point, we can not fully explain this contradiction between our clinical impression about the treatment response of the tongue SCC and higher MVD% in the tongue. However we believe that this trend might be more clearly identified by evaluating more patients and prospectively measuring tissue oxygen tension directly.

In conclusion, in this preliminary study, we saw large inter-tumoral heterogeneity in Ki67, MI, MVD, and EGFR in feline oral SCC. The negative trend between EGFRtotal and OST suggests a similarity between feline oral SCC and human H&N SCC. The current study identifies the role of EGFR as a potential prognostic indicator for patient survival and suggests that therapeutic interference of the EGFR pathway might be a novel means to control this aggressive cancer. A prospective characterization study may help identify further prognostic factors and enhance understanding of the biology of this devastating tumor.

Table 4.1: Summary of mitotic index (MI), Ki67, microvascular density (MVD), and epidermal growth factor receptor (EGFR) in feline oral SCC; median (range)

	MI		Ki67			MVD		EGFR		
	Ave	Max	%	Int	Total	%	#	%	Int	Total
Total (22)	2.3 (0.1-6.4)	6 (1-10)	4 (2-4)	3 (2-4)	12 (6-16)	2.8 (0.9-4.4)	208 (107-532)	2 (0-4)	2 (0-3)	2 (0-12)
Mandible/maxilla (9)	1.4(0.1-6.4)	3(1-9)	4(2-4)	3(2-4)	12(6-16)	1.4(0.9-4.1)	181(128-325)	1(0-4)	1(0-3)	2(0-8)
Tongue/sublingual (9)	3.6(0.2-5.5)	6(1-10)	3(2-4)	3(3-4)	12(6-16)	3.01(1.1-4.4)	212(107-532)	2(1-4)	2(1-3)	4(1-12)
P-value	0.380	0.420	0.600	0.350	0.890	0.088	0.410	0.280	0.520	0.250

Ave, Average of total MI in up to 10 high power fields (HPF); Max, Maximum number of mitotic cells in these HPF; %, Percent of positively stained tumor cells; Int, intensity of each marker; Total, product of % and Int

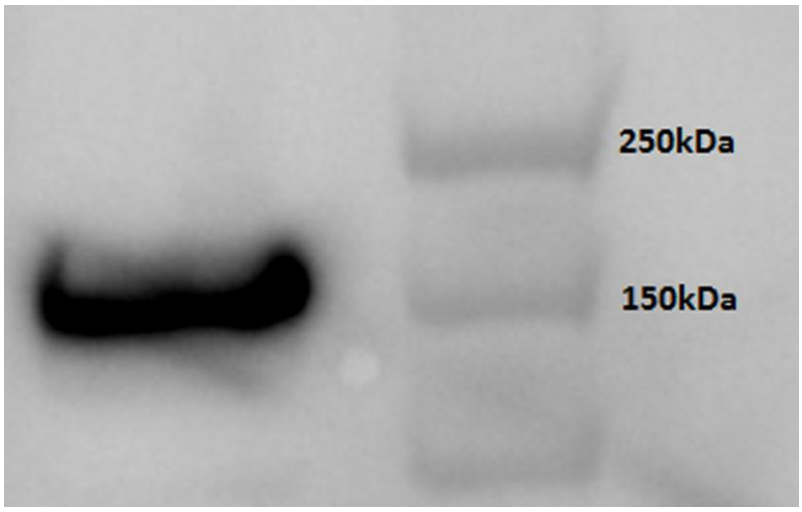

Figure 4.1: Western blot assay to verify cross-reactivity of an epidermal growth factor receptor antibody against a feline squamous cell carcinoma cell line. Note the single intense band seen in the left lane. Molecular weight marker was run in the right lane.

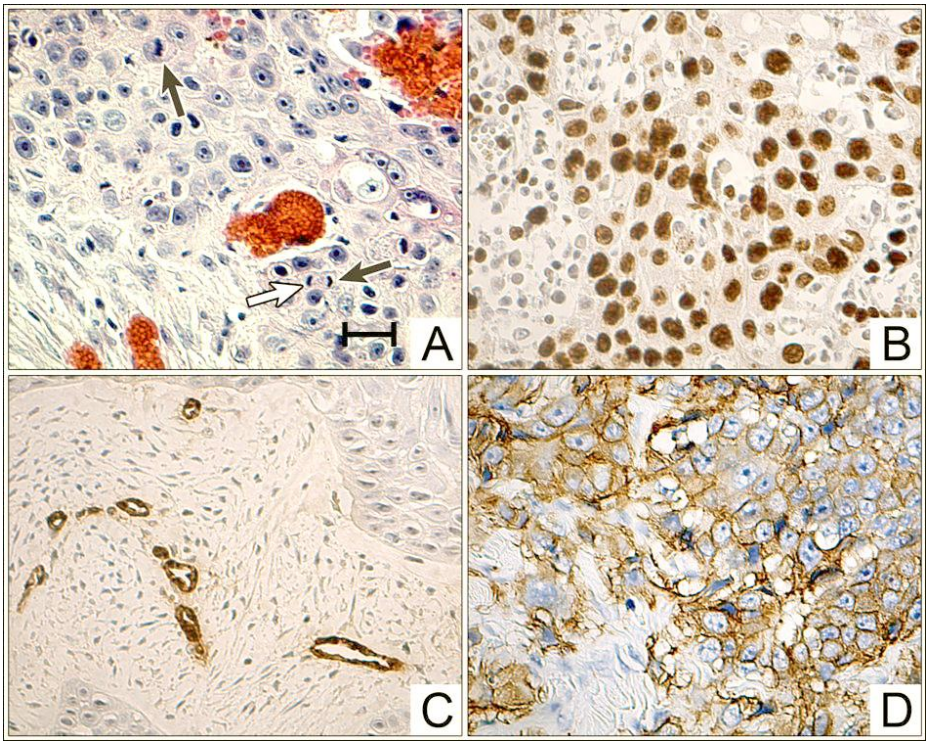

Figure 4.2: Representative images of biological markers evaluated with hematoxylin and eosin (A) and immunohistochemical staining (B-D) in feline oral squamous cell carcinoma [Mitotic index (A), Ki67 (B), Microvascular density (C), epidermal growth factor (D)]. Bar=20µm.

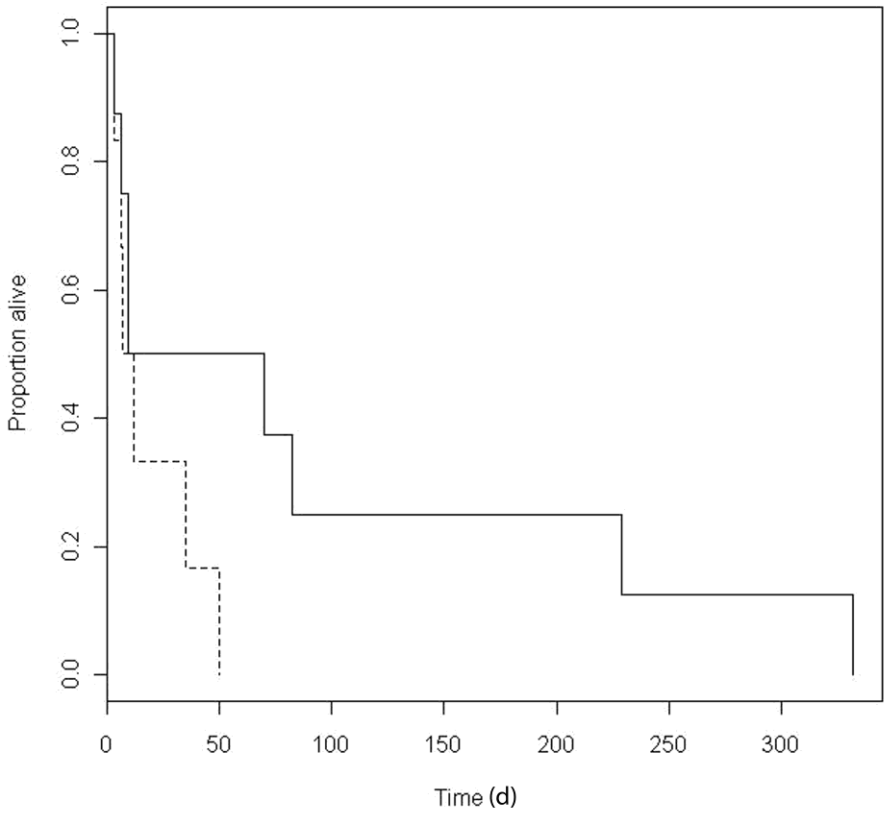

Figure 4.3: Kaplan–Meier graph showing overall survival time of cats with low (<=2) EGFRtotal and high (>2) EGFRtotal. Although not statistically significant, patients with EGFRtotal >2 tended to have a shorter survival times than patients with EGFRtotal<=2. (*P*=0.097, hazard ratio=1.91, 95% confidence interval: 0.97-1.47).

BIBLIOGRAPHY

1. Moore AS, Ogilvie GK. In: Y Stecher ed. *Feline Oncology*. Trenton, NJ: Veterinary Learning Systems, 2001;271-294.

2. Head KW, Else RW, Dubielzig RR. In: DJ Meuten, ed. *Tumors in Domestic Animals* 4th ed. Ames, IA: Iowa State Press Co, 2002;425-427.

3. Bregazzi VS, LaRue SM, Powers BE, et al. Response of feline oral squamous cell carcinoma to palliative radiation therapy. *Veterinary Radiology and Ultrasound* 2000;42:77-79.

4. Northrup NC, Selting KA, Rassnick KM, et al. Outcomes of cats with oral tumors treated with mandibulectomy: 42 cases. *Journal of the American Animal Hospital Association* 2006;42:350-360.

5. Hayes AM, Adams VJ, Scase TJ et al. Survival of 54 cats with oral squamous cell carcinoma in United Kingdom general practice. *Journal of Small Animal Practice* 2007;48:394-399.

6. Emms SG, Harvey CE. Preliminary results of maxillectomy in the dog and cat. *Journal of Small Animal Practice* 1986;27:291-306.

7. Hutson CA, Willauer CC, Walder EJ, et al. Treatment of mandibular squamous cell carcinoma in cats by use of mandibulectomy and radiotherapy: seven cases (1987-1989). *Journal of the American Veterinary Medical Association* 1992;201:777-781.

8. Bostock DE. The prognosis in cats bearing squamous cell carcinoma. *Journal of Small Animal Practice* 1972;13:119-125.

9. Fidel JL, Sellon RK, Houston RK, et al. A nine-day accelerated radiation protocol for feline squamous cell carcinoma. *Veterinary Radiology and Ultrasound* 2007;48:482-485.

10. Laroye GJ, Minkin S. The impact of mitotic index on predicting outcome in breast carcinoma: a comparison of different counting methods in patients with different lymph node status. *Modern Pathology* 1991;4:456-460.

11. Sealy R, Immerman A, Shepstone B. Mitotic index in human squamous cell carcinoma. *Acta radiologica: oncology, radiation, physics, biology* 1972;11:59-64.

12. Nakano T, Oka K, Ishikawa A, et al. Immunohistochemical prediction of radiation response and local control in radiation therapy for cervical cancer. *Cancer Detection and Prevention* 1998; 22:120-128.

13. Suzuki Y, Oka K, Ohno T, et al. Prognostic impact of proliferating cell populations in cervical cancer patients treated with carbon ion beam. *Cancer* 2009;115:1875-1882.

14. Nakano T, Oka K. Differential values of ki-67 index and mitotic index of proliferating cell population. *Cancer* 1993;72:2401-2408.

15. Kraxber H, Tamas L, Jaray B, et al. Search for prognostic factors in head and neck cancer. *Acta Oto-laryngologica. Supplementum* 1997;527:145-149.

16. Tannehill-Gregg SH. Feline head and neck squamous cell carcinoma: a natural model for the human disease and development of a mouse model. *Veterinary and Comparative Oncology* 2006;4:84–97.

17. Scholzen T, Gerdes J. The Ki-67 protein: From the known and the unknown. *Journal of Cellular Physiology* 2000;182:311-322.

18. Melzer K, Guscetti F, Bley CR, et al. Ki67 reactivity in nasal and periocular squamous cell carcinomas in cats treated with electron beam radiation therapy. *Journal of Veterinary Internal Medicine* 2006;20:676-681.

19. Raybaud-Diogene H, Fortin A, Morency R, et al. Markers of radioresisntance in squamous cell carcinomas of the head and neck a clinicopathologic and immunohistochemical study. *Journal of Clinical Oncology* 1997;15:1030-1038.

20. Liu M, Lawson G, Delos M, et al. Prognostic value of cell proliferation markers, tumor suppressor proteins and cell adhesion molecules in primary squamous cell carcinoma of the larynx and hypopharynx. *European archives of oto-rhino-laryngology* 2003;260:28-34.

21. Acikalin MF, Oner U, Tel N, et al. Prognostic significance of Ki-67 expression for patients with laryngeal squamous cell carcinoma primarily treated by total laryngectomy. *European archives of oto-rhino-laryngology* 2004;261:376-380.

22. Artese L, Rubini C, Ferrero G, et al. Microvascular density (MVD) and vascular endothelial growth factor expression (VEGF) in human oral squamous cell carcinoma. *Anticancer Research* 2001;21:689-696.

23. Weidner N. Current pathologic methods for measuring intratumoral microvessel density within breast carcinoma and other solid tumors. *Breast Cancer Research and Treatmen*t 1995; 36:169-180.

24. Weidner N, Semple JP, Welch WR, et al. Tumor angiogenesis and metastasis- correlation in invasive breast carcinoma. *The New England journal of Medicine* 1991;324:1-8.

25. Albo D, Granick MS, Jhala N, et al. The relationship of angiogenesis to biological activity in human squamous cell carcinomas of the head and neck. *Annals of Plastic Surgery* 1994;32:588-594.

26. Lentsch EJ, Goudy S, Sosnowski J, et al. Microvessel density in head and neck squamous cell carcinoma primary tumors and its correlation with clinical staging parameters. *The laryngoscope* 2006;116:397-400.

27. Ascani G, Balercia P, Messi M, et al. Angiogenesis in oral squamous cell carcinoma. *Acta Otorhinolaryngologica Italica* 2005;25:13-17.

28. Herbst RS. Review of epidermal growth factor receptor biology. *International Journal of Radiation Oncology, Biology, Physics* 2004;59:21-26.

29. Ang KK, Andratschke NH, Milas L. Epidermal growth factor receptor and response of head-and-neck carcinoma to therapy. *International Journal of Radiation Oncology, Biology, Physics* 2004;58:959-965.

30. Looper JS, Malarkey DE, Ruslander D, et al. Epidermal growth factor receptor expression in feline oral squamous cell carcinomas. *Veterinary and Comparative Oncology* 2006;4:33-40.

31. Sabattini S, Marconato L, Zoff A, et al. Epidermal growth factor receptor expression is predictive of poor prognosis in feline cutaneous squamous cell carcinoma. *Journal of Feline Medicine and Surgery* 2010;12:760-768.

32. Bergkvist GT, Argyle DJ, Pang LY, et al. Studies on the inhibition of feline EGFR in squamous cell carcinoma: Enhancement of radiosensitivity and rescue of resistance to small molecule inhibitors. *Cancer Biology and Therapy* 2011;11:927-937.

33. Christgau M, Caffesse RG, Newland JR, et al/ Characterization of immunocompetent cells in the diseased canine periodontium. *Journal of Histochemistry and Cytochemistry* 1998;46:1443-1454.

34. Bergkvist GT, Yool DA. Epidermal growth factor receptor as a therapeutic target in veterinary oncology. *Veterinary and Comparative Oncology* 2011;9:81-94.

35. Minke JMH, Schuuring Ed, van den Berghe R, et al. Isolation of two distinct epidermal cell lines from a single feline mammary carcinoma with different tumorigenic potential in nude mice and expressing different levels of epidermal growth factor receptors. *Cancer Research* 1991;51:4028-4037.

36. Maglennon GA, Murphy S, Adams V, et al. Association of Ki67 index with prognosis for intermediate-grade canine cutaneous mast cell tumours. *Veterinary and Comparative Oncology* 2008;6:268-274.

37. Yerushalmi R, Woods R, Ravdin PM, et al. Ki67 in breast cancer: prognostic and predictive potential. *The Lancet Oncology* 2010;11:174-83.

38. Niemiec J, kolodziejski L, Dyczek S. EGFR LI and ki67 LI are independent prognostic parameters influencing survivals of surgically treated squamous cell lung cancer patients. *Neoplasma* 2005;52:231-237.

39. Kazantseva IA, Potapov luN, Linell' F, et al. Mitotic index as a prognostic factor in ductal breast cancer. *Arkhiv patologii* 1995;57:18-21.

40. Arteaga CL. Epidermal growth factor receptor dependence in human tumor: more than just expression?. *The Oncologist* 2002;7:31-39.

41. Weinberg RA. Dialogue replaces monologue: Heterotypic interactions and the biology of angiogenesis. In: *the Biology of Cancer*, New York, Garland Science, Taylor & Francis Group, LLC, 2006:556-574.

42. Jain RK. Molecular regulation of vessel maturation. *Nature Medicine* 2003;9:685-693.

CHAPTER 5: ASSESSMENT OF PREDICTIVE MOLECULAR VARIABLES IN FELINE ORAL SQUAMOUS CELL CARCINOMA TREATED WITH STEREOTACTIC RADIATION THERAPY

Brief Summary

This study evaluated molecular characteristics that are potentially prognostic in cats with oral squamous cell carcinoma (SCC) that underwent stereotactic radiation therapy (SRT). Survival time (ST) and progression-free interval (PFI) were correlated with mitotic index, histopathological grades, Ki67 and epidermal growth factor receptor expressions, tumor microvascular density (MVD), and tumor oxygen tension (pO_2). Median ST and PFI were 106 and 87 days, respectively. Overall response rate was 38.5% with rapid improvement of clinical symptoms in many cases. Patients with higher MVD or more keratinized SCC had significantly shorter ST or PFI than patients with lower MVD or less keratinized SCC (P=0.041 and 0.049, respectively). Females had significantly longer PFI and ST than males ($P \leq 0.016$). Acute toxicities were minimal. However, treatment-related complications such as fractured mandible impacted quality of life. In conclusion, SRT alone should be considered as a palliative treatment. MVD and degree of keratinization may be useful prognostic markers.

Introduction

Feline oral squamous cell carcinoma (SCC) is one of the most devastating veterinary cancers due to its high rate of treatment failure. Although traditional and novel treatment modalities have been evaluated, there has been no major improvement in tumor control or survival time.[1-9] Given that almost all patients with oral SCC that undergo any treatment type

eventually succumb to local tumor recurrence or tumor progression, primary tumor control is the most critical treatment goal. However, lack of our knowledge about the biology of SCC limits development of more effective treatment modalities.

In human SCC and feline SCC, possible prognostic markers have been evaluated and those include histopathological grading, Ki67, epidermal growth factor receptor (EGFR), and microvascular density (MVD). Histopathological grading has been used to evaluate and prognosticate human oral SCC and parameters include degree of keratinization, mitotic index, and stage of invasion.[10-13] Ki67 is a protein specifically expressed in the nucleus of actively proliferating cells.[14] One study evaluated the correlation between immunohistochemically-evaluated Ki67 expression and treatment outcome after electron radiation therapy (XRT) in feline cutaneous SCC.[15] In this study, patients with higher Ki67 expression had better treatment outcome compared to patients with lower Ki67 expression. EGFR is a transmembrane receptor coupled with tyrosine kinase. This receptor has been shown to play key roles in multiple cellular events including cell proliferation, apoptosis, and migration in human tumors.[16, 17] High EGFR immunoreactivity has been shown to be prognostic for shorter survival and local control after fractionated radiation therapy in human H&N SCC.[18] Our previous study revealed that EGFR expression may be a prognostic factor in feline oral SCC.[19] MVD is a technique to evaluate tumor angiogenesis that has been identified as a prognostic factor in some human malignancies including breast carcinoma, ovarian carcinoma, and head and neck (H&N) SCC.[20-23]

XRT plays an important role in management of human and veterinary cancer patients. Stereotactic XRT (SRT) is a novel technique recently introduced in veterinary medicine. This new technique allows increasing dose to the target yet spares adjacent normal structures because of the steep dose drop-off outside the treatment target and higher delivery accuracy. It has been

suggested that the biological responses/events occur in the human tumor and its microenvironment after SRT is different from those after conventional fractionated XRT.[24, 25] Previous studies with xenograft models have shown that significant number of tumor vasculature endothelial cells undergo apoptosis when tumors are treated with a larger dose/fraction such as >10 Gy/fraction.[25] In addition, tumors irradiated with a larger dose/fraction (8-10 Gy) have been shown to undergo mitotic death following G2 phase-arrest and those receiving an extremely large dose/fraction (>15-20 Gy) have been shown to undergo interphase death regardless of the cell cycle phase.[25] Clinically, SRT has been evaluated as a primary treatment modality for human H&N SCC.[26-28] In these studies, most patients showed clinical responses and the authors concluded that SRT is a useful treatment option for human patients with H&N SCC although its long-term treatment outcome was not as favorable as that of more aggressive combination treatment of surgery, XRT, and chemotherapy. However, because SRT is a completely new XRT technique in veterinary medicine, knowledge about its efficacy for a variety of veterinary malignancies including feline oral SCC is scarce.

Oxygen status in tissue is a well-known factor that affects the biological response of cells to photon irradiation.[29] Human cancer contains hypoxic regions due to abnormal tumor vascular function, structure, and organization.[30] Also, hypoxic tumors are known to have less apoptotic potential.[31, 32] In human H&N SCC and cervical carcinoma, tumor hypoxia, which is typically defined as median or mean oxygen tension (pO_2) < 5-10 mm Hg, predicts tumor control and survival time after fractionated XRT.[2, 33-40] Fractionated XRT has been advocated to increase post-treatment tumor pO_2 theoretically.[29] One study has shown an improvement in tumor pO_2 in human patients with cervical SCC after treatments including fractionated XRT although results

of clinical studies are not consistent.[34, 41, 42] Post-SRT *in vivo* oxygen measurement in spontaneous cancer patients has not been reported in human or veterinary medicine.

The main purpose of the current study was to prospectively evaluate the prognostic significance of variety of different markers (histopathological grades, Ki67, EGFR, MVD, tumor pO_2 and patient parameters) for the patients with feline oral SCC treated by SRT.

Materials and methods

Patient population: Twenty feline oral SCC patients who were referred to the Flint Animal Cancer Center, Colorado State University (CSU-ACC) between January 2010 and July 2011 were enrolled into the study at owner's consent. All patients underwent diagnostic evaluations including chest radiographs, complete blood count, serum chemistry profile, and urinalysis. All patients were clinically staged using an established WHO clinical staging scheme (Table5.1).[43] This study protocol was approved by institutional animal care and use committee (IACUC). All biopsy samples were confirmed to be SCC by a boarded pathologist.

CT or PET/CT examination and stereotactic radiation Therapy: All patients underwent either CT or PET/CT examination for radiation therapy planning, using an integrated PET/CT scanner (Philips Gemini TF Big Bore 16-slice scanner, Philips Medical Systems, Andover, MA). After inducing general anesthesia (typically with atropine, methadone or hydromorphone, and ketamine or propofol induction, followed by maintenance with oxygen/isoflurane or sevoflurane admixture), patients were positioned on the CT couch in either ventral or dorsal recumbency using custom-made immobilization devices reported in our previous study.[44, 45] Patients who underwent PET/CT examination were injected intravenously (IV) with 0.17 mCi per kg +/- 10%

^{18}F-FDG and the time recorded. A detailed PET/CT protocol is described in our previous report.[45] For the patients who did not undergo PET/CT, regular pre- and post-contrast CT studies were performed with the same patient setup apparatus.

Post-contrast simulation CT images were imported into the Eclipse treatment planning workstation (version 8.6.0, Varian Medical Systems, Palo Alto, CA). Normal organs at risk (OAR) such as eyes, lenses, brain, skin, oral mucosa, bones, trachea, esophagus, mandibular salivary glands, spinal cord, optic chiasm, and tongue were identified and contoured. Mandibular and retropharyngeal lymph nodes were also contoured. Grossly identifiable tumor was delineated as the gross tumor volume (GTV) based on contrast enhancement and PET avidity. No expansion for potential subclinical diseases {GTV-to-clinical target volume (CTV) margin} was used. This is because SRT delivers a higher dose per fraction to the target and irradiating the surrounding normal tissues (that could be included in the CTV) with high dose per fraction increases the risk of late radiation toxicities. A uniform planning target volume (PTV) expansion (2 mm) was added to the GTV, lymph nodes, and all OARs. Computerized, three-dimensional image-based treatment planning using an inverse planning algorithm, tissue heterogeneity correction, and intensity modulation (sliding leaf technique with multi-leaf collimator) was used for all patients. 6 MV and/or 10 MV photon energies were used for all patients and typical plans consisted of equally-spaced 6-10 co-planar beams. Isocentric (100 cm) technique was used for all patients. Tissue-equivalent bolus was used when required. Plans were evaluated by visual inspection of dose color-wash and dose volume histograms and approved by an American College of Veterinary Radiology board-certified veterinary radiation oncologist. The regional lymph nodes were irradiated either prophylactically or with curative intent depending on the result of physical examination, CT or PET/CT images, and cytological examination. Quality

assurance of the plan and dose delivery was performed for each case by an American Board of Radiology certified therapeutic medical physicist.

On the day of treatment, patients were anesthetized and positioned on the treatment couch with the immobilization devices made at the time of CT/PET-CT examination. A Varian Trilogy linear accelerator (Varian Medical Systems, Palo Alto, CA) was used to administer SRT. Alignment of patient positioning was done by comparing digitally reconstructed radiographs that are created in the Eclipse workstation and/or original planning CT to two orthogonal kV images and/or cone-beam CT that were obtained with on-board imaging device.[44] Using an image comparison tool, appropriate couch shifts (X, Y, and Z directions, as well as couch rotation) were applied.

In this study, the proposed SRT protocol was 10 Gy x 3 fx (3 consecutive days) to the PTV but this was modified to 20 Gy x 1 fx because many patients had concurrent medical issues that precluded repeated anesthesia. This change was also approved by the IACUC.

Patient follow-up and evaluation of treatment response, outcome and toxicities: Patients were checked two weeks after the SRT either at the CSU-ACC or at the referring animal hospitals. All patients were followed-up every 2-3 months thereafter until their death or as needed. A follow-up CT or ^{18}FDG-PET/CT examination was performed to evaluate treatment response four weeks after SRT. Only contrast-enhanced CT images were used for this purpose to maintain consistency between patients. Complete remission (CR), partial response (PR), progressing disease (PD), and stable disease (SD) were defined as follows; CR = disappearance of detectable diseases, PR $\geq$ 30% reduction in the largest tumor dimension, PD $\geq$ 20 % increase in the largest tumor dimension, SD = between PR and PD. The severity of SRT-related acute and

late toxicities was evaluated at the time of recheck appointments and scored based on the published scoring schemes from the Veterinary Radiation Therapy Oncology Group (VRTOG).[46] Progression free interval (PFI) was defined as the time from the start of SRT to the clinically noticeable tumor recurrence or patient death, whichever comes first. Survival time (ST) was defined as the time from the start of the SRT to the patient death. Patients who died of disease-unrelated to the tumor/treatment were censored from PFI and ST analyses. Kaplan-Meier analysis was performed to estimate median PFI and median ST.

Histophathological grading: Grading system used was modified from a published system for human H&N tumors.[47] This system consisted of histological grading of malignancy of tumor cell population (degree of keratinization, nuclear polymorphism, and number of mitosis) and tumor-host relationship (pattern of invasion, stage of invasion, and lympho-plasmacytic infiltraion). Modifications were determined by the primary author and a boarded veterinary pathologist (EJE) (Table 5.2). This system was applied to the feline oral SCC of this study by the primary author with all grading overseen by this pathologist (EJE).

Mitotic index: MI was evaluated as described in our previously published study.[19] Briefly, MI was determined by counting mitotic cells in ten random HPFs (400x magnification) of H&E stained slides. The slides were read twice by a single author in a blind manner and the total numbers of cells in mitosis were divided by the numbers of HPFs counted to obtain an average MI (MIave). The maximum number of mitotic cells in these HPFs for each patient was also recorded as MImax and used as one of the variables. These results were confirmed by a boarded veterinary pathologist.

Immunohitochemistry for Ki67, Von-Willebrand factor (vWf, for MVD), and EGFR: The IHC protocol for Ki67, vWf, and EGFR are described in our previously published study.[19] Briefly, After antigen retrieval [citrate buffer (Dako target retrieval solution, Dako, Carpinteria, CA) for Ki67 and vWf, and with protease (Dako cytomation proteolytic enzyme, Dako, Carpinteria, CA) for EGFR for 1 min at 125 ℃] and blocking (Background sniper, Biocare medical, Concord, CA) for non-specific binding (10 minutes at room temperature), primary antibody [mouse anti-human Ki67 monoclonal (MIB-1, Dako, Carpinteria, CA) 1:50 dilution; rabbit anti-human vWf (A0082, Dako, Carpinteria, CA) polyclonal 1:300 dilution; mouse anti-human EGFR monoclonal (ab-10, Thermo Fisher Scientific, Fremont CA)1:50 dilution] was applied and incubated overnight at 4 ℃. After blocking endogenous peroxidase (3% hydrogen peroxide for 10 minutes), the slides were incubated with a universal secondary antibody (Dako Envision+ Dual link, Dako, Carpinteria, CA) for 20 min at room temperature. A diaminobenzidine substrate kit (DAB substrate kit for peroxidase, Vector Laboratories, Burlingame, CA) was utilized to detect immunoreactive complexes. The slides were counterstained with Mayer's hematoxylin and permanently mounted. Appropriate positive control slides were used for each batch and for all antibodies (feline lymph nodes for Ki67 and feline urinary bladder for vWf and EGFR). Negative controls were stained exactly the same as the tumor slides except for omission of the primary antibody.

Grading of IHC stains: The evaluation of Ki67 and EGFR was completed as our previously reported study.[19] Briefly, two readers graded all slides independently based on criteria described below. Grading was performed in a blind manner. Discrepancies were reviewed together at a multi-head microscope and consensus was reached. Grading was confirmed by a boarded veterinary pathologist. If no consensus was obtained, the reading was repeated.

Scoring of the protein expression of Ki67 and EGFR: Ki67 and EGFR staining was evaluated as previously reported by our group.[19] Briefly, the percent of positively-stained tumor cells (0; 0%, 1; 1-5%, 2; 6-20%, 3; 21-50%, 4; ≥51%)(Ki67%) and the average intensity of positively stained tumor cells (0; negative, 1; weak, 2; moderate, 3; strong, 4; very strong)(Ki67int) were recorded and these were multiplied to obtain a total score of 0 - 16 (Ki67total) for Ki67. For the EGFR, the percent of positively stained tumor cells (0; 0%, 1; <10%, 2; 11-30%, 3; 31-60%, and 4; ≥61%) (EGFR%) and the average intensity of positively stained tumor cells (0; negative, 1; weak, 2; moderate, 3; strong) (EGFRint) were scored and these were multiplied to obtain a total score (EGFRtotal).

Microvascular density analysis: MVD was evaluated as described in our previous study.[19] Briefly, blood vessels positive for vWf was quantified using a microscope equipped with a CCD camera (Carl Zeiss Axioplan 2 imaging scope, Carl Zeiss, Thornwood, New York) and image analysis software (Axio Vision 4.3 system software, Carl Zeiss, Thornwood, New York). After scanning the entire field under low power field (40x magnification), the highest microvascular density area (hot spot) close to tumor cells was determined subjectively.[48] Then, at 200x magnification, two distinct hot spots were picked from each slide and captured. MVD was expressed as the ratio of positively-stained pixels of representative endothelium over the total amount of image pixels and the results from these two slides were averaged (Auto%Ave). Higher percentile among these two images was also recorded as Auto%Max. We also counted the number of microvessels manually as a previous study and averaged them to obtain ManualAve and the maximum count among the two hot-spot images was also recorded as ManualMax.[48]

pO_2 measurement: pO_2 in the tumor was measured immediately before and 24 hours after SRT. pO_2 was also measured in an accessible normal-looking area of mucus membrane outside of the

treatment field to serve as an internal control. Tissue pO_2 was measured using a fiber-optic pO_2 measurement system (OxyLite system, Oxford Optronics, UK) with a "large area" probe with an 8 mm window for pO_2 measurement. After inducing general anesthesia, patients inhaled admixed oxygen which was set to 28% of pO_2 and were maintained for at least 15 minutes to equalize the oxygen concentration in the body. This produces a pO_2 within the normal range for patients at altitude.[49] The site and insertion angle of the probe were decided based upon the planning CT. The site for the normal tissue pO_2 was decided for each case, depending on the patient position and tumor location. Sites were then gently cleaned with 4% chlorhexidine and saline. A small skin/mucosal incision was made with a #11 scalpel blade. The sheath of a 24 G intravenous catheter was used to pass the oxygen probe into the tumor and the normal tissues. Probe positioning was visually confirmed. Once the probes were placed in the tissues, pO_2 measurement was started. All data was recorded using software provided by the manufacturer (Chart5, Oxford Optronics, UK). Typically, it took approximately 5 to 10 minutes until the measurement reading stabilized. Once the measurement was completed, probes were pulled out and the incision sites were cleaned appropriately. All probes were calibrated before each measurement following manufacturer's instructions. After the measurement, the pO_2 data was reviewed using the provided software. Final data was obtained by averaging approximately 10 seconds of reading after reached stable status. Two-tailed, paired t-test was performed to evaluate changes in pre- and post-SRT pO_2 in tumor and normal tissue.

Evaluating markers as a prognostic factor for ST and PFI: Patients were divided into two groups; above or below the median result of each marker ("high" and "low" groups, respectively). A Log-Rank test was performed to evaluate for a prognostic significance for ST and PFI. Univariate Cox-proportional hazard analysis was also performed. Patient factors

included for those analyses were sex, age at the time of diagnosis of oral SCC, body weight at the time of SRT, clinical stage, volume of GTV, and tumor location. Variables with those *P*-values < 0.05 in either Log-Rank or univariate Cox-proportional hazard analysis were included in multivariate Cox-proportional hazard analysis.

Difference of IHC markers, histopathological grading, pre-SRT tumor pO_2, and volume of GTV between clinical stages or tumor locations: Patients were sorted into either clinical stage II or stage III/IV. Patients were also grouped into either mandibular/maxillary or tongue/laryngeal group. Between these groups, statistical analyses were performed to evaluate any difference in IHC scores, pre-SRT tumor pO_2, and volume of GTV. Student's t-test was performed for the pre-SRT tumor pO_2 and the volume of GTV. Mann-Whitney rank sum test was performed for the MI and the MVDs. Fisher exact test was performed for the Ki67, the EGFR, and the histopathological grading.

Statistical analysis: All statistical analysis was performed using commercially available software (SigmaStat version 3.5 and SigmaPlot version 12, Systat Software, San Jose, CA). A *P*-value < 0.05 was considered statistically significant.

Results

Patient information, ST, and PFI: Fifteen domestic short hair, four domestic long hair, and one Siamese were included in the study. Tumor locations included mandible (11), lingual/laryngeal (6), and maxilla (3). There were twelve neutered males, seven neutered females, and one intact female. Mean patient age and body weight at diagnosis were 12.5 y.o. and 4.4 kg, respectively. There were nine each patients in clinical stage II and stage III and two patients were in stage IV.

All histopathological grading criteria were (Table 5.2) subjectively evenly distributed except the stage of invasion since most cases had invaded into the adjacent muscles (data not shown). Information regarding sex, age, and body weight of the patients, tumor location, clinical stage, volume of GTV, prescribed dose, maximum, mean, and 95% doses of PTV, ST, PFI, and reason of death are listed in Tables 5.3 and 5.4. One of the two patients who received 10 Gy x 3 fractions (#3) received an additional fraction of 20 Gy when the tumor recurred 104 days after the first fraction of SRT. One of the 17 patients (#19) who received 20 Gy x 1 fraction underwent multiple cytoreductive surgeries when the tumor recurred 108 days after the start of SRT. For these two patients, PFI was determined at time of first recurrence. Among the 20 patients, twelve had PET/CT examination and eight had CT examination for SRT planning. There were two patients with metastatic lymph nodes. One of them had a large SCC at left side of the neck and the mandibular and retropharyngeal lymph nodes were considered contiguous to the original tumor mass. The other patient had a metastatic superficial cervical lymph node. This patient received 16.2-16.6 Gy to its mandibular, retropharyngeal, and cervical lymph nodes.

Among the 20 cats, two cats were euthanized due to tumor/treatment-unrelated problems both at day 21 (Case#4: heart failure, case#6: acute renal failure) (Table.5.4). These two cats had no obvious progression of disease when they were euthanized. They were censored from ST and PFI analysis. Median ST was 106 days (range: 14-359 days) (Figure 5.1A). Median PFI was 87 days (range: 14-206 days) (Figure 5.1B) (range: 14-206 days)

Thirteen cats underwent either CT or ^{18}F-FDG PET/CT 30 days post-SRT in average. Among them, two cats (15.4 %) showed CR, eight cats (61.5 %) showed SD, and three cats (23.1 %) showed PR. Overall response rate was 38.5 % (Table 5.4).

Evaluating markers as a prognostic factor for ST and PFI: As previously reported, Ki67 showed nuclear staining.[19] vWf and EGFR showed cytoplasmic and membranous staining, respectively.[19] Log-Rank test revealed multiple variables that were significantly prognostic for ST and PFI. For ST, EGFRint, ManualAve, patient sex, and volume of GTV showed statistically significant differences between the two groups. To evaluate prognostic importance of these variables by accounting for mutual impact, we conducted multivariate Cox-proportional hazard analysis (Table 5.5). This test revealed that patients with higher ManualAve (P=0.041, RR=1.06, 95% CI=1.002, 1.1) (Figure 5.2 A-B, Figure 5.3 A) or male patients (P=0.025, for female: RR=0.26, 95% CI=0.08, 0.84) had significantly shorter ST than patients with lower ManualAve or female patients (Table 5.5). For PFI, EGFRint, degree of keratinization and patient sex are statistically significant in the Log-Rank analysis. In the multivariate Cox-proportional hazard analysis, patients with higher degree of keratinization (P=0.049, RR=0.087, 95% CI=0.0076, 0.99) (Figure 5.2 C-D, Figure 5.3 B) or male patients (P=0.016, for female: RR=0.17, 95% CI=0.042, 0.72) had significantly shorter PFI (Table 5.6). No other histopathological grading parameters showed a statistical significance.

Patients #1 and #3 received 10 Gy x 3 fractions whereas other 18 patients received 20 Gy x 1 fx. Also, patient #19 underwent multiple cytoreductive surgeries when the tumor recurred. Therefore, we conducted the same ST analysis but this time, without these three cases. When patient #1, 3, 19 were excluded from the ST analysis, patients with higher ManualAve (P=0.014, RR=1.1, 95% CI=1.02, 1.3) or male patients (P=0.007, for female: RR=0.042, 95% CI=0.0039, 0.42) still had significantly shorter ST in the multivariate Cox-proportional hazard analysis. Because patients #1 and 3 underwent different SRT protocol from other 18 patients, PFI analysis without these 2 patients were also performed. In this analysis, male patients (P=0.038, for

female: RR=0.13, 95% CI=0.019, 0.89) still had significantly shorter PFI in the multivariate Cox-proportional hazard analysis.

pO_2 measurement: Pre- and post-SRT pO_2 in tumor and normal tissue were summarized in Figure 5.4. pO_2 measurement was not performed in one patient (SCC# 10) due to the patient's condition while under anesthesia. Four of the 19 patients had only the pre-SRT pO_2 measurement (SCC#2,4,16: poor general condition, SCC#8: equipment failure). Paired t-test revealed that post-SRT tumor pO_2 was significantly lower than pre-SRT tumor pO_2 (n=15, mean 19.2 mm Hg vs 11.02 mm Hg, P=0.047) (Figure 5.4). Paired t-test also revealed that pO_2 in pre-SRT tumor (n=18) and post-SRT tumor (n=15) are significantly lower than those in pre-SRT normal tissue and post-SRT normal tissue, respectively (both $P < 0.001$, 21.5 mm Hg vs 75.8 mm Hg and 11.02 mm Hg vs 68.8 mm Hg, respectively) (Figure 5.4). pO_2 in the normal tissues was normal in both pre- and post-SRT.

Difference of IHC markers, pre-SRT pO_2, and volume of GTV between patients with different clinical stages or tumor locations: Statistically significant difference was not found between clinical stages II and III/IV. Statistical analyses revealed that patients with Tongue/Laryngeal tumors had significantly higher ManualAve and ManualMax than patients with Mandibular/Maxillary tumors (both $P \leq 0.001$).

SRT-related toxicities: Toxicities and treatment-related complications are summarized in Table 5.7. No patients showed acute toxicity in skin or mucous membrane with (VRTOG) scores 2 or higher. Patient #13 showed refractory glaucoma in the left eye approximately 2 months after SRT. CT examination which was performed at this time revealed local tumor progression but the exact cause of glaucoma of the left eye could not be determined. Other patients showed no late

effects or score 1 late effect in their skin/hair or eyes. Fractured/displaced mandible was observed in 6 of 11 mandibular cases, fibrosis in 3 of 6 lingual/laryngeal cases, and oro-nasal fistula in 1 of 3 maxillary cases.

Discussion

Feline oral SCC is a locally aggressive cancer that responds to local treatment initially but almost always recurs locally.[43] Although our knowledge about its etiology/biology has been deepened by previous studies,[19, 50, 51] knowledge about tumor biology that possibly leads to better local tumor control is still scarce.[7, 9, 52-55] Our current study was to evaluate the biological variables that possibly act as a prognostic marker in feline patients with oral SCC treated by the novel type of radiation therapy, SRT.

We found that patients with higher MVD had shorter ST compared to patients with lower MVD. This finding is in contrast to a previous human study in which treatment outcome of patients with H&N SCC was worse in patients with lower MVD.[23] In that study, patients underwent fractionated radiation therapy instead of SRT. Although not proven in human patients, it has been presumed that the tumoricidal effect of SRT, which typically delivers higher dose per fraction, consists of radiation damage directly to the cancer cells and indirect damage secondary to tumor vasculature damage whereas the effect of fractionated XRT is mainly from the direct killing of the cancer cells.[24] It has also been shown that the MVD decreases immediately after a large single dose of radiation (10-15 Gy), remains reduced for varying periods, and occasionally re-grows to the original level.[24] In a study with human glioblastoma, tumor started re-growing when blood perfusion recovered 3 weeks after an initial reduction in MVD and perfusion and an

increase of hypoxic fraction caused by a single large dose of radiation (15 Gy).[56] Although we did not evaluate MVD serially and the correlation between MVD and tissue hypoxia is still unclear, patients with higher pre-SRT MVD may have had more surviving tumor vasculature and a lower hypoxic fraction compared to patients with lower pre-SRT MVD, resulting in continuous proliferation of cancer cells. This may have led to significantly earlier local failure in patients with higher pre-SRT MVD in the current study. This result suggests that additional treatments targeting tumor vasculature such as metronomic chemotherapy may be beneficial although this additional treatment may also increase the chance of normal tissue late toxicities by damaging normal endothelial cells unless the treatment is targeted to the tumor vasculature. Further study of serial evaluation of the change in MVD before and post-SRT is needed.[57]

Statistical analyses revealed that patients with less keratinized SCC had longer PFI compared to patients with more keratinized SCC. In human H&N SCC, one study reported that lower degree of keratinization correlates to better treatment outcome.[58] Other studies also showed that human patients with more differentiated SCC had significantly poorer local tumor control than patients with less differentiated SCC.[59, 60] The patients in these three studies underwent conventional fractionated XRT. Keratinized SCC is generally considered to be more differentiated. Less differentiated tumors are generally considered to be more aggressive. Although these results seem counterintuitive, our result regarding the degree of keratinization is in accordance with the findings in human SCC studies. Because this variable is easily evaluated using H&E stained tumor specimens, it might be worth continuing to evaluate the prognostic significance to verify its usefulness in a larger patient population.

We found that the male patients had significantly shorter ST and PFI compared to female patients. As of our knowledge, this has never been reported and a plausible reason for the difference between males and females still needs to be investigated in a larger patient population.

Patients with low scores of EGFR intensity had significantly shorter ST and PFI than those with high scores in the Log-Rank analyses although this was not significant in the multivariate Cox-proportional hazard analysis. Further investigation is needed to exclude the chance of type II error caused by the small sample population in the current study.

In the current study, median ST and median DFI were 106 and 87 days, respectively. Although inter-study comparison is difficult, these outcomes in the current study do not appear to be superior to previous studies.[3, 5, 8] However, advantages of the current study include fewer anesthesia events, less cosmetic and functional changes compared to more radical surgery, and lower probability of side effects compared to other type of palliative radiation therapy.[1] The major disadvantage of SRT is its cost. Because the current study failed to prove an advantage in long term local control over other treatment modalities and SRT showed about 40% of overall response rate with rapid improvement of clinical symptoms in many cases, it should be considered as a palliative treatment as is in human H&N SCC.[26-28]

Tumor vasculature is not the same as normal tissue vasculature.[61] Tumor vasculature is characterized by its tortuous, dilated, dead-ended, and leaky structure.[30, 61] It has been shown that the tumor vasculature is less dense and less effective to deliver oxygen and nutrients to the surrounding cells.[61] Moreover, blood flow in the tumor is slow and bi-directional.[61] Although no study has evaluated the blood flow dynamics and vascular structure in feline oral SCC, it might be reasonable to assume that these well-known characteristics of tumor vasculature can be

applied to this feline cancer. In our study, we performed direct measurement of tissue pO_2 in the oral SCC and nearby normal tissues using a fiber-optic system. In human H&N SCC, tumor pO_2 as a prognostic value has been extensively studied with controversial results.[2, 34, 41, 62]. In the current study, no correlations were found between pre-SRT tumor pO_2 and ST or PFI. There are a couple of possible explanations for this result. First, the treatment protocol in the current study (SRT) was different from these previous studies that used fractionated protocols. Second, the oxygen measurement probe used in the current study was different from the one used in previous reports, in which polarographic oxygen probes were used.[34, 62] In our study, we used the fiber-optic probe. Although histogram analysis is probably the most ideal technique that is currently available to evaluate tissue oxygen status, we obtained a single-point reading of pO_2 with a wide window probe. This probe has an 8 mm of reading window and therefore, the pO_2 readout is the average of the pO_2 around the window. Given the fact that the tissue pO_2 changes dramatically in less than 100 um,[29] hypoxic areas may have been masked by non-hypoxic areas with this averaging. However, the fiber-optic probe has some advantages over the polarographic probes and those include higher sensitivity in the lower range (pO_2<10 mm Hg) of pO_2 and no oxygen consumption by the probe.[63] Even with those advantages, fiber-optic probes lack spatial information of pO_2 and a novel pO_2 measurement modality which allows us quick and accurate measurement in multiple points and is as practical as the fiber-optic system will be needed to deepen our knowledge about tumor pO_2.

In the current study, pre-SRT mean pO_2 in the tumor was significantly lower than that in the normal tissues. A statistically significant difference between the tumor and normal tissues was also seen at 24 hrs after SRT. These findings are in accordance with the general consensus that tumor is more hypoxic than normal tissues.[62, 64] On the other hand, as is shown in Figure 5.4,

we observed a large inter-patient variation of pO_2 in normal tissues. This variation has been reported in human literature too.[62, 64, 65] These previous studies have also shown that there is a large intra-patient/intra-organ heterogeneity of pO_2, by using the histogram technique. Although we performed only a "single-point measurement" in the normal subcutaneous tissues, the inter-patient heterogeneity we observed may suggest that the oxygenation status in feline normal tissues is similar to that in human normal tissues. Previous reports have also shown that there is some inter-patient heterogeneity in tumor pO_2.[2, 34, 41, 62] Although different measurement techniques were used among the previous studies as well as between these studies and our current studies, the heterogeneity in tumor pO_2 we observed may suggest that it might be worth further investigation for prognostication. Tumor oxygenation status is an important tumor-microenvironmental factor that affects the response of tumor to radiation therapy especially photon therapy.[29] For photon radiation therapy, oxygen enhancement ratio (OER), an indicator of how much higher dose is required under hypoxic condition to obtain the same radiobiological effects seen under oxygenated condition, has been reported to be around 2.5 at lower dose range (~3 Gy) and become higher up to 3.5 as the dose increases (5-25 Gy) in Chinese hamster cells.[29] Although we showed that the pO_2 in the tumor is lower than that in the surrounding normal tissues, an obvious question would be the magnitude of hypoxia at which level we see a significant reduction in radiobiological effects. A study that was reported in 1953 has shown that about 3 mm Hg of pO_2 (0.5 %) is required to obtain 50 % radiosensitivity of fully oxygenated tumors and under 30 mm Hg of pO_2, cells are 100 % radiosensitive.[66] This data, however, was obtained by using mouse tumor cells and some plant cells and therefore, it may not be appropriate to extrapolate these numbers directly to feline oral SCC and other types of malignancies. Clinically, there are studies that evaluated significance of pre-treatment tumor pO_2

as a prognostic marker for human H&N SCC patients treated with fractionated radiation therapy.[2, 33, 34, 41, 62, 67] One of these studies evaluated pO_2 in 397 patients with H&N SCC.[33] In this study, patients whose fraction of $pO_2 \leq 2.5$ mm Hg was less than 19% of total measurement had significantly better overall survival than those whose fraction of $pO_2 < 2.5$ mm Hg was more than 19 %. Moreover, the fraction of $pO_2 \leq 2.5$ mm Hg was the most statistically significant prognostic marker for patient survival.[33] Patients in this study underwent curative intent fractionated XRT with or without chemotherapy/surgery. Four other studies set the cut-off value pO_2 between 2.5-10 mm Hg and found significantly worse prognosis in patients with higher hypoxic fraction.[2, 34, 41, 67] Therefore, it may be reasonable to assume that clinically significant cut-off value for the pO_2 histogram in human patients with H&N SCC treated with fractionated radiation therapy is between 2.5-10 mm Hg. In the current study, however, we treated patients with feline oral SCC with SRT, not fractionated protocol. As mentioned below, it seems like that there is a substantial difference in the events occurring in the tumor cells and their microenvironment in response to radiotherapy between SRT and fractionated regimen. Furthermore, because the method we performed averages the pO_2 around the probe, it does not provide us a histogram. And finally, our study has smaller patient population compared to these human H&N SCC studies. Because of these differences/limitations in the current study, our future direction to understand the clinical impact of tumor oxygenation includes a more detailed pO_2 measurement such as histogram evaluation in a larger patient population.

In contrast to the well-accepted concept of re-oxygenation after a small fraction of radiation, we did not observe an increase of tumor pO_2.[29] Instead, we observed a significant reduction of tumor pO_2 after SRT. Previous studies with xenograft models suggested that when higher dose per fraction is used, radiation damage to the endothelial cells becomes critical and

leads these cells to initiate apoptotic cascades as early as 3 hours post-irradiation [68, 69] In the mouse xenograft model, the threshold dose for endothelial cell death has been suggested to be around 10 Gy.[68] In a study with human H&N SCC mouse xenograft, a single dose of 10 Gy caused a significant reduction of hypoxic fraction with a minimum value reached at 7 hrs post-irradiation followed by a steady increase of the hypoxic fraction until 11 days post-irradiation.[70] The hypoxic fraction at that time (11 days post-irradiation) was significantly higher than that at between 2 hrs and 96 hrs post-irradiation.[70] Although the endothelial cell damage, at least partially, may be the cause of the significant reduction of tumor pO_2 after SRT observed in the current study, spatial and serial information of pO_2 and MVD is essential to understand the *in vivo* effect of SRT on the tumor endothelial cells and tumor microenvironment more in detail.

In our previous study, we reported that the MVD in lingual SCC tended to be higher than that in mandibular/maxillary SCC.[19] In the current study, we found the same difference between tongue/laryngeal group and mandibular/maxillary group, but this time the difference was statistically significant ($P<0.001$). The impact of this significant difference to the patient outcome is unclear because the tumor location (mandibular/maxillary vs tongue/laryngeal) was not a prognostic factor in our current study. In order to clarify this discrepancy between our current and previous studies, we think that it is important to increase the patient population and continue evaluating the difference in MVD between lingual/laryngeal SCC and mandibular/maxillary SCC.

In the current study, no patients showed acute or late toxicities with score of 3 in the skin/mucous membrane, however, survival time was not long enough to adequately study late effects (Table 5.7). No patients showed acute toxicities or if they did, the score was 1 in skin, or mucous membrane. These acute toxicities were self-limiting and no treatment was indicated.

There was a patient with possible radiation-induced glaucoma in the left eye recognized 8 weeks post-SRT (patient #13). This patient had left maxillary SCC and received a single fraction of 20 Gy. The left eye was in the treatment field. Although the multileaf collimator was used to minimize the dose to the left eye, approximately 30 % of the eye, mostly the ventral aspect, received 10 Gy. Postmortem examination of the eye was not performed due to owner's request. A CT examination at the time of diagnosis of the glaucoma revealed significant progression of SCC but could not differentiate whether the glaucoma was caused by tumor progression or toxicity of SRT. Because there are only three maxillary SCC cats whose ST is more than 2 months, it is difficult to decide the precise incidence rate of SRT-related glaucoma at this point. In the future, patients with maxillary SCC should be closely watched post-SRT for any signs of intra-ocular inflammation or glaucoma. In the other patients with mandibular, laryngeal, or lingual SCC, there was no sign of acute/late toxicity in their eyes, demonstrating the advantage of a sharp drop-off of radiation dose outside the treatment target for intensity modulation and SRT. We also observed fracture of mandible, lingual fibrosis, and oro-nasal fistula formation typically 2-3 months post-SRT. Those complications were seen in 50 % of cats in the current study. Although clear distinction of the cause of those complications is impossible (radiation-induced toxicity vs tumor invasion or tumor-induced inflammation), it may be safe to assume that the complication rate following SRT is relatively high in cats with locally advanced oral SCC. Unless effective reconstruction techniques or tissue engineering is developed, it is likely that these complications will continue to be a problem in patients with any type of destructive oral malignancies.

In conclusion, although the tumor rapid response to SRT with alleviation of clinical symptoms and fewer anesthesia episode are advantages of SRT, the associated cost, the higher

chance of late complications, and relatively short period of local tumor control limit the use of this modality as a sole treatment, especially the protocol of a single fraction of 20 Gy, to a palliative purpose only. MVD and degree of keratinization appear to be prognostic indicators for patients undergoing SRT and anti-angiogenic treatment may help improving local tumor control. Changes in tumor pO_2 following SRT in feline oral SCC suggests tumor vasculature in this tumor responds in a similar fashion as is reported in human H&N SCC but serial monitoring might allow more detailed insight about its dynamics. This may also help identify possible treatment targets that amplify the effect of SRT. Acute toxicity was minimal, although late toxicities/treatment-related toxicities impacted patient quality of life.

Table 5.1: Clinical staging scheme for feline oral tumors

Primary Tumor (T)	
T1	Tumor <2 cm in diameter at greatest dimension, without evidence of bone invasion (a) or with evidence of bone invasion (b)
T2	Tumor 2-4 cm in diameter at greatest dimension, without evidence of bone invasion (a) or with evidence of bone invasion (b)
T3	Tumor >4 cm in diameter at greatest dimension, without evidence of bone invasion (a) or with evidence of bone invasion (b)

Regional Lymph Nodes (N)	
N0	No regional lymph node metastasis
N1	Movable ipsilateral lymph nodes, without evidence of lymph node metastasis (a) or with evidence of lymph node metastasis (b)
N2	Movable contralateral lymph nodes, without evidence of lymph node metastasis (a) or with evidence of lymph node metastasis (b)
N3	Fixed lymph nodes

Distant Metastasis (M)	
M0	Distant metastasis not detected
M1	Distant metastasis detected

Stage Grouping	**Tumor (T)**	**Nodes (N)**	**Metastasis (M)**
I	T1	N0, N1a, N2a	M0
II	T2	N0, N1a, N2a	M0
III	T3	N0, N1a, N2a	M0
	Any T	N1b	M0
IV	Any T	N2b, N3	M0
	Any T	Any N	M1

Table 5.2: A modified histopathological grading scheme for feline oral squamous cell carcinoma.

Morphologic parameter	Points			
	1	2	3	4
Histologic grading of malignancy of tumor cell population				
Degree of keratinization	Highly keratinized (>50% of the cell)	Moderately keratinized (20-50% 0f the cells)	Minimal keratinization (5-20% of the cells)	No keratinization (0-5% of the cells)
Nuclear polymorphism	Little nuclear polymorphism (>75% mature cells)	Moderately abundant nuclear polymorphism (50-75% mature cells)	Abundant nuclear polymorphism (20-50% mature cells)	Extreme nuclear polymorphism (0-25% mature cells)
Number of mitosis/HPF (x400)	$0 < MI \leq 1.5$	$1.5 < MI \leq 3.0$	$3.0 < MI \leq 5$	$MI > 5$
Histologic grading of malignancy of tumor-host relationship				
Pattern of invasion	Pushing, well-delineated infiltrating borders	Infiltrating, solid cords, bands and/or strands	Small groups or cords of infiltrating cells (n>15)	Marked and widespread cellular dissociation in small groups of cells (n<15) and/or in single cells
Stage of invasion (depth)	Carcinoma *in situ* and/or questionable invasion	Distinct invasion, but involving lamina propria only	Invasion below lamina propria adjacent to muscles, salivary gland tissues and periosteum	Extensive and deep invasion replacing most of the stromal tissue and infiltrating jaw bone
Lympho-plasmacytic infiltration (at x20)	throughout every field	some within every field	only in some fields	None

Table 5.3: Summary of patients' profile

Patient#	Sex	Age (years)	BW (kg)	Tumor location	Clinical Stage	GTV volume (cm^3)
1	FS	12.7	5.1	R mandible	II: T2b, N0, M0	4.9
2	MI	14.2	3.8	R mandible	III: T3b, N0, M0	12.8
3	FS	6.2	3.3	R maxilla	II: T2b, N0, M0	5.9
4	FS	13.3	4.5	R mandible	II: T2b, N0, M0	11.8
5	MC	12.2	5.6	R mandble	III: T3b, N0, M0	38.9
6	MC	13.3	7.3	L mandible	III: T3b, N0, M0	22.9
7	MC	9.8	6.1	L mandible	III: T3b, N0, M0	18.1
8	FS	12.8	2.5	R mandible	II: T2b, N0, M0	2.6
9	MC	12.5	4.3	sublingual	II: T2a, N0, M0	5.3
10	MC	17.7	2.8	R mandible	III: T3b, N0, M0	13.2
11	MC	10.5	4.1	laryngeal	IV: T3a, N3, M0	29.3
12	MC	13	5.2	sublingual	III: T3a, N0, M0	13.5
13	MC	16.7	4	L maxilla	II: T2b, N0, M0	13
14	MC	8.1	4.8	laryngeal/lingual	II: T2a, N0, M0	5.1
15	FS	13.5	5	R mandible	III: T3b, N0, M0	18.8
16	MC	11.1	2.8	R mandible	IV: T3b, N1b, M0	21.3
17	FS	14.3	4.5	sublingual	II: T2a, N0, M0	6.8
18	MC	15	3.2	R mandible	III: T3b, N0, M0	24.7
19	MC	10.7	4.5	sublingual	II: T2a, N0, M0	1.3
20	FS	11.5	4.1	R maxilla	III: T3b, N0, M0	31.7

BW, Body weight; GTV, Gross tumor volume; MC, Male castrated; MI, Male intact; FS, Female spayed; L, Left; R, Right

Table 5.4: Summary of prescribed protocol, doses to planning target volume, survival time, progression free interval, reason of death, and treatment response.

Patient#	SRT prescription	Dose to PTV (Gy)			ST (days)	PFI (days)	Reason of death	Treatment response
		Maximum	Mean	95%				
1	10 Gy x 3	33.1	29.8	28.8	132	131	PD	SD
2	20 Gy x 1	27.8	18.6	15	156	156	PD	-
3	10 Gy x 3 + 20Gy x 1	35.9	30.7	26.2	359	104	PD	SD
4	20 Gy x 1	27.7	18.9	15.8	21	21	Heart failure	-
5	20 Gy x 1	27.4	20.2	16.8	69	69	PD	-
6	20 Gy x 1	31.6	22.4	17.4	21	21	Acute Renal Failure	-
7	20 Gy x 1	32.8	22.7	18.2	84	84	PD	SD
8	20 Gy x 1	27.3	20.7	19.5	206	206	PD	CR
9	20 Gy x 1	30.7	22.3	19	77	75	PD	CR
10	20 Gy x 1	27.3	20.5	13	23	23	PD	-
11	20 Gy x 1	30	21.8	15.3	106	87	PD	SD
12	20 Gy x 1	30.8	22.4	19.7	44	44	PD	SD
13	20 Gy x 1	31.2	22.6	19.2	104	54	PD	SD
14	20 Gy x 1	28	19.2	15.8	84	59	PD	-
15	20 Gy x 1	31	21.5	18.2	190	164	PD	SD
16	20 Gy x 1	34.4	22.7	19.2	14	14	PD	-
17	20 Gy x 1	29.2	21.8	19.4	140	140	PD	PR
18	20 Gy x 1	28.7	21.8	17.7	70	57	PD	PR
19	20 Gy x 1 + cytoreductive surgery	26.7	21.4	19.8	355	108	PD	PR
20	20 Gy x 1	3.03	23.1	18.3	145	128	PD	SD

CR: complete response, PD: progressed disease, PFI: progression-free interval, PR: partial response, PTV: planned target volume, SD: stable disease, SRT: stereotactic radiation therapy, ST: survival

Table 5.5: Results of survival analysis. For each group, number of patient, median and range of survival time, *P*-value of Log Rank test, *P*-value of multivariate Cox proportional hazard analysis, relative risk, and lower/upper 95% confidence interval are shown.

MVD (ManualAve)	n, (median), range	Sex	n, (median), range
Low	10 (156), 70-359	**Female**	7 (145), 132-359
High	10 (77), 14-145	**Male**	13 (84), 14-156
Log Rank *P*-value	0.011	**Log Rank *P*-value**	0.029
Cox *P*-value	0.041	**Cox *P*-value**	0.025
RR (95% CI)	1.06 (1.002, 1.1)	**RR (95% CI)**	0.26 (0.08, 0.84)

CI: Confidence interval, MannualAve: average of manually counted microvessels, MVD: microvascular density, RR: risk ratio.

Table 5.6: Results of progression-free interval analysis. For each group, number of patient, median and range of progression-free interval, *P*-value of Log Rank test, *P*-value of multivariate Cox proportional hazard analysis, relative risk, and lower/upper 95% confidence interval are shown.

Degree of keratinization	n (median), range	Sex	n (median), range
Low	14 (69), 14-131	**Female**	7 (131), 104-206
High	6 (156), 75-206	**Male**	13 (69), 14-156
Log Rank *P*-value	0.003	**Log Rank *P*-value**	0.005
Cox *P*-value	0.049	**Cox *P*-value**	0.016
RR (95% CI)	0.087 (0.0076, 0.99)	**RR (95% CI)**	0.17 (0.042, 0.72)

CI: Confidence interval, RR: risk ratio

Table 5.7: Treatment-related toxicities and complications.

Patient#	Acute effects			Late effects		Treatment-related complications
	Skin	Mucous membrane	Eyes	Skin/hair	Eyes	
1	0	0	0	1	0	Fractured mandible
2	0	0	0	0	0	Fractured mandible
3	0	0	0	1	0	
4	0	0	0	-	-	Fractured mandible
5	1	0	0	-	-	Fractured mandible
6	0	0	0	-	-	Fractured mandible
7	0	0	0	-	-	
8	0	0	0	0	0	
9	0	0	0	-	-	
10	1	0	0	-	-	
11	0	0	0	0	0	
12	0	0	0	-	-	Fibrosis
13	0	0	1	1	2	
14	0	1	0	0	0	
15	1	0	0	1	0	Fractured mandible
16	1	0	1	-	-	
17	1	0	0	0	0	Fibrosis
18	1	1	0	0	0	
19	0	0	0	0	0	Fibrosis
20	1	0	0	1	0	Oro-nasal fistula

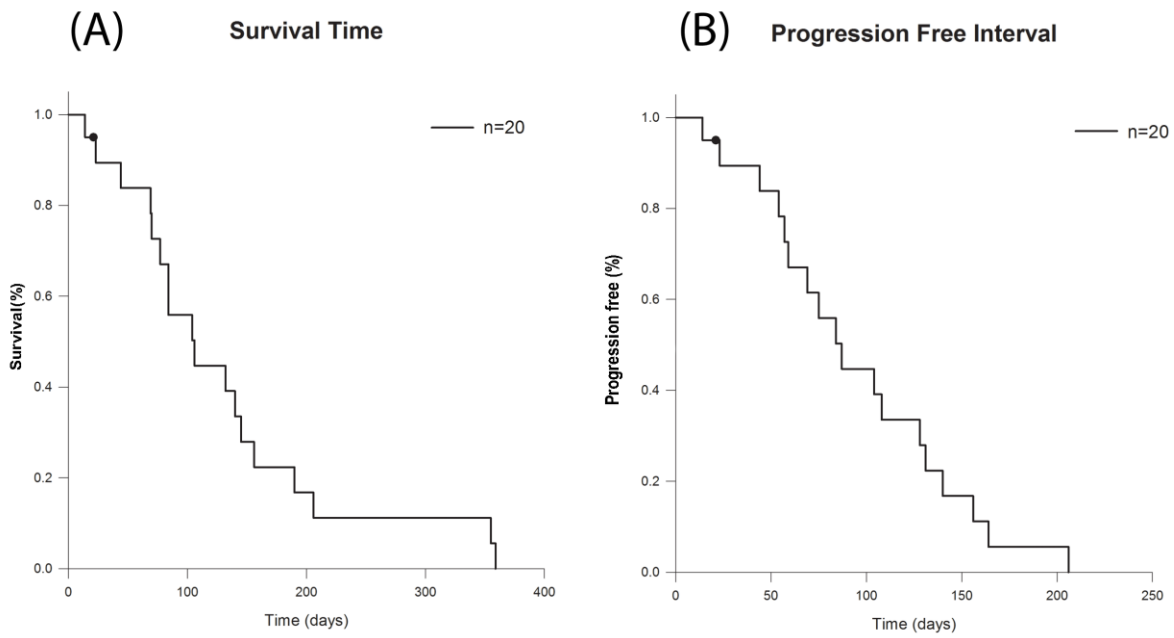

Figure 5.1: Kaplan-Meier graphs representing (A) survival time and (B) progression free interval of feline patients with oral squamous cell carcinoma treated by stereotactic radiation therapy. Black circles indicate censored patients.

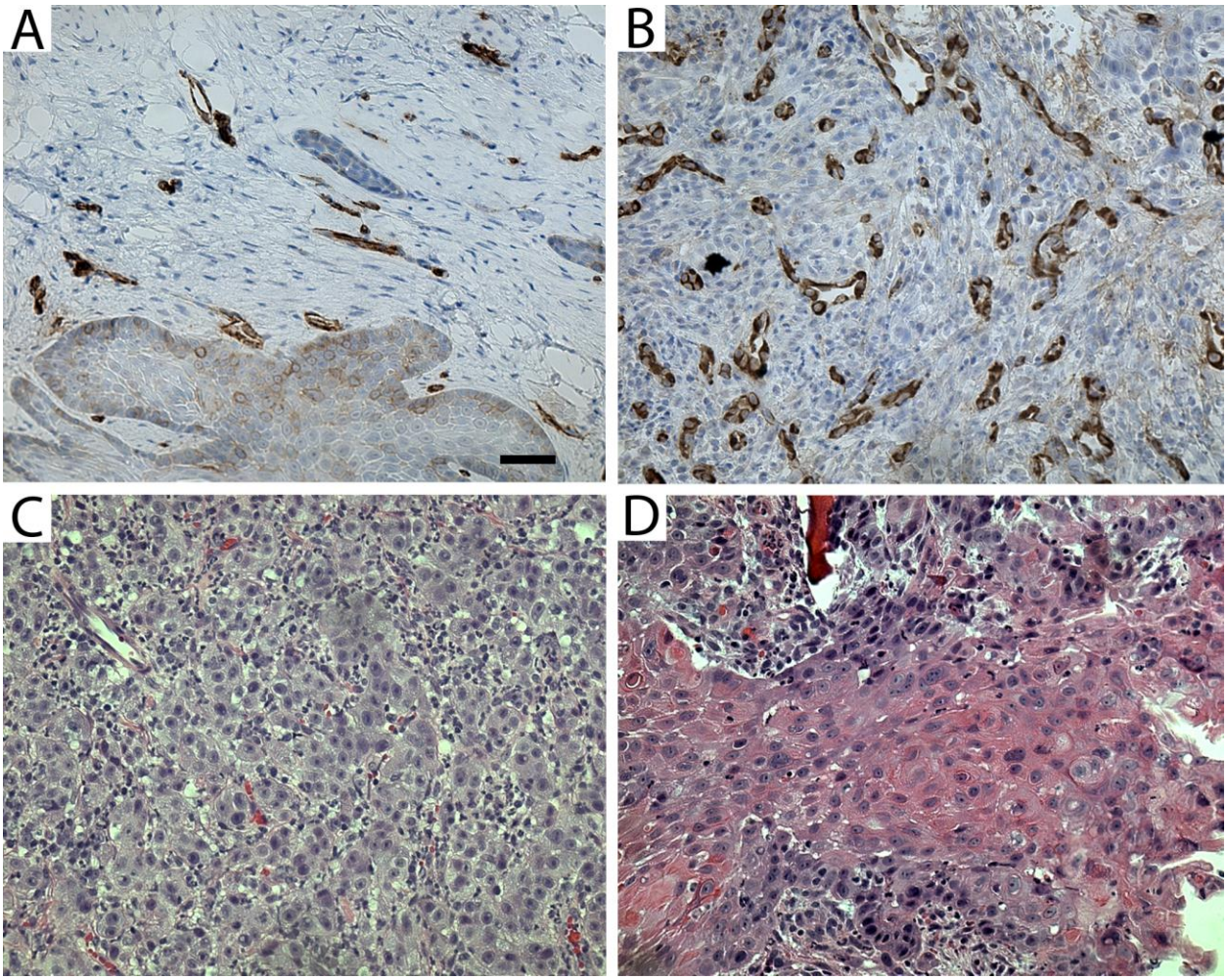

Figure 5.2: Representative microscopic images of (A) low and (B) high microvascular density and (C) low and (D) high degree of keratinization. Bar=20 µm.

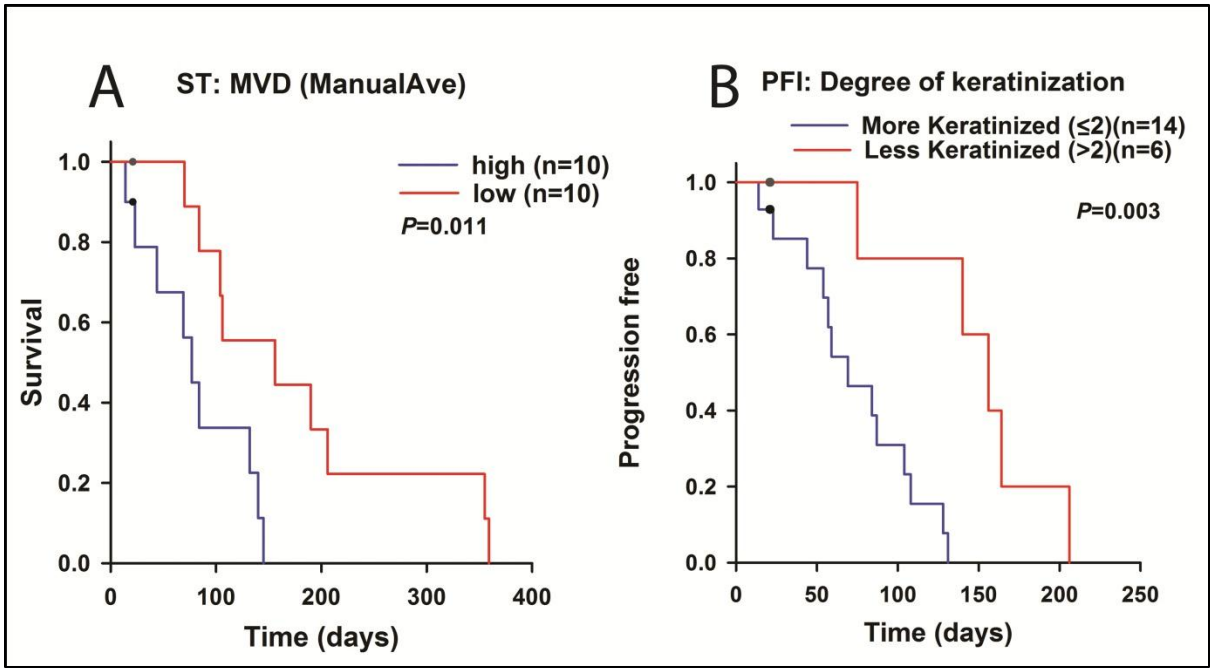

Figure 5.3: Kaplan-Meier graphs representing outcome of feline patients with oral squamous cell carcinoma treated by stereotactic radiation therapy. (A) Survival time stratified by low (red) or high (blue) in the microvascular density (ManualAve). (B) Progression free interval stratified by low (blue, more keratinized group) or high (red, less keratinized group) in scoring of the degree of keratinization histopathological grading system. Black circles indicate censored patients.

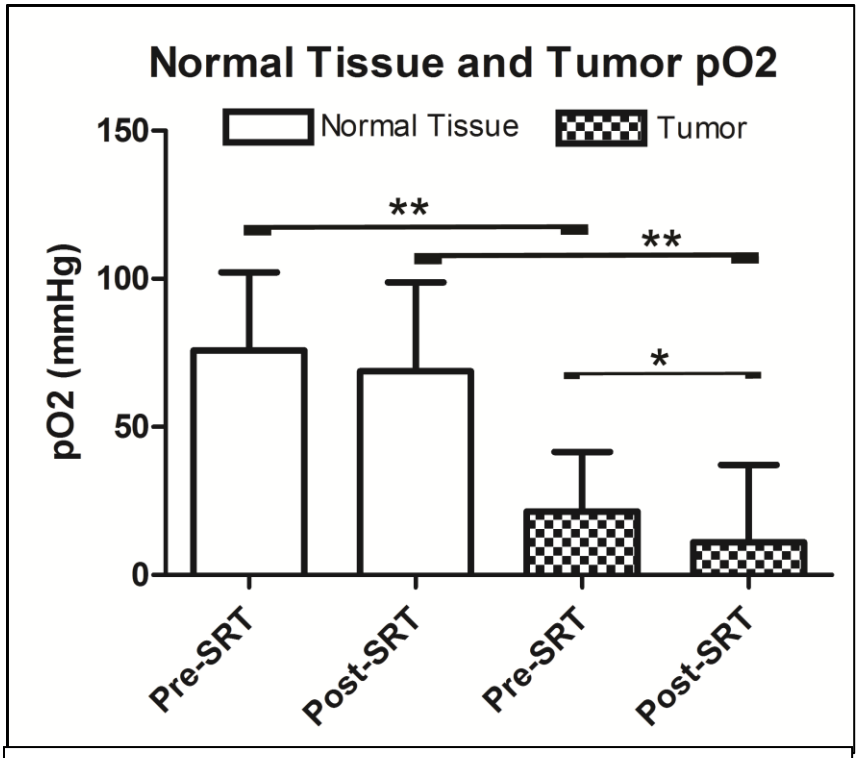

Figure 5.4: Bar graphs representing changes of oxygen tension in the tumor (checked pattern) and nearby normal tissues (blank) measured in feline patients with oral squamous cell carcinoma, measured immediately before SRT and 24hrs post-SRT. Asterisk represents P=0.047 and double asterisk represents P<0.001.

BIBLIOGRAPHY

1. Bregazzi VS, LaRue SM, Powers BE, Fettman MJ, Ogilvie GK and Withrow SJ. Response of feline oral squamous cell carcinoma to palliative radiation therapy. *Vet Radiol Ultrasound*. 2001; 42(1): 77-9.

2. Brizel DM, Sibley GS, Prosnitz LR, Scher RL and Dewhirst MW. Tumor hypoxia adversely affects the prognosis of carcinoma of the head and neck. *Int J Radiat Oncol Biol Phys*. 1997; 38(2): 285-9.

3. Fidel J, Lyons J, Tripp C, Houston R, Wheeler B and Ruiz A. Treatment of oral squamous cell carcinoma with accelerated radiation therapy and concomitant carboplatin in cats. *J Vet Intern Med*. 2011; 25(3): 504-10.

4. Fidel JL, Sellon RK, Houston RK and Wheeler BA. A nine-day accelerated radiation protocol for feline squamous cell carcinoma. *Vet Radiol Ultrasound*. 2007; 48(5): 482-5.

5. Hutson CA, Willauer CC, Walder EJ, Stone JL and Klein MK. Treatment of mandibular squamous cell carcinoma in cats by use of mandibulectomy and radiotherapy: seven cases (1987-1989). *J Am Vet Med Assoc*. 1992; 201(5): 777-81.

6. Jones PD, de Lorimier LP, Kitchell BE and Losonsky JM. Gemcitabine as a radiosensitizer for nonresectable feline oral squamous cell carcinoma. *J Am Anim Hosp Assoc*. 2003; 39(5): 463-7.

7. Martin CK, Werbeck JL, Thudi NK, Lanigan LG, Wolfe TD, Toribio RE and Rosol TJ. Zoledronic acid reduces bone loss and tumor growth in an orthotopic xenograft model of osteolytic oral squamous cell carcinoma. *Cancer Res*. 2010; 70(21): 8607-16.

8. Northrup NC, Selting KA, Rassnick KM, Kristal O, O'Brien MG, Dank G, Dhaliwal RS, Jagannatha S, Cornell KK and Gieger TL. Outcomes of cats with oral tumors treated with mandibulectomy: 42 cases. *J Am Anim Hosp Assoc*. 2006; 42(5): 350-60.

9. Wypij JM, Fan TM, Fredrickson RL, Barger AM, de Lorimier LP and Charney SC. In vivo and in vitro efficacy of zoledronate for treating oral squamous cell carcinoma in cats. *J Vet Intern Med*. 2008; 22(1): 158-63.

10. Anneroth G, Batsakis J and Luna M. Review of the literature and a recommended system of malignancy grading in oral squamous cell carcinomas. *Scand J Dent Res*. 1987; 95(3): 229-49.

11. Nakano T and Oka K. Differential values of Ki-67 index and mitotic index of proliferating cell population. An assessment of cell cycle and prognosis in radiation therapy for cervical cancer. *Cancer*. 1993; 72(8): 2401-8.

12. Nakano T, Oka K, Ishikawa A and Morita S. Immunohistochemical prediction of radiation response and local control in radiation therapy for cervical cancer. *Cancer Detect Prev*. 1998; 22(2): 120-8.

13. Suzuki Y, Oka K, Ohno T, Kato S, Tsujii H and Nakano T. Prognostic impact of mitotic index of proliferating cell populations in cervical cancer patients treated with carbon ion beam. *Cancer*. 2009; 115(9): 1875-82.

14. Scholzen T and Gerdes J. The Ki-67 protein: from the known and the unknown. *J Cell Physiol*. 2000; 182(3): 311-22.

15. Melzer K, Guscetti F, Rohrer Bley C, Sumova A, Roos M and Kaser-Hotz B. Ki67 reactivity in nasal and periocular squamous cell carcinomas in cats treated with electron beam radiation therapy. *J Vet Intern Med*. 2006; 20(3): 676-81.

16. Arteaga CL. Epidermal growth factor receptor dependence in human tumors: more than just expression? *Oncologist*. 2002; 7 Suppl 4: 31-9.

17. Herbst RS. Review of epidermal growth factor receptor biology. *Int J Radiat Oncol Biol Phys*. 2004; 59(2 Suppl): 21-6.

18. Ang KK, Berkey BA, Tu X, Zhang HZ, Katz R, Hammond EH, Fu KK and Milas L. Impact of epidermal growth factor receptor expression on survival and pattern of relapse in patients with advanced head and neck carcinoma. *Cancer Res*. 2002; 62(24): 7350-6.

19. Yoshikawa H, Ehrhart E, Charles JB, Thamm DH and Larue SM. Immunohistochemical characterization of feline oral squamous cell carcinoma. *Am J Vet Res*. 2012; 73(11): 1801-6.

20. Alvarez AA, Krigman HR, Whitaker RS, Dodge RK and Rodriguez GC. The prognostic significance of angiogenesis in epithelial ovarian carcinoma. *Clin Cancer Res*. 1999; 5(3): 587-91.

21. Erovic BM, Neuchrist C, Berger U, El-Rabadi K and Burian M. Quantitation of microvessel density in squamous cell carcinoma of the head and neck by computer-aided image analysis. *Wien Klin Wochenschr*. 2005; 117(1-2): 53-7.

22. Weidner N, Folkman J, Pozza F, Bevilacqua P, Allred EN, Moore DH, Meli S and Gasparini G. Tumor angiogenesis: a new significant and independent prognostic indicator in early-stage breast carcinoma. *J Natl Cancer Inst*. 1992; 84(24): 1875-87.

23. Kaanders JHAM, Wijffels KIEM, Marres HAM, Ljungkvist ASE, Pop LAM, van den Hoogen FJA, de Wilde PCM, Bussink J, Raleigh JA and van der Kogel AJ. Pimonidazole Binding and Tumor Vascularity Predict for Treatment Outcome in Head and Neck Cancer. *Cancer Research*. 2002; 62(23): 7066-74.

24. Park HJ, Griffin RJ, Hui S, Levitt SH and Song CW. Radiation-Induced Vascular Damage in Tumors: Implications of Vascular Damage in Ablative Hypofractionated Radiotherapy (SBRT and SRS). *Radiat Res*. 2012; 177(3): 311-27.

25. Song CW, Park HJ, Griffin RJ and Levitt SH. Radiobiology of stereotactic radiosurgery and stereotactic body radiation therapy. In: *Technical basis of radiation therapy,* 5th edn., SH Levitt, J Purdy, C Perez and S Vijayakumar, eds., Springer-Verlag, 2012: 51-61.

26. Kawaguchi K, Yamada H, Horie A and Sato K. Radiosurgical treatment of maxillary squamous cell carcinoma. *Int J Oral Maxillofac Surg*. 2009; 38(11): 1205-7.

27. Kodani N, Yamazaki H, Tsubokura T, Shiomi H, Kobayashi K, Nishimura T, Aibe N, Ikeno H and Nishimura T. Stereotactic body radiation therapy for head and neck tumor: disease control and morbidity outcomes. *J Radiat Res*. 2011; 52(1): 24-31.

28. Siddiqui F, Patel M, Khan M, McLean S, Dragovic J, Jin JY, Movsas B and Ryu S. Stereotactic body radiation therapy for primary, recurrent, and metastatic tumors in the head-and-neck region. *Int J Radiat Oncol Biol Phys*. 2009; 74(4): 1047-53.

29. Hall E and Giaccia A. Oxygen effect and reoxygenation. In: *Radiobiology for the radiologist,* 6th edn., 2006: 85-105.

30. Weinberg R. Dialogue replaces monologue: heterotypic interactions and the biology of angiogenesis. In: *The biology of cancer,* edn., Garland Science, Taylor & Francis Group, 2007: 527-86.

31. Hockel M, Schlenger K, Hockel S and Vaupel P. Hypoxic cervical cancers with low apoptotic index are highly aggressive. *Cancer Res*. 1999; 59(18): 4525-8.

32. Graeber TG, Osmanian C, Jacks T, Housman DE, Koch CJ, Lowe SW and Giaccia AJ. Hypoxia-mediated selection of cells with diminished apoptotic potential in solid tumours. *Nature*. 1996; 379(6560): 88-91.

33. Nordsmark M, Bentzen SM, Rudat V, Brizel D, Lartigau E, Stadler P, Becker A, Adam M, Molls M, Dunst J, Terris DJ and Overgaard J. Prognostic value of tumor oxygenation in 397 head and neck tumors after primary radiation therapy. An international multi-center study. *Radiother Oncol*. 2005; 77(1): 18-24.

34. Nordsmark M, Overgaard M and Overgaard J. Pretreatment oxygenation predicts radiation response in advanced squamous cell carcinoma of the head and neck. *Radiother Oncol*. 1996; 41(1): 31-9.

35. Fyles A, Milosevic M, Hedley D, Pintilie M, Levin W, Manchul L and Hill RP. Tumor hypoxia has independent predictor impact only in patients with node-negative cervix cancer. *J Clin Oncol*. 2002; 20(3): 680-7.

36. Knocke TH, Weitmann HD, Feldmann HJ, Selzer E and Potter R. Intratumoral pO2-measurements as predictive assay in the treatment of carcinoma of the uterine cervix. *Radiother Oncol*. 1999; 53(2): 99-104.

37. Milosevic M, Fyles A, Hedley D and Hill R. The human tumor microenvironment: invasive (needle) measurement of oxygen and interstitial fluid pressure. *Semin Radiat Oncol*. 2004; 14(3): 249-58.

38. Lyng H, Sundfor K, Trope C and Rofstad EK. Disease control of uterine cervical cancer: relationships to tumor oxygen tension, vascular density, cell density, and frequency of mitosis and apoptosis measured before treatment and during radiotherapy. *Clin Cancer Res*. 2000; 6(3): 1104-12.

39. Nordsmark M and Overgaard J. A confirmatory prognostic study on oxygenation status and loco-regional control in advanced head and neck squamous cell carcinoma treated by radiation therapy. *Radiother Oncol*. 2000; 57(1): 39-43.

40. Stadler P, Becker A, Feldmann HJ, Hansgen G, Dunst J, Wurschmidt F and Molls M. Influence of the hypoxic subvolume on the survival of patients with head and neck cancer. *Int J Radiat Oncol Biol Phys*. 1999; 44(4): 749-54.

41. Brizel DM, Dodge RK, Clough RW and Dewhirst MW. Oxygenation of head and neck cancer: changes during radiotherapy and impact on treatment outcome. *Radiother Oncol*. 1999; 53(2): 113-7.

42. Dunst J, Hansgen G, Lautenschlager C, Fuchsel G and Becker A. Oxygenation of cervical cancers during radiotherapy and radiotherapy + cis-retinoic acid/interferon. *Int J Radiat Oncol Biol Phys*. 1999; 43(2): 367-73.

43. Liptak JM and SJ W. Cancer of the gastrointestinal tract. In: *Small Animal Clinical Oncology,* edn., Withrow SJ and V DM, eds., 2007: 455-35.

44. Yoshikawa H, Harmon JF, Custis JT and Larue SM. Repeatability of a Planning Target Volume Expansion Protocol for Radiation Therapy of Regional Lymph Nodes in Canine and Feline Patients with Head Tumors. *Vet Radiol Ultrasound*. 2012; 53(6): 667-72.

45. Yoshikawa H, Randall EK, Kraft SL and Larue SM. Comparison between 2-(18) F-Fluoro-2-Deoxy-D-Glucose Positron Emission Tomography and Contrast-Enhanced Computed Tomography for Measuring Gross Tumor Volume in Cats with Oral Squamous Cell Carcinoma. *Vet Radiol Ultrasound*. 2013.

46. Ladue T and Klein MK. Toxicity criteria of the veterinary radiation therapy oncology group. *Vet Radiol Ultrasound*. 2001; 42(5): 475-6.

47. Okada Y, Mataga I, Katagiri M and Ishii K. An analysis of cervical lymph nodes metastasis in oral squamous cell carcinoma. Relationship between grade of histopathological malignancy and lymph nodes metastasis. *Int J Oral Maxillofac Surg*. 2003; 32(3): 284-8.

48. Weidner N. Current pathologic methods for measuring intratumoral microvessel density within breast carcinoma and other solid tumors. *Breast Cancer Res Treat*. 1995; 36(2): 169-80.

49. Thrall DE, Larue SM, Pruitt AF, Case B and Dewhirst MW. Changes in tumour oxygenation during fractionated hyperthermia and radiation therapy in spontaneous canine sarcomas. *Int J Hyperthermia*. 2006; 22(5): 365-73.

50. Snyder LA, Bertone ER, Jakowski RM, Dooner MS, Jennings-Ritchie J and Moore AS. p53 expression and environmental tobacco smoke exposure in feline oral squamous cell carcinoma. *Vet Pathol*. 2004; 41(3): 209-14.

51. Bertone ER, Snyder LA and Moore AS. Environmental and lifestyle risk factors for oral squamous cell carcinoma in domestic cats. *J Vet Intern Med*. 2003; 17(4): 557-62.

52. Marconato L, Buchholz J, Keller M, Bettini G, Valenti P and Kaser-Hotz B. Multimodal therapeutic approach and interdisciplinary challenge for the treatment of unresectable head and neck squamous cell carcinoma in six cats: a pilot study. *Vet Comp Oncol*. 2012.

53. Hayes A, Scase T, Miller J, Murphy S, Sparkes A and Adams V. COX-1 and COX-2 expression in feline oral squamous cell carcinoma. *J Comp Pathol*. 2006; 135(2-3): 93-9.

54. Bergkvist GT, Argyle DJ, Pang LY, Muirhead R and Yool DA. Studies on the inhibition of feline EGFR in squamous cell carcinoma: enhancement of radiosensitivity and rescue of resistance to small molecule inhibitors. *Cancer Biol Ther*. 2011; 11(11): 927-37.

55. Looper JS, Malarkey DE, Ruslander D, Proulx D and Thrall DE. Epidermal growth factor receptor expression in feline oral squamous cell carcinomas. *Vet Comp Oncol*. 2006; 4(1): 33-40.

56. Kioi M, Vogel H, Schultz G, Hoffman RM, Harsh GR and Brown JM. Inhibition of vasculogenesis, but not angiogenesis, prevents the recurrence of glioblastoma after irradiation in mice. *J Clin Invest*. 2010; 120(3): 694-705.

57. Kerbel RS and Kamen BA. The anti-angiogenic basis of metronomic chemotherapy. *Nat Rev Cancer*. 2004; 4(6): 423-36.

58. Reddy SP, Raslan WF, Gooneratne S, Kathuria S and Marks JE. Prognostic significance of keratinization in nasopharyngeal carcinoma. *Am J Otolaryngol*. 1995; 16(2): 103-8.

59. Johansen LV, Grau C and Overgaard J. Squamous cell carcinoma of the nasopharynx--an analysis of treatment results in 149 consecutive patients. *Acta Oncol*. 2001; 40(7): 801-9.

60. Taguchi T, Tsukuda M, Mikami Y, Matsuda H, Tanigaki Y, Horiuchi C, Nishimura G and Nagao J. Treatment results and prognostic factors for advanced squamous cell carcinoma of the head and neck treated with concurrent chemoradiotherapy. *Auris Nasus Larynx*. 2009; 36(2): 199-204.

61. Bergers G and Benjamin LE. Tumorigenesis and the angiogenic switch. *Nat Rev Cancer*. 2003; 3(6): 401-10.

62. Eschwege F, Bourhis J, Girinski T, Lartigau E, Guichard M, Deble D, Kepta L, Wilson GD and Luboinski B. Predictive assays of radiation response in patients with head and neck squamous cell carcinoma: a review of the Institute Gustave Roussy experience. *Int J Radiat Oncol Biol Phys*. 1997; 39(4): 849-53.

63. Griffiths JR and Robinson SP. The OxyLite: a fibre-optic oxygen sensor. *Br J Radiol*. 1999; 72(859): 627-30.

64. Terris DJ and Dunphy EP. Oxygen tension measurements of head and neck cancers. *Arch Otolaryngol Head Neck Surg*. 1994; 120(3): 283-7.

65. Braun RD, Lanzen JL, Snyder SA and Dewhirst MW. Comparison of tumor and normal tissue oxygen tension measurements using OxyLite or microelectrodes in rodents. *Am J Physiol Heart Circ Physiol*. 2001; 280(6): H2533-44.

66. Gray LH, Conger AD, Ebert M, Hornsey S and Scott OC. The concentration of oxygen dissolved in tissues at the time of irradiation as a factor in radiotherapy. *Br J Radiol*. 1953; 26(312): 638-48.

67. Gatenby RA, Kessler HB, Rosenblum JS, Coia LR, Moldofsky PJ, Hartz WH and Broder GJ. Oxygen distribution in squamous cell carcinoma metastases and its relationship to outcome of radiation therapy. *Int J Radiat Oncol Biol Phys*. 1988; 14(5): 831-8.

68. Fuks Z and Kolesnick R. Engaging the vascular component of the tumor response. *Cancer Cell*. 2005; 8(2): 89-91.

69. Garcia-Barros M, Paris F, Cordon-Cardo C, Lyden D, Rafii S, Haimovitz-Friedman A, Fuks Z and Kolesnick R. Tumor response to radiotherapy regulated by endothelial cell apoptosis. *Science*. 2003; 300(5622): 1155-9.

70. Bussink J, Kaanders JH, Rijken PF, Raleigh JA and Van der Kogel AJ. Changes in blood perfusion and hypoxia after irradiation of a human squamous cell carcinoma xenograft tumor line. *Radiat Res*. 2000; 153(4): 398-404.

CHAPTER 6: Feline oral squamous cell carcinoma: Use of telomere length in putative tumor initiating cells and expression levels of telomerase activity and tumor initiating cell marker proteins to predict clinical outcome after stereotactic radiation therapy

Brief summary

Tumor initiating cell (TIC) and cancer stem cell theory and telomere biology are actively studied fields in human head and neck (H&N) cancer. Feline oral squamous cell carcinoma (SCC), which has been advocated as a feline model of human H&N cancer, is the most common feline oral cancer with a very poor prognosis. Little is known about the TIC and telomere biology of this feline malignancy. We conducted a retrospective study to immunohistochemically evaluate protein expression levels of the putative TIC markers of human H&N cancer, CD44 and Bmi-1, for their possible role as prognostic markers in 20 patients with feline oral SCC who underwent SRT. A combined technique of fluorescent in-situ hybridization and immunofluorescent staining was used to evaluate telomere length in the putative TICs that are positive for CD44 and Bmi-1 and correlated with treatment outcome. And finally, we performed a quantitative analysis of telomerase activity using pre-treatment samples. Significant inverse correlations were found between progression-free interval (PFI) or survival time and Bmi-1 protein expression in the Log-Rank and the multivariate Cox proportional hazard analyses. Telomere length ratio (fractions of very short telomere/average length telomere) and relative telomerase activity did not show any correlations with patient outcome. Relative telomerase activity in many cases was lower than that in normal feline oral mucosa. Our study suggests that Bmi-1 may play important roles in local tumor recurrence and be used as a novel therapeutic target. Although further investigation is needed, telomerase inhibition may not be effective in many of those cases.

Introduction

The goal of most cancer therapies is to eradicate all cancer cells indiscriminately. Despite this, some tumor types respond poorly to treatment, leading to tumor recurrence. One hypothesis to explain treatment failure is the idea that the tumor does not consist of a population of identical cells, but rather is a conglomerate of heterogeneous cell populations. It is thought that cancer cells with specific phenotypes are more resistant to conventional treatments and thus are responsible for treatment outcome. These cancer cells, called tumor initiating cells (TICs), are thought to initiate the entire population of the cancer cells [1] and the TIC theory was first reported in human myeloid leukemia in 1971 [2]. That study showed that cancer cells with less-differentiated markers were able to cause cancers in immunocompromised mice more efficiently than cancer cells without these markers. A number of studies have been conducted to characterize TICs in various human malignancies [3]. In human head and neck squamous cell carcinoma (H&N SCC), cancer cells with stem cell-like markers have been shown to be resistant to cytotoxic agents such as chemotherapeutic drugs and ionizing radiation. In addition, these cells possess the ability to reproduce a heterogeneous cancer cell population and self-renewal properties [4,5]. In human H&N SCC, cancer cells positive for CD44, a hyaluronic acid receptor on the cell surface, have been shown to be more tumorigenic than cancer cells negative for CD44 [5]. Other studies have demonstrated that human H&N SCC patients with greater numbers of CD44-positive cancer cells had more advanced clinical tumor stages, higher rates of tumor recurrence and of successful tumor implantation in immunocompromised mice, and significantly lower survival rate [6-8]. The study that originally advocated CD44 as a TIC marker showed that CD44-positive cancer cells, but not CD44-negative cancer cells, differentially express Bmi-1 at RNA and protein levels [5]. Bmi-1 is an oncogene responsible for suppression of cell cycle inhibitors

and is necessary for self-renewal [9]. Several studies have shown that Bmi-1 protein confers radio- and chemo-resistance in some human malignancies [10,11]. Clinically, Bmi-1 expression has been suggested as a prognostic indicator in human malignancies including H&N SCC [12-14]. We are unaware of studies that evaluated the prognostic value of CD44 and Bmi-1 protein expression in feline oral SCC. This feline cancer is one of the most refractory malignancies in veterinary medicine and most patients succumb to local disease [15]. Even though multimodal treatment approaches have been used to tackle this devastating disease, treatment outcome is disappointing. A more thorough understanding of the underlying biology is necessary to inform new clinical strategies.

The telomere is a highly conserved tandem repeat DNA sequence found at the end of eukaryotic chromosomes [16]. Telomere provides a protective "cap" of important DNA coding regions but shortens by up to 100 base pairs during each cell division due to the end-replication problem [17]. When telomere sequence becomes too short, cells are forced to enter senescence [17]. If a cell with a shortened telomere can somehow bypass senescence and continues to proliferate, the telomere becomes critically short. At this point, most cells die of apoptosis due to an abnormal chromosomal segregation such as breakage-fusion-bridge [17]. Thus the telomere allows most cells to divide a limited number of times (Hayflick limit) and this is thought to be a defense mechanism against cancer development [17,18]. Cancer cells, however, are capable of unlimited proliferation (immortalized) [19]. This can be achieved by maintaining telomere length either via activation of telomerase, which is a DNA reverse-transcriptase, or alternative lengthening of telomere (ALT), which is a non-homologous end joining-based process [17]. Most human cancers have been shown to express telomerase activity [17]. Therefore, telomerase is an attractive target for cancer therapy and many studies have attempted to counteract telomerase expression/activity

and to shorten telomere length so that the cancer cells undergo apoptosis or at least stop proliferating [20]. One report suggested that the anti-telomerase therapy can radio-sensitize human H&N SCC cancer cells most effectively when their telomere length is critically short [21]. This implies that the telomere length (TL) may be used as a predictor of radiation therapy response. Indeed, many studies have evaluated a possible correlation between TL and treatment outcome in human oncology with varying conclusions [22]. In human H&N SCC, patients with longer TL in their tumor had significantly shorter post-surgical disease-free survival compared to those with shorter TL [23]. Studies about feline telomere and telomerase biology are limited [24-26].

If the TIC is a more important cell population than non-TICs for tumor control, there could be potential benefit in evaluating TL in the TICs, not in the heterogeneous cancer cell population. The gold standard for TL measurement is a southern blot-based assay which is called telomere restriction fragment (TRF) assay and other methods include fluorescence-activated cell sorting-based assay and chemiluminescent slot blot assay [22,27-29]. However, when clinically obtained samples (which include non-cancer cells) are used, it is impossible to discriminate different phenotypes using these techniques. To solve this issue, we employed fluorescence in-situ hybridization- (FISH) and immunofluorescent staining-based techniques called TELI-FISH. This technique uses formalin-fixed, paraffin embedded tissues and therefore, allows us to evaluate TL in specific cells [30]. We evaluated TL of the putative TICs by TELI-FISH assay and protein expression levels of CD44 and Bmi-1 immunohistochemically for their role as a prognostic marker in patients with feline oral SCC who underwent stereotactic radiation therapy (SRT). Based on the clinical and biological similarities between human H&N SCC and feline oral SCC, we hypothesized that high protein expression level of CD44 and Bmi-1is prognostic for poor treatment outcome in cats with oral SCC treated with SRT. In addition, we evaluated

telomerase activity using real-time quantitative polymerase chain reaction (RTQ-PCR). We hypothesized that longer TL in the putative TICs is prognostic for poorer treatment outcome.

Materials and Methods

Patient population: Twenty cats with histopathologically confirmed oral SCC who were enrolled in a prospective clinical trial with SRT at the Animal Cancer Center, Colorado State University between January 2010 and July 2011were included. All patients were clinically staged.

Radiation therapy: All patients underwent either CT or 2-[^{18}F]-fluoro-2-deoxy-D-glucose positron emission tomography/CT examination for tumor extent evaluation and SRT planning. Detailed protocols are described in our previous reports [31,32]. SRT was delivered in either 10 Gy x 3 fx or 20 Gy x 1 fx schedule using a SRT-capable linear accelerator (Trilogy, Varian Medical System).

Western analysis for Bmi-1: The SCCF1 cell line (supplied by Dr. Thomas Rosol, the Ohio State University) was maintained as published previously [33]. Cells were lysed and the extracted protein was electrophoresed , blotted, hybridized, and visualized as described [34]. A mouse anti-human Bmi-1 monoclonal antibody (ab-14389, Abcam) was used to detect feline Bmi-1 protein. Anti-CD44 antibody [rat anti-human CD44 monoclonal (IM7, eBioscience)] has been shown to cross-react with feline cells [35].

Immunohistochemistry: Tumor biopsy samples obtained before SRT were sectioned and processed as a previous study [34]. The anti-CD44 and anti-Bmi-1 primary antibodies described

above (in the western analysis section) were used with immunoperoxidase technique. 3,3'-diaminobenzidine was used to visualize an antibody-antigen interaction.

Scoring immunoreactivity of CD44 and Bmi-1: The immunohistochemical evaluation of CD44 and Bmi-1 was completed by two readers who graded all slides independently based on criteria described in previous studies (table 6.1)[7,12,14,36]. The scoring was confirmed by a boarded veterinary pathologist. For CD44 and Bmi-1, percent of positively stained cells (CD44% and Bmi-1%, respectively) and average intensity of positively stained cells (CD44intensity and Bmi-1intensity, respectively) were created and multiplied to calculate total score (CD44total and Bmi-1total, respectively).

TELI-FISH stain: The basic protocol is described in detail in a previous study [30]. Briefly, the slides were deparaffinized and rehydrated and then antigen retrieval was conducted with citrate buffer (Target retrieval solution, Dako) for 1 min at 125℃. The slides were then incubated with a blocking reagent (Background sniper, Biocare medical, for 15 minutes at RT). Slides were hybridized with PNA telomere hybridization probe (G-rich probe, Cy3-labeled; red, Biosynthesis, Lewisville, TX) for 5 min at 84℃ first then overnight at 37℃. The slides were then incubated with a primary antibody cocktail for CD44 and Bmi-1 (described above, in the western analysis section) for 2 hrs at 37℃. This was followed by incubation with a secondary antibody cocktail (goat anti-rat Alexa Fluor 647 conjugated; goat anti-mouse Alexa Fluor466 conjugated, both Life Technologies) for 45 min at RT. Slides were then mounted and cover-slipped with anti-fade medium with DAPI (ProLong Gold, Invitrogen).

Image acquisition and quantification of telomere length of putative tumor initiating cells: Image Z stacks were obtained using a Zeiss Axio Imager Z2 microscope (capturing fluorescent

images with a Coolsnap ES2 camera using Metamorph software) (Molecular Devices, Sunnyvale, CA). For each cell population 15 to 20 images were obtained by taking twenty-six stacks of 0.2 um per plane in 2 different wavelengths (Dapi and Cy3). Three-dimensional deconvolution was performed to obtain a maximum projection of the 26 stacks which allowed analysis of all telomere signals visible in the whole extension of each cell nuclei (DeconvolutionJ: http://rsbweb.nih.gov/ij/plugins/deconvolutionj.html) (Figure 6.1).

Analysis of telomere fluorescence intensity (TFI) was performed using Telometer, available from http://demarzolab.pathology.jhmi.edu/telometer/downloads/index.html. Telomere signals from cells that were positive for CD44 and Bmi-1 were analyzed using custom program settings (minimum object size: 1; maximum object size: 350; despeckle ratio: 0.3, rolling ball size: 1). At least 45 cells were counted per cat. Mean sample TFI was calculated and individual TFI frequency histograms were created for each sample group. We calculated the ratio between very short telomeres (VS) (define as telomeres with ½ or less the average TFI in the sample) and the average (AV) TFI for the sample. In other words, the ratio= VS/AV represents the proportion VS in relation to the average TL. Therefore, VS/AV = 1 represents samples that had an equal proportion of VST and AV TL. VS/AV <1 represents samples with a higher proportion of AV TL. Finally, VS/AV > 1 represents samples with a higher proportion of VS. A block of a normal cat skin was included in each batch of staining and used as a reference to monitor technical errors. Linear regression analysis was performed to evaluate a possible correlation between VS/AV and patient age.

RTQ-TRAP Telomerase Assay and Analysis: Pre-SRT tissues of feline squamous cell carcinoma were collected and flash frozen in liquid nitrogen immediately and stored at -80℃ until analysis. The SYBR Green RTQ-TRAP assay was adapted from previous reports [37,38]. Samples were weighed (10 to 20 mg), suspended in cold M-PER lysis buffer (Thermofisher, Lafayette, CO) with protease inhibitor (Roche, Indianapolis, IN) and ribonuclease inhibitor (25 µl/100 µl lysis buffer; Promega, Madison, WI) at the ratio of 100 µl per 10 mg of sample. Protein extraction was performed using a glass on glass homogenizer on ice. Following homogenization, samples were immediately refrozen on dry ice and moved to -80℃ within 15 min. The lysate was processed using RNase-free conditions. Briefly, the sample was thawed on ice and centrifuged at 13000rcf, 4℃ for 10 min. The supernatant was removed. Lysates were aliquoted and refrozen in -80℃. Each sample was not freeze-thawed more than 3 times. Protein content was determined using a Bradford protein assay (Biorad, Hercules, CA).

The SYBR green master mix (Biorad, Hercules, CA) included all necessary dNTP's, $MgCl_2$, enzyme and Sybr green to complete the RTQ-PCR reaction. Each well contained 0.25µg of protein lysate, 50% volume of SYBR green master mix, 0.2µg T4 gene32 protein (New England Biolabs, Ipswitch, MA), 0.1µg of each primer TS (5'-AATCCGTCGAGCAGAGTT-3') and ACX (5'-GCGCGG(CTTACC)3CTAACC-3') (Integrated DNA Technologies, Coralville, IA) and RNase/DNase free water to achieve a final well volume of 25ul. The samples were loaded into a real-time 96-well microtiter plate (Thermofisher, Lafayette, CO) and sealed with a real time PCR sealant film (Thermofisher, Lafayette, CO). The PCR and detection was performed on a CFX 96 (Biorad, Hercules, CA). In addition to the treatment samples, a series of controls were also included on each plate: (1) no template control with TS primer only, (2) no template control with ACX primer only, (3) no template control with TS and ACX primers, (4)

heat inactivated control with template (protein lysate) and TS and ACX primers, (5) HeLa cell lysate with TS and ACX primers (a positive control robust in telomerase) and (6) feline skin tissue as a tissue control.

The RTQ-PCR program includes the following steps: Step 1- 1cycle 25℃ 20 min (used to allow telomerase in the protein extracts to elongate the TS primer by adding TTAGGG repeat sequences to it); Step 2- 1cycle 95℃ 3 min (provides heat activation of the enzyme in the SYBR master mix); Step 3- 40 cycles of 95℃ for 20 sec, 50℃ for 30 sec and 72℃ for 1min 30 sec (PCR amplification of already elongated TS oligo, allows for detection by real time instrument); Step 4- 80 cycles 0.10 sec per cycle (melt curve, ensures no primer dimer formation). The more telomerase activity in the sample, the more rapidly the threshold of amplification (Ct) is achieved. Each sample is run in triplicate on a 96 well plate format allowing for an average Ct to be obtained per sample. Utilizing the average Ct value, the relative percent telomerase activity in each sample is calculated using the Livak method, or Delta Delta Ct method ($2^{-\Delta\Delta Ct}$) [39]. Briefly, to calculate the percent relative activity for each sample one must first normalize the average Ct for a sample to the no template control with TS and ACX primers (control run on each plate). This is referred to as the delta Ct value. The delta Ct value of each sample is then subtracted from the delta Ct value of a chosen comparative sample, a normal feline mucous membrane cell lysate, yielding a delta delta Ct value ($\Delta\Delta Ct$). Using the $2^{-\Delta\Delta Ct}$, a relative value is generated for each sample comparison and when multiplied by 100 is the relative percent of telomerase activity in the sample of oral SCC compared to the normal feline mucous membrane. A percent value can then be compared between samples assayed across different plates. Results from two runs were averaged and used as a variable in the statistical analyses. To evaluate any correlation

between telomerase activity and patient age, sex, body weight, clinical stage, tumor location, or tumor volume, linear regression test and/or Fisher exact test were performed.

Survival analysis: For each variable, patients were sorted into two groups; higher or lower than median of each variable. Log-Rank analysis and univariate Cox proportional hazard analysis were performed to evaluate for a statistical significance. Patient parameters were also evaluated in these analyses and those included patient age, sex, body weight, clinical stage, tumor location, and tumor volume. Variables that were significant in those analyses were further evaluated by multivariate Cox proportional hazard analysis. Survival time (ST) was defined as the time from the start of the SRT to the patient death. Progression-free interval (PFI) was defined as the time from the start of SRT to the clinically noticeable tumor recurrence or patient death, whichever came first. All statistical analyses were performed with commercially available software (SigmaPlot version 12, Systat Software) and *P*-values <0.05 were considered statistically significant.

Results

Patient population: 15 domestic short hair, four domestic long hair, and one Siamese were evaluated. Tumor locations included mandible (11), lingual/sublingual (6), and maxilla (3). There were twelve neutered males, seven neutered females, and one intact female. Mean patient age and body weight at diagnosis were 12.5 y.o. and 4.4 kg, respectively. Two of the 20 cats received 10 Gy x 3 fx. One of them underwent additional single fraction of 20 Gy after the tumor recurred locally. The rest of the 18 cats received 20 Gy x 1 fx and one cat underwent multiple

cytoreductive surgeries after the tumor recurred locally. For these two patients, PFI was determined at time of first recurrence.

Western analysis for Bmi-1: Molecular weight of mouse and human Bmi-1 proteins are reported to be around 37-45 kDa in size [40]. In our experiment, an intense band was observed at around 40 kDa, suggesting the positive cross-reactivity of the antibody with feline Bmi-1 protein (Figure 6.2).

Immunohistochemistry: Immunohistochemistry was performed in all of the 20 patients. CD44 exhibited membranous and Bmi-1 exhibited mainly nuclear and minor cytoplasmic localization (Figure 6.3). The mean and range of each score were as following: CD44% (3.7, 3-4), CD44intensity (1.8, 1-2), CD44total (6.5, 3-8), Bmi-1% (2.5, 2-3), Bmi-1intensity (2.1, 1-3), Bmi-1total (5.4, 2-9).

Telomere length measurement: Telomere length was measured in all of the 20 patients. In the TELI-FISH analysis, CD44 exhibited membranous and Bmi-1 exhibited mainly nuclear and minor cytoplasmic localization (Figure 6.1). The cells showing double-positive staining for CD44 and Bmi-1 were subjectively 1-5 % in the entire cancer cell population (data not shown). The mean VS/AV was 1.12 [standard deviation (SD) = 0.32] and median VS/AV was 1.051 (Table 6.2). There was no significant correlation between VS/AV and patient age.

RTQ-TRAP Telomerase Assay and Analysis: Telomerase analysis was performed in the 15 of 20 cats. A large inter-patient variability was noticed in the relative telomerase activity with median = 39.2 %, mean = 67.5 %, and SD = 75.1 % (Table 6.2). No statistically significant correlation was found between the relative telomerase activity and VS/AV, patient age, sex, body weight, clinical stage, tumor location, or tumor volume.

Survival analysis: In the 20 cats, median ST and PFI and the range were 106 days (14-359) and 87 days (14-206), respectively. In the Log-Rank analysis and the multivariate Cox proportional hazard analysis, cats with low Bmi-1% or female cats had significantly longer ST and PFI than cats with high Bmi-1% (Table 6.3 and Figure 6.4) (ST: P=0.013 and P=0.019, risk ratio (RR)=0.22 and 95%CI=0.061 and 0.78 for lower group, respectively) (PFI: P=0.047 and P=0.034, RR=0.28 and 95%CI=0.087 and 0.91 for lower group). The Log-Rank and univariate Cox proportional hazard analysis revealed no statistically significant correlations between ST or PFI and the VS/AV or the relative telomerase activity.

Discussion

We verified the cross-reactivity of the anti-Bmi-1 antibody for feline oral SCC cells by western analysis. According to a previous report, feline Bmi-1 protein is 99% and 97% homologous to the human and mouse Bmi-1 protein, respectively [41]. Our result and the protein sequence similarity between human and feline Bmi-1 support that feline oral SCC expressed Bmi-1 protein. We also verified staining pattern of CD44 by using several feline normal tissues as controls. The antibody used has been shown to cross-react with feline cells [35]. In this study, it showed the expected staining pattern in feline skin, small intestine and lymph nodes (data not shown) as described in murine and human studies [42-44].

Bmi-1 is a transcription repressor and a member of the polycomb group protein [45]. Bmi-1 has been shown to be essential for self-renewal of some types of human stem cells and to be present in higher percent in TICs of human H&N SCC compared to cells without TIC characteristics [5]. Furthermore, in rodent models of human H&N SCC, knocking down the Bmi-1

gene improved radiochemosensitivity, implying that this gene plays an important role in the response to radiation therapy [46]. Our study revealed that higher Bmi-1% is prognostic for poor treatment outcome (ST and PFI). This is the first study which evaluated the prognostic role of Bmi-1 in feline oral SCC treated with SRT. This result, however, is in contrary to a previous report in human H&N SCC which found low or negative expression of Bmi-1 protein as an predictor of shorter disease-free interval after surgery [12]. The human patients in that study all underwent surgery whereas the feline patients in the current study underwent SRT. Moreover, other studies in human H&N SCC and non-small cell lung cancer have shown that Bmi-1 expression is higher in more advanced disease and co-expression of Bmi-1 and a cell surface glycoprotein podoplanin is a negative prognostic factor in patients who underwent radiation therapy [13,14]. These studies support our finding that high Bmi-1 protein expression is a negative prognostic factor in patients with feline oral SCC who underwent SRT. Because of the small patient population in the current study, validation of this result in a future study is needed.

CD44 was first described as a TIC marker for human H&N SCC in 2006, and since then, many researchers have utilized anti-CD44 antibody to detect/isolate putative TICs [5,47]. Although some studies in human H&N and other malignancies showed that the immunohistochemically-evaluated CD44 expression is prognostic for treatment outcome, our current study did not find a significant correlation between CD44 protein expression and either ST or PFI [6-8,36,48-50]. One plausible reason for this discrepancy could be due to the wide variety of isoforms of CD44 protein. In human, at least eleven different CD44 isoforms are created through alternative splicing from a single CD44 gene [51]. Although the hydrophobic transmembrane domain has been reported to be 100% conserved between mammalian species, details about cytoplasmic and extracellular domain of feline CD44 are unknown [51]. The anti-CD44 antibody used in the current

study (IM7) is a pan-CD44 antibody that is designed to detect all isoforms of human CD44 protein. Although this antibody has been used for feline cells [35], it is not clear whether this monoclonal antibody binds to all isoforms of feline CD44 protein or binds to a specific isoform preferentially. Also, the number of patients in our study was limited, and overall prognosis was poor, with little difference in PFI and ST between groups. In addition to this, there seems to be a large inter-study variability in the percentile of CD44-positive cancer cells. A study that first reported CD44 as a TIC marker in human H&N SCC found that CD44-positive H&N SCC cells are typically <10% of the clinically obtained H&N cancer cell population [5]. By contrast, our feline oral SCC patients showed a higher percentage of CD44-positive cancer cells with median and mean scores of 4/4 and 3.7/4, respectively. Recent reports in human H&N SCC found that almost all cancer cells are positive for CD44 [52,53]. A plausible explanation for this difference includes the difference in antibodies and experimental methods (flow cytometry vs immunohistochemistry). There might be a difference in the expression pattern of CD44 protein between felines and humans. To clarify this discrepancy, a detailed research to identify specific CD44 isoform expressed in the feline oral SCC is essential. Furthermore, a functional study such as tumor sphere assay to assess whether CD44-positive feline oral SCC cells possess characteristics of TIC is also needed.

Because telomeres are involved in cell cycle control, proliferation, apoptosis, and DNA repair, many clinical studies have been carried out with a goal of finding a correlation between the TL and clinical outcome [17,22,54]. Researches used the southern blot-based assay or florescence-activated cell sorting-based assay to measure telomere length of the cancer cells [22]. However these methods are not ideal for clinically obtained samples which include non-cancer cells such as inflammatory cells and stromal cells. With the TELI-FISH technique, we were able

not only to discriminate cancer cells from the non-cancer cells, but also to identify putative TICs by co-staining samples with anti-CD44 and anti-Bmi-1 antibodies. Because the intensity of the fluorescence signal corresponds to the length of the telomeric sequence, we evaluated telomere length specifically of the TICs [30]. In addition, we used the three-dimensional deconvolution technique to decrease the impact of the halo artifact inherently seen in a point fluorescent source.[55,56]

The current study revealed a large inter-patient variability in the relative telomerase activity. One study reported telomerase activity in a variety of feline malignancies, including one feline oral SCC [57]. Since the current study used RTQ-PCR and the previous study used a more traditional technique, telomeric repeat amplification protocol (TRAP), simple comparison of the results between the current and the previous studies is not appropriate. Interestingly, however, a previous study showed that TRAP assay frequently overestimates telomerase activity and RTQ-PCR is accurate and reproducible [38]. In our study, many patients showed very low telomerase activity compared to normal feline oral mucosal epithelium. This result suggests that a high percent of patients with feline oral SCC do not activate telomerase and that telomerase inhibition may not be an effective treatment strategy. Although RTQ-PCR enables us accurate quantification of telomerase activity, when clinically obtained biopsy samples are used, it is important to keep in mind that only immunohistochemistry can provide us information about cell types that are expressing telomerase (i.e. tumor cells vs inflammatory cells vs fibroblast). Ideally, a combinational analysis using RTQ-PCR and immunohistochemistry with a reliable primary antibody against feline telomerase should be performed.

In the current study, no statistically significant correlations between the TL ratio or the relative telomerase activity and PFI or ST were found. Those non-significant findings could be

due to the type II error from the small sample population. Another possible explanation for the non-significant result between TL ratio and PFI or ST is due to the validity of these putative TIC markers. As mentioned above, the current study lacks a functional assay such as tumor sphere formation assay and Hoechst dye exclusion assay. Although CD44 and Bmi-1 have been advocated as TIC markers in human H&N SCC [5], their role in feline oral SCC has yet to be evaluated. Whereas the fraction of CD44-positive cancer cells in the current study is higher than the previous study in human H&N SCC [5], the fraction of cells positive for both CD44 and Bmi-1 in the current study was subjectively less than 5 % of the entire cancer cell population, which is similar to the finding in other studies [5,58]. Again, future functional studies are essential to validate this finding.

In conclusion, our study revealed that high Bmi-1 protein expression might be a poor prognostic factor in patients with feline oral SCC who undergo SRT. Further studies focusing on functional aspects of these putative TICs are mandatory to strengthen our findings in the current study. Many patients with feline oral SCC may not activate telomerase and this suggests that anti-telomerase treatment may not effective.

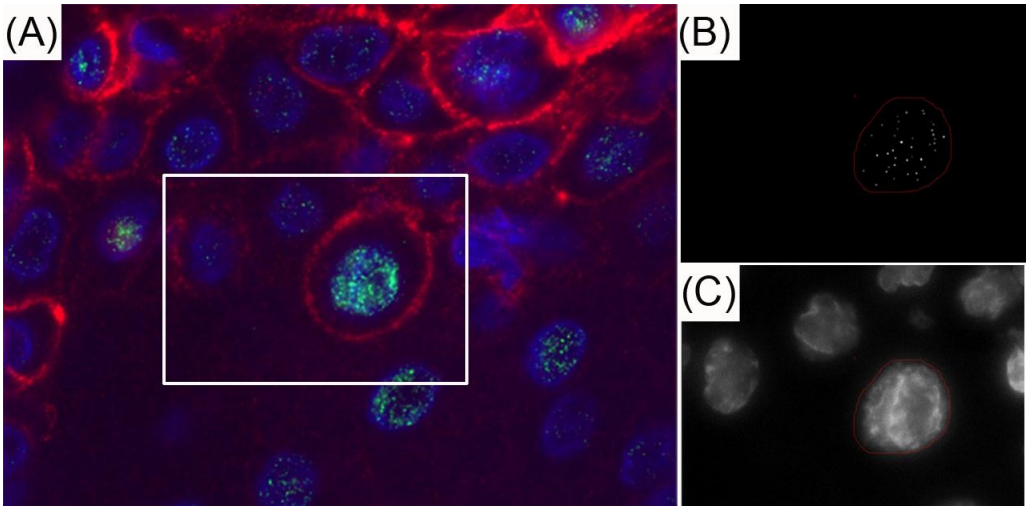

Figure 6.1: Representative images of telomere length measurement in putative tumor initiating cells of feline oral squamous cell carcinoma. (A) Cancer cells positive for CD44 (CD44; red) and Bmi-1 (green) were selected and (B) 26 serial images were captured by moving the microscope table vertically. The image set was proposed to create a single stacked image. Telomere signal intensity was quantified by using special software (Telometer). (C) A nucleus was contoured based on the positivity for these two putative tumor initiating cell markers. The line drawn to select the nucleus was then automatically copied on a different window (B). The software quantifies telomere intensity only inside the line. White rectangular box in (A) represents the image field of (B) and (C). Blue: DAPI.

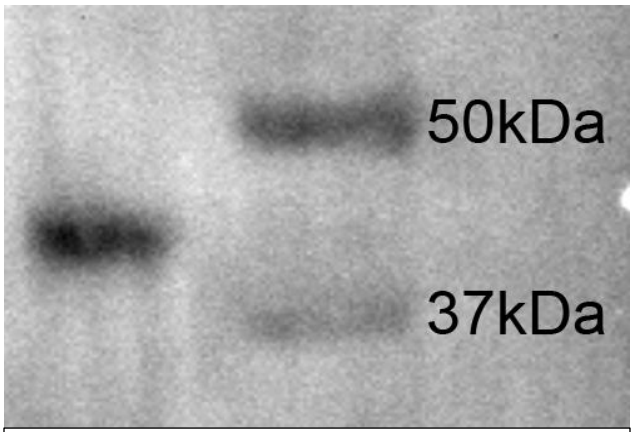

Figure 6.2: Result of western blot assay to verify cross-reactivity of an anti-Bmi-1 antibody against a feline oral SCC cell line. Notice the single intense band in the left lane. Molecular weight marker was run in the right lane.

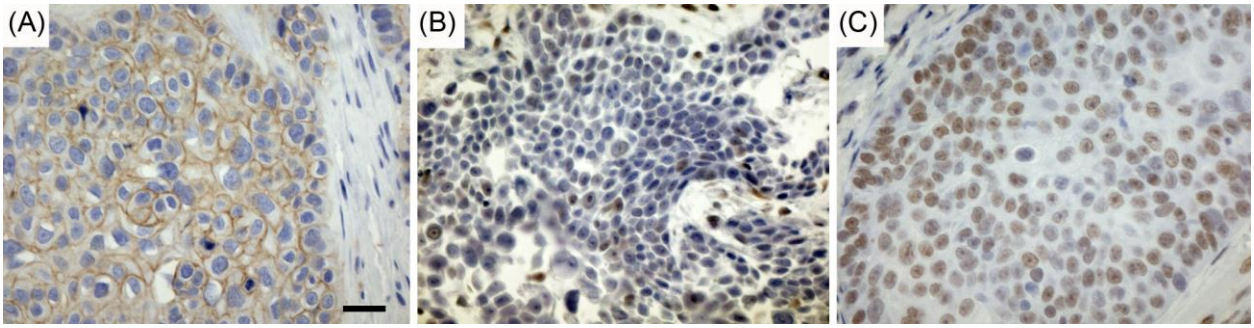

Figure 6.3: Representative photomicrographs of (A) CD44, (B) low Bmi-1 expression, and (C) high Bmi-1 expression in biopsy samples of feline oral squamous cell carcinoma analyzed in the current study. Bar=20µm.

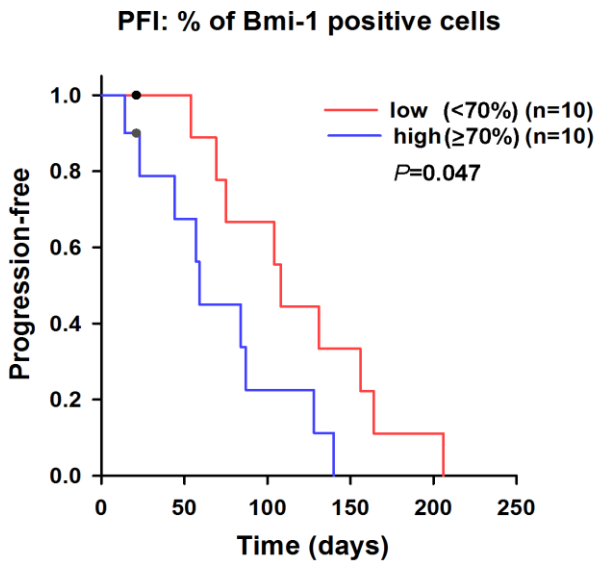

Figure 6.4: Kaplan-Meier graph of progression-free interval of patients with feline oral squamous cell carcinoma stratified by low (solid line) or high (dashed line) Bmi-1 protein expression evaluated immunohistochemically.

Table 6.1: Scoring schemes for the CD44 and Bmi-1 protein expression fraction and its average intensity in patients with feline oral squamous cell carcinoma.

CD44		
positive fraction	0	0%
	1	<25%
	2	25-49%
	3	50-74%
	4	≥75%
Intensity	0	negative
	1	weak
	2	strong

Bmi-1		
positive fraction	0	0%
	1	<20%
	2	20-69%
	3	≥70%
Intensity	0	negative
	1	weak
	2	moderate
	3	strong

Table 6.2: Results of Log Rank analysis and multivariate Cox proportional hazard analysis of immunohistochemical evaluation of Bmi-1 protein expression. ST: survival time. PFI: progression-free interval. Int: intensity. RR: risk ratio. CI: confidence interval.

ST **Bmi-1 %**	**n** **median (range)**
Low	10 156 (69-359)
High	10 84 (14-145)
***P*-value (Log Rank)**	**0.013**
Cox *P*-value	**0.019**
RR	0.22
95% CI lower	0.061
95% CI upper	0.78

PFI **Bmi-1 %**	**n** **median (range)**
Low	10 108 (54-206)
High	10 59 (14-140)
***P*-value (Log Rank)**	**0.047**
Cox *P*-value	**0.034**
RR	0.28
95% CI lower	0.087
95% CI upper	0.91

Table 6.3: Summary of telomere length ratio and relative telomerase activity. VS; very short length telomere, AV; average length telomere, SD; standard deviation

Patient	VS/AV ratio	Relative telomerase activity (%)
		Mean of 2 runs
1	1.1	-
2	2.2	214.7
3	1.2	-
4	1.0	44.1
5	1.3	-
6	0.9	4.2
7	0.8	10.0
8	1.1	53.0
9	1.0	3.1
10	1.0	-
11	1.0	159.4
12	1.1	163.8
13	1.5	-
14	1.2	26.8
15	1.4	39.2
16	1.0	161.6
17	0.8	1.2
18	1.3	0.9
19	0.9	5.4
20	0.7	125.8
Mean	1.1	67.5
SD	0.32	75.1

BIBLIOGRAPHY

1. Dalerba P, Cho RW, Clarke MF. Cancer stem cells: models and concepts. *Annu Rev Med* 2007;58:267-284.

2. Park CH, Bergsagel DE, McCulloch EA. Mouse myeloma tumor stem cells: a primary cell culture assay. *J Natl Cancer Inst* 1971;46:411-422.

3. Harper LJ, Costea DE, Gammon L, et al. Normal and malignant epithelial cells with stem-like properties have an extended G2 cell cycle phase that is associated with apoptotic resistance. *BMC Cancer* 2010;10:166.

4. Okamoto A, Chikamatsu K, Sakakura K, et al. Expansion and characterization of cancer stem-like cells in squamous cell carcinoma of the head and neck. *Oral Oncol* 2009;45:633-639.

5. Prince ME, Sivanandan R, Kaczorowski A, et al. Identification of a subpopulation of cells with cancer stem cell properties in head and neck squamous cell carcinoma. *Proc Natl Acad Sci U S A* 2007;104:973-978.

6. Joshua B, Kaplan MJ, Doweck I, et al. Frequency of cells expressing CD44, a head and neck cancer stem cell marker: correlation with tumor aggressiveness. *Head Neck* 2012;34:42-49.

7. Kokko LL, Hurme S, Maula SM, et al. Significance of site-specific prognosis of cancer stem cell marker CD44 in head and neck squamous-cell carcinoma. *Oral Oncol* 2011;47:510-516.

8. Uwa N, Kataoka TR, Torii I, et al. CD44 expression is related to poor prognosis of hypopharyngeal squamous cell carcinoma. *Acta Otolaryngol* 2011;131:323-329.

9. Park IK, Qian D, Kiel M, et al. Bmi-1 is required for maintenance of adult self-renewing haematopoietic stem cells. *Nature* 2003;423:302-305.

10. Facchino S, Abdouh M, Chatoo W, et al. BMI1 confers radioresistance to normal and cancerous neural stem cells through recruitment of the DNA damage response machinery. *J Neurosci* 2010;30:10096-10111.

11. Wang E, Bhattacharyya S, Szabolcs A, et al. Enhancing chemotherapy response with Bmi-1 silencing in ovarian cancer. *PLoS One* 2011;6:e17918.

12. Hayry V, Makinen LK, Atula T, et al. Bmi-1 expression predicts prognosis in squamous cell carcinoma of the tongue. *Br J Cancer* 2010;102:892-897.

13. Vormittag L, Thurnher D, Geleff S, et al. Co-expression of Bmi-1 and podoplanin predicts overall survival in patients with squamous cell carcinoma of the head and neck treated with radio(chemo)therapy. *Int J Radiat Oncol Biol Phys* 2009;73:913-918.

14. Vrzalikova K, Skarda J, Ehrmann J, et al. Prognostic value of Bmi-1 oncoprotein expression in NSCLC patients: a tissue microarray study. *J Cancer Res Clin Oncol* 2008;134:1037-1042.

15. Liptak JM, Withrow SJ. Cancer of the gastrointestinal tract In: Withrow SJ,Vail DM, eds. *Small Animal Clinical Oncology*. 4th ed: Saunders Elsevier, 2007;455-510.

16. Moyzis RK, Buckingham JM, Cram LS, et al. A highly conserved repetitive DNA sequence, (TTAGGG)n, present at the telomeres of human chromosomes. *Proc Natl Acad Sci U S A* 1988;85:6622-6626.

17. Weinberg R. Eternal life: Cell immortalization and tumorigenesis. *The biology of cancer*: Garland Science, Taylor & Francis Group 2007;357-398.

18. Hayflick L, Moorhead PS. The serial cultivation of human diploid cell strains. *Exp Cell Res* 1961;25:585-621.

19. Hanahan D, Weinberg RA. Hallmarks of cancer: the next generation. *Cell* 2011;144:646-674.

20. Cunningham AP, Love WK, Zhang RW, et al. Telomerase inhibition in cancer therapeutics: molecular-based approaches. *Curr Med Chem* 2006;13:2875-2888.

21. McCaul JA, Gordon KE, Minty F, et al. Telomere dysfunction is related to the intrinsic radio-resistance of human oral cancer cells. *Oral Oncol* 2008;44:261-269.

22. Svenson U, Roos G. Telomere length as a biological marker in malignancy. *Biochim Biophys Acta* 2009;1792:317-323.

23. Patel MM, Parekh LJ, Jha FP, et al. Clinical usefulness of telomerase activation and telomere length in head and neck cancer. *Head Neck* 2002;24:1060-1067.

24. Hirota J, Usui R, Satoh T, et al. Telomere position on the cat chromosome. *J Vet Med Sci* 1996;58:1025-1026.

25. McKevitt TP, Nasir L, Wallis CV, et al. A cohort study of telomere and telomerase biology in cats. *Am J Vet Res* 2003;64:1496-1499.

26. Brummendorf TH, Mak J, Sabo KM, et al. Longitudinal studies of telomere length in feline blood cells: implications for hematopoietic stem cell turnover in vivo. *Exp Hematol* 2002;30:1147-1152.

27. Fordyce CA, Heaphy CM, Griffith JK. Chemiluminescent measurement of telomere DNA content in biopsies. *Biotechniques* 2002;33:144-146, 148.

28. Slijepcevic P. Telomere length measurement by Q-FISH. *Methods Cell Sci* 2001;23:17-22.

29. Baerlocher GM, Vulto I, de Jong G, et al. Flow cytometry and FISH to measure the average length of telomeres (flow FISH). *Nat Protoc* 2006;1:2365-2376.

30. Meeker AK, Gage WR, Hicks JL, et al. Telomere length assessment in human archival tissues: combined telomere fluorescence in situ hybridization and immunostaining. *Am J Pathol* 2002;160:1259-1268.

31. Yoshikawa H, Harmon JF, Custis JT, et al. Repeatability of a Planning Target Volume Expansion Protocol for Radiation Therapy of Regional Lymph Nodes in Canine and Feline Patients with Head Tumors. *Vet Radiol Ultrasound* 2012;53:667-672.

32. Yoshikawa H, Randall EK, Kraft SL, et al. Comparison between 2-(18) F-Fluoro-2-Deoxy-D-Glucose Positron Emission Tomography and Contrast-Enhanced Computed Tomography for Measuring Gross Tumor Volume in Cats with Oral Squamous Cell Carcinoma. *Vet Radiol Ultrasound* 2013.

33. Tannehill-Gregg SH, Levine AL, Rosol TJ. Feline head and neck squamous cell carcinoma: a natural model for the human disease and development of a mouse model. *Vet Comp Oncol* 2006;4:84-97.

34. Yoshikawa H, Ehrhart E, Charles JB, et al. Immunohistochemical characterization of feline oral squamous cell carcinoma. *Am J Vet Res* 2012;73:1801-1806.

35. Quimby JM, Webb TL, Gibbons DS, et al. Evaluation of intrarenal mesenchymal stem cell injection for treatment of chronic kidney disease in cats: a pilot study. *J Feline Med Surg* 2011;13:418-426.

36. Gonzalez-Moles MA, Bravo M, Ruiz-Avila I, et al. Adhesion molecule CD44 as a prognostic factor in tongue cancer. *Anticancer Res* 2003;23:5197-5202.

37. Herbert BS, Hochreiter AE, Wright WE, et al. Nonradioactive detection of telomerase activity using the telomeric repeat amplification protocol. *Nat Protoc* 2006;1:1583-1590.

38. Hou M, Xu D, Bjorkholm M, et al. Real-time quantitative telomeric repeat amplification protocol assay for the detection of telomerase activity. *Clin Chem* 2001;47:519-524.

39. Kim NW, Wu F. Advances in quantification and characterization of telomerase activity by the telomeric repeat amplification protocol (TRAP). *Nucleic Acids Res* 1997;25:2595-2597.

40. Alkema MJ, Wiegant J, Raap AK, et al. Characterization and chromosomal localization of the human proto-oncogene BMI-1. *Hum Mol Genet* 1993;2:1597-1603.

41. Kinnon S, Fulton R. Nucleotide sequence of the feline Bmi-1 coding region. *DNA Seq* 1999;10:335-338.

42. Fox SB, Fawcett J, Jackson DG, et al. Normal human tissues, in addition to some tumors, express multiple different CD44 isoforms. *Cancer Res* 1994;54:4539-4546.

43. Kennel SJ, Lankford TK, Foote LJ, et al. CD44 expression on murine tissues. *J Cell Sci* 1993;104 (Pt 2):373-382.

44. Oliveira DT, Odell EW. Expression of CD44 variant exons by normal oral epithelia. *Oral Oncol* 1997;33:260-262.

45. Park IK, Morrison SJ, Clarke MF. Bmi1, stem cells, and senescence regulation. *J Clin Invest* 2004;113:175-179.

46. Chen YC, Chang CJ, Hsu HS, et al. Inhibition of tumorigenicity and enhancement of radiochemosensitivity in head and neck squamous cell cancer-derived ALDH1-positive cells by knockdown of Bmi-1. *Oral Oncol* 2010;46:158-165.

47. Zhang Z, Filho MS, Nor JE. The biology of head and neck cancer stem cells. *Oral Oncol* 2012;48:1-9.

48. Baumann M, Krause M. CD44: a cancer stem cell-related biomarker with predictive potential for radiotherapy. *Clin Cancer Res* 2010;16:5091-5093.

49. Rodriguez-Rodriguez L, Sancho-Torres I, Mesonero C, et al. The CD44 receptor is a molecular predictor of survival in ovarian cancer. *Med Oncol* 2003;20:255-263.

50. de Jong MC, Pramana J, van der Wal JE, et al. CD44 expression predicts local recurrence after radiotherapy in larynx cancer. *Clin Cancer Res* 2010;16:5329-5338.

51. Goodison S, Urquidi V, Tarin D. CD44 cell adhesion molecules. *Mol Pathol* 1999;52:189-196.

52. Faber A, Barth C, Hormann K, et al. CD44 as a stem cell marker in head and neck squamous cell carcinoma. *Oncol Rep* 2011;26:321-326.

53. Pries R, Wittkopf N, Hasselbacher K, et al. Constitutive expression of the potential stem cell marker CD44 in permanent HNSCC cell lines. *HNO* 2008;56:461-466.

54. Blasco MA. Telomeres and human disease: ageing, cancer and beyond. *Nat Rev Genet* 2005;6:611-622.

55. Chuang TC, Moshir S, Garini Y, et al. The three-dimensional organization of telomeres in the nucleus of mammalian cells. *BMC Biol* 2004;2:12.

56. Klonisch T, Wark L, Hombach-Klonisch S, et al. Nuclear imaging in three dimensions: a unique tool in cancer research. *Ann Anat* 2010;192:292-301.

57. Cadile CD, Kitchell BE, Biller BJ, et al. Telomerase activity as a marker for malignancy in feline tissues. *Am J Vet Res* 2001;62:1578-1581.

58. Weinberg R. Multi-step tumorigenesis. *The biology of cancer*: Garland Science, Taylor & Francis Group, 2007;399-462.

CHAPTER 7: CONCLUSIONS

Although each of the five studies in this dissertation stands alone, integrating information from the studies is important to help us understand feline oral SCC.

^{18}F-FDG PET for treatment planning in cats with oral SCC

^{18}F-FDG PET imaging is an imaging examination that helps to include all possible tumoral regions in the GTV, and is invaluable to identify lingual/laryngeal SCC appropriately. However, because many of the currently available PET radioisotopes including ^{18}F-FDG and ^{18}F-fluorothymidine (FLT) are to highlight areas of increased metabolic activity such as glucose consumption and DNA replication, PET imaging is not cancer-specific.[1] Although other radioisotopes such as ^{18}F-fluoromisonidazole (MISO) as a hypoxia marker that are designed to detect intra-tumoral regions where may impact treatment outcome have been evaluated, as of my knowledge, there are no radioisotopes to depict gene/protein expression levels that are responsible for tumor's resistance to treatments.[1] Since tumors are heterogeneous, it is important to localize tumor cells with more treatment-refractory characteristics. Recent studies indicate that tumor cells with stem cell characteristics are more resistant to conventional treatment modalities due to more efficient DNA damage repair machineries and existence of drug-efflux protein.[2] Those cells are called cancer stem cells or tumor-initiating cells (TIC). Because those cells are thought to be neither quiescent nor rapidly proliferating, it is unlikely that PET proliferation markers such as ^{18}F-FLT can detect TICs. Therefore, although improving the resolution of PET images is essential, ideally the PET imaging that would highlight areas with more TICs might improve treatment outcome such as local tumor control by helping us treating those areas more aggressively. Potential targets include protein expression of Bmi-1, Oct3/4, Nanog, and

CD133.[2,3] Caution should be paid, however, because normal stem cells around the tumor may also express those proteins.

PTV expansions for a simultaneous irradiation of primary tumor and regional lymph nodes

Based on this work, when the mandibular and retropharyngeal lymph nodes are treated simultaneously with the primary tumor, PTV expansions larger than 2 mm (dogs; 4-9 mm, cats; 2-4 mm) are needed to deliver the dose to the target. When lymph nodes are the only treatment target, smaller PTV expansions (dogs; 3-5 mm, cats; 2-3 mm) should be adequate. Since the guidelines for PTV expansions established in this study can be applied to other organs at risk, there are many possible research opportunities. For example salivary glands, trachea, esophagus, and eyes can be evaluated for head and neck setups. For pelvic and lower abdomen setups, medial iliac and inguinal lymph nodes and ureters can be evaluated. Those PTV expansions should be specific for patient immobilization devices and linear accelerators.

Immunohistochemical evaluation of feline oral SCC using archival tumor samples

Immunohistochemical and imaging techniques established in the chapter 4 provided tools for the evaluation of Ki67, MVD, and EGFR in feline oral SCC using formalin-fixed, paraffin-embedded blocks. Those markers can be applied to other feline malignancies.

Since immunohistochemistry provides us valuable information about protein expression while preserving tissue architecture, I am eager to establish staining and quantification techniques for feline and canine malignancies using antibodies for other target proteins. Since the specificity of the primary antibodies is the key factor influencing the validity of the examination, I view, establishing a facility to develop tailor-made monoclonal antibodies using hybridomas as an important direction in my professional development.

Characterization of feline oral SCC using various markers in cats with oral SCC who underwent SRT

The finding that cats with higher MVD had shorter ST compared to those with lower MVD might indicate that tumor microvasculature is playing an important role in treatment response after SRT. Additional treatment to suppress tumor angiogenesis, such as metronomic chemotherapy that is targeted to tumor angiogenesis and small molecule inhibitors such as anti-VEGF therapy, might improve local tumor control. However, since combining those treatments and SRT may compromise normal endothelial cells and cause unacceptable toxicities in the normal tissues, a novel method to deliver those drugs specifically to the tumor or to maintain a high drug concentration in the tumor might reduce potential toxicities. Since we found that feline oral SCC expresses high levels of CD44 on their cell surface, anti-endothelial cell drugs conjugated with anti-CD44 antibody may be able to concentrate and slowly release the anti-angiogenic drug in the tumor. However, since CD44 has many isoforms in humans, it is critical to determine the type and level of isoform expressed in feline oral SCC.

This study also revealed that cats with more keratinized SCC had shorter PFI compared to those with less keratinized SCC. This finding has also been reported in human nasopharyngeal SCC.[4] Although the underlying mechanism has yet to be investigated and might be complicated, oncologists should consider utilizing this variable for prognostication since it is easily evaluated. One possible explanation of this finding is the effect of inflammation. Since extracellular keratin is thought to cause inflammatory response, it is possible that this immune reaction triggered by the extracellular keratin causes more malignant transformation of the SCC cells and as a result, deteriorates tumor control.[5] Evaluating the correlation between degrees of inflammation and keratinization would be another future study to dissect the biology of this cancer. Degree of

inflammation may be evaluated by quantifying amount of specific inflammatory cells such as macrophage and lymphocytes.

The SRT protocol evaluated in the current study can be used as a palliative treatment, with advantages of the short treatment course and minimal acute toxicities. Since we encountered relatively high rate of treatment/tumor-related complications, especially several months after SRT, the SRT protocol needs further modifications. The most commonly-seen complication was related to a tissue-defect that developed at the original tumor site. SRT showed rapid reduction of tumor volume in many cases whereas granulation reaction was seen at slower speed and tissue defect became a clinical concern. Therefore, I would suggest modifying the SRT protocol to kill the tumor "more slowly" so that the granulation can catch up with the speed of tumor reduction. At the same time, we should avoid an unnecessary increase of anesthesia episodes. To achieve those goals, a moderately fractioned protocol such as 8 Gy x 4 fx or 7 Gy x 5 fx may be feasible. Methods to stimulate granulation/epithelialization may also be beneficial to minimize the complication.

Putative tumor initiating cells and telomere and telomerase biology in feline oral SCC

The telomere length and telomerase assays established in the chapter 6 can be applied to other tumor types in cats and possibly in dogs. The validity of putative TICs (feline oral SCC positive for both CD44 and Bmi-1) needs to be established. This could be achieved by using functional evaluations such as tumor sphere formation and side population assay. Since little is known about the degree of telomerase expression in feline oral SCC, further studies to evaluate its expression level are needed. Since the currently available assays to evaluate telomerase expression (TRAP and RTQ-PCR) cannot discriminate cell types if clinically obtained samples

are used, a reliable primary antibody or probe against the telomeric protein has to be developed. Following development of the primary antibody, I would like to evaluate its expression status in the putative TICs, using co-staining immunohistochemistry or immunofluorescent assay or flow cytometry. And finally, if the TICs express telomerase, a study blocking its function in those putative TICs might be beneficial to evaluate its role in tumor control.

Since the study in the chapter 6 revealed the possible role of Bmi-1 protein in the treatment response after SRT, protein expression level of Bmi-1 should be evaluated to estimate progression free intervals for cats with oral SCC who undergo SRT. However, since its function in feline oral SCC has not been studied yet, a further study to investigate the role of this protein is essential. An *in vitro* experiment to evaluate potential therapeutic effects of small interference RNA (siRNA) on feline oral SCC should be investigated. The effects of anti-Bmi-1 therapy that should be evaluated include the efficacy of tumor sphere formation and successful tumor inoculation to experimental animals, cell survival assay after irradiation. Those studies should give us further insights about the function of this protein in feline oral SCC.

BIBLIOGRAPHY

1. Lawrence J, Rohren E, Provenzale J. PET/CT today and tomorrow in veterinary cancer diagnosis and monitoring: fundamentals, early results and future perspectives. *Vet Comp Oncol* 2010;8:163-187.

2. Dalerba P, Cho RW, Clarke MF. Cancer stem cells: models and concepts. *Annu Rev Med* 2007;58:267-284.

3. Okamoto A, Chikamatsu K, Sakakura K, et al. Expansion and characterization of cancer stem-like cells in squamous cell carcinoma of the head and neck. *Oral Oncol* 2009;45:633-639.

4. Reddy SP, Raslan WF, Gooneratne S, et al. Prognostic significance of keratinization in nasopharyngeal carcinoma. *Am J Otolaryngol* 1995;16:103-108.

5. Weinberg R. Multi-step tumorigenesis. *The biology of cancer*: Garland Science, Taylor & Francis Group, 2007;399-462.